

# **Comparison Studies of Zone and CFD Fire Simulations**

**BY**

**André Lovatt**

**Supervised by**

**Dr Charley Fleischmann**

**Fire Engineering Research Report 98/5  
June 1998**

This report was presented as a project report  
as part of the M.E. (Fire) degree at the University of Canterbury

School of Engineering  
University of Canterbury  
Private Bag 4800  
Christchurch, New Zealand

Phone 643 364-2250  
Fax 643 364-2758



# Abstract

Comparisons between the results of zone and computational fluid dynamics (CFD) fire model simulations have been made; the zone model used was FAST (Peacock et al., 1997) and the CFD model used was SOFIE (Welch and Rubini, 1996). The underlying goal of this research is to investigate the limitations of zone models for the fire safety design of large enclosures.

Three different sized fires have been simulated in two different sized enclosures:

1. A domestic-sized enclosure measuring 3.7m long x 2.5m wide x 2.5m high.
2. An industrial-sized enclosure measuring 41m long x 11m wide x 11m high.

The fire sizes simulated were 330, 430, and 500kW for the domestic-sized enclosure and 300, and 600kW for the industrial-sized enclosure.

The results of these simulations have been compared based on interface height and average upper layer temperature. Two definitions of interface height have been used - the N-percent method by Cooper et al. (1982) and a height derivative of temperature approach, which defines an interface at the point of maximum change in temperature with height.

The comparisons between the two fire simulation techniques show that the comparisons are dependant on which definition of interface height is used; the N-percent method was not preferred because of the lack of any theoretical basis for its use, and its inability to define an interface in locations where the temperature gradient from the floor to the ceiling was small.

The comparisons between the zone and CFD simulations show that for the domestic-sized enclosure, the CFD results derived average upper layer temperatures between 30 and 40% of the average upper layer temperature derived by the zone model. The CFD results indicated that the interface height was between 50 and 80% of the interface height derived by the zone model.

For the industrial-sized enclosure, the CFD results derived average upper layer temperatures between 56 and 96% of the average upper layer temperature derived by the zone model. The CFD results indicated that the interface height was between 0 and 183% of the interface height derived by the zone model. Generally, the interface height predicted by the CFD model was higher than the interface height predicted by the zone model.

When the enclosure boundaries are assumed to be adiabatic, zone models over-predict (compared to the CFD simulations) the average upper layer temperature for cases where the volumetric heat release rate is large.

# Acknowledgments

Throughout the course of this project I have received assistance and support from a large number of people who I would like to acknowledge, including:

- My supervisor, Dr Charley Fleischmann.
- The Building Research Association of New Zealand (BRANZ) who provided the suggestion for this project and financial support through a grant from the Foundation for Research, Science and Technology.
- Dr Philip Rubini, of Cranfield University, United Kingdom, and author of Sofie. I would not have made it through this project had it not been for Dr Rubini's willingness to provide first class technical assistance with Sofie; thank you.
- Associate Professor Andrew Buchanan, thank you for reading sections of this report and for all your enthusiasm and support.
- Mr Peter Collier of BRANZ who read sections of this report and provided technical advise.
- The staff of the School of Engineering's computer laboratories: Messrs Coursey, Earl, Hutchison, and Stenfert-Kroese, for providing unlimited computing facilities and much assistance throughout the whole project.
- The staff of the Engineering and Physical Sciences libraries, especially Mrs Pat Roddick and Mrs Christine McKee, for assistance in finding papers.
- Mr David James and the Partners of Powell Fenwick Consultants Limited for their support during the 1997-98 academic year.
- Doctoral students, Messrs Clement and Enright, for counsel and advise.
- The other MEFÉ students, particularly Per Olsson and Ee Yii.
- My family, and especially Kate who, along with my Mum, bore the brunt of my many frustrations (two lines of acknowledgment can't say enough!).
- My supportive friends: Boyd, Clark, Gareth, Jeff, Morrissey, Murray, Anne-Marie & Zoë, Nigel, Ryan & Michele, Tom, and particularly Keith for having the great gift of being able to make you see familiar things differently.
- Lastly I would like to acknowledge my brother Nicholas, in whose memory I have chosen to dedicate this project.



# Contents

<b>Abstract</b> .....	<b>i</b>
<b>Acknowledgments</b> .....	<b>iii</b>
<b>List of Figures</b> .....	<b>xi</b>
<b>List of Tables</b> .....	<b>xvii</b>
<b>1 Introduction</b> .....	<b>1</b>
1.1 Zone and CFD Models	1
1.2 Impetus for the Research	2
1.3 Goals of the Research	3
1.4 Outline of this Report	3
1.5 Limitations of this Study	4
<b>2 Literature Review</b> .....	<b>5</b>
2.1 Introduction	5
2.2 Fires in Domestic-Sized Enclosures	6
2.3 Fires in Large Structures	11
2.3.1 Aircraft Hangars	11
2.3.2 Tunnel Fires	16
2.3.3 Other	18
2.4 Simulation of Fire Plumes	20
2.5 CFD in Consulting Engineering	22
2.6 Other	22
2.7 The Future of CFD in Fire Engineering	22
2.8 Summary	23
<b>3 Full-Scale Fire Experiments</b> .....	<b>25</b>

3.1 Collier (1997)	25
3.1.1 Issues Arising	26
3.1.2 Conclusion	26
<b>4 Zone Modelling Simulations.....</b>	<b>27</b>
4.1 Aims	27
4.2 Theoretical Background to FAST	27
4.2.1 Introduction	27
4.2.2 The Equation Set	28
4.2.3 Empirical Relationships	29
4.3 Method	31
4.3.1 Other modelling notes	32
4.4 Results	35
4.4.1 Enclosure 1	35
4.4.2 Enclosure 2	37
4.4.3 Summary	38
4.5 Discussion	39
4.5.1 Enclosure 1	39
4.5.2 Enclosure 2	39
4.5.3 General	39
<b>5 SOFIE - Simulation of Fires in Enclosures.....</b>	<b>41</b>
5.1 SOFIE Structure	41
5.2 Governing Equations of Fluid Flow	44
5.2.1 Conservation of Mass Equation	44
5.2.2 Conservation of Momentum Equation	44
5.2.3 Conservation of Energy Equation	45



5.2.4 Chemical Species Conservation	46
5.2.5 General Conservation Equation	47
5.3 Physical Models	49
5.3.1 Turbulence Modelling	49
5.3.2 Eddy Breakup Combustion Model	53
5.3.3 Heat Transfer	53
5.4 Numerical Solution Procedure	54
5.4.1 Discretisation Methods	54
5.4.2 Interpolation Methods	55
5.4.3 Algebraic Equation Solver	56
5.4.4 Calculating the Flow Field	57
<b>6 CFD Simulation Methodology .....</b>	<b>59</b>
6.1 Introduction	59
6.2 Computer Hardware and Software	59
6.2.1 Solution Type	60
6.2.2 Grid Generation	60
6.2.3 Blockages	63
6.2.4 Boundary Types	64
6.2.5 Boundary Values	64
6.2.6 Convergence Limits and Numerical Solution	67
6.2.7 Running the Simulation	68
6.2.8 Result File Exporting	68
<b>7 CFD Results and Discussion.....</b>	<b>69</b>
7.1 Enclosure 1	69
7.1.1 330kW	70

7.1.2 430kW	73
7.1.3 500kW	76
7.1.4 Remarks for Enclosure 1	79
7.2 Enclosure 2	80
7.2.1 300kW	80
7.2.2 600kW	86
7.2.3 300kW - central location	92
7.2.4 Remarks for Enclosure 2	98
7.3 Discussion	99
7.3.1 Enclosure 1	99
7.3.2 Enclosure 2	101
7.3.3 Computer Run Time	103
7.3.4 Limitations	104
<b>8 Comparisons .....</b>	<b>107</b>
8.1 Aim	107
8.2 Method	107
8.2.1 Locations for Comparisons	107
8.2.2 Interface Height	109
8.2.3 Average Upper Layer Temperature	112
8.3 Results	113
8.3.1 Enclosure 1	113
8.3.2 Enclosure 2	120
8.4 Discussion	127
8.4.1 Enclosure 1	127
8.4.2 Enclosure 2	129

8.4.3 Overall	131
<b>9 Conclusions .....</b>	<b>133</b>
9.1 Conclusions from the Zone Modelling Simulations	133
9.2 Conclusions from the CFD Simulations	133
9.3 Conclusions from the Comparisons	134
9.4 Further Research	135
<b>10 Nomenclature.....</b>	<b>137</b>
<b>11 References .....</b>	<b>139</b>
B1 Communication	B-1
B2 Planning	B-1
B3 User Manuals	B-2
B4 Heap Space Memory	B-2
B5 Databases	B-3
B6 Grids	B-4
B7 Active Blockages	B-4
B8 Tracking CO Concentration	B-5
B9 Convergence Problems	B-5
B10 Post-Processing	B-7



# List of Figures

Figure 2.1. Visualisation of 600kW methane fire in a domestic-sized enclosure showing half of the enclosure with a soot volume fraction isosurface at 0.5ppm (Moss and Rubini, 1997a).....	9
Figure 2.2 Visualisation of smoke layer within a domestic-sized enclosure for a 600kW methane fire (Moss and Rubini, 1997a).....	10
Figure 2.3. Temperature contours at $y = 5.5\text{m}$ for a square kerosene pool fire burning at $11\text{kg/s}$ (Sinai and Owens, 1995). ....	21
Figure 4.1. The two zone model with no mass exchange between the zones except the plume (Walton, 1995). ....	29
Figure 4.2. Upper layer gas temperature history for enclosure 1.....	35
Figure 4.3. Interface height history for enclosure 1. ....	36
Figure 4.4. Upper layer gas temperature history for enclosure 2.....	37
Figure 4.5. Interface height history for enclosure 2. ....	37
Figure 5.1. The top level of SOFIE's command interface.....	42
Figure 5.2. Graphical representation of the elements of the SOFIE CFD package system.....	43
Figure 5.3. A two-dimensional control volume surrounding a grid point P (Patankar, 1980). ....	55
Figure 6.1. The domain for enclosure 1, the shaded region indicates the fuel source. Note: a mirror line boundary exists down the doorway centre-line and the boundary in the x-y plane outside the doorway is the static pressure boundary.	61
Figure 6.2. The computational grid for enclosure 1.....	63
Figure 7.1. Gas temperature profile throughout enclosure 1, 330kW fire at 20 minutes.....	70

Figure 7.2. Vertical temperature profile at the fire source centre-line for enclosure 1, 330kW fire.....	71
Figure 7.3. Vertical temperature profile at the doorway centre-line for enclosure 1, 330kW fire.....	71
Figure 7.4. Vertical temperature profile at the corner adjacent to the doorway for enclosure 1, 330kW fire. ....	72
Figure 7.5. Gas temperature profile throughout enclosure 1, 430kW fire at 20 minutes. ....	73
Figure 7.6. Vertical temperature profile at the fire source centre-line for enclosure 1, 430kW fire.....	74
Figure 7.7. Vertical temperature profile at the doorway centre-line for enclosure 1, 430kW fire.....	74
Figure 7.8. Vertical temperature profile at the corner adjacent to the doorway for enclosure 1, 430kW fire. ....	75
Figure 7.9. Gas temperature profile throughout enclosure 1, 500kW fire at 20 minutes. ....	76
Figure 7.10. Vertical temperature profile at the fire source centre-line for enclosure 1, 500kW fire.....	77
Figure 7.11. Vertical temperature profile at the doorway centre-line for enclosure 1, 500kW fire.....	77
Figure 7.12. Vertical temperature profile at the corner adjacent to the doorway for enclosure 1, 500kW fire. ....	78
Figure 7.13. Gas temperature profile throughout enclosure 2, 300kW fire at 10 minutes. ....	80
Figure 7.14. Gas temperature profile throughout enclosure 2, 300kW fire at 20 minutes. ....	81
Figure 7.15. Gas temperature profile throughout enclosure 2, 300kW fire at 30 minutes. ....	82

Figure 7.16. Vertical temperature profile at the fire source centre-line for enclosure 2, 300kW fire. ....	83
Figure 7.17. Vertical temperature profile at thermocouple 1 for enclosure 2, 300kW fire. ....	83
Figure 7.18. Vertical temperature profile at thermocouple 2 for enclosure 2, 300kW fire. ....	84
Figure 7.19. Vertical temperature profile at the vent centre-line for enclosure 2, 300kW fire. ....	84
Figure 7.20. Vertical temperature profile at the corner adjacent to the vent for enclosure 2, 300kW fire. ....	85
Figure 7.21. Gas temperature profile throughout enclosure 2, 600kW fire at 10 minutes. ....	86
Figure 7.22. Gas temperature profile throughout enclosure 2, 600kW fire at 20 minutes. ....	87
Figure 7.23. Gas temperature profile throughout enclosure 2, 600kW fire at 30 minutes. ....	88
Figure 7.24. Vertical temperature profile at the fire source centre-line for enclosure 2, 600kW fire. ....	89
Figure 7.25. Vertical temperature profile at thermocouple 1 for enclosure 2, 600kW fire. ....	89
Figure 7.26. Vertical temperature profile at thermocouple 2 for enclosure 2, 600kW fire. ....	90
Figure 7.27. Vertical temperature profile at the vent centre-line for enclosure 2, 600kW fire. ....	90
Figure 7.28. Vertical temperature profile at the corner adjacent to the vent for enclosure 2, 600kW fire. ....	91
Figure 7.29. Gas temperature profile throughout enclosure 2, centrally-located 300kW fire at 10 minutes. ....	92

Figure 7.30. Gas temperature profile throughout enclosure 2, centrally-located 300kW fire at 20 minutes.....	93
Figure 7.31. Gas temperature profile throughout enclosure 2, centrally-located 300kW fire at 30 minutes.....	94
Figure 7.32. Vertical temperature profile at the fire source centre-line for enclosure 2, centrally-located 300kW fire.....	95
Figure 7.33. Vertical temperature profile at thermocouple 1 for enclosure 2, centrally-located 300kW fire.....	95
Figure 7.34. Vertical temperature profile at thermocouple 2 for enclosure 2, centrally-located 300kW fire.....	96
Figure 7.35. Vertical temperature profile at the vent centre-line for enclosure 2, centrally-located 300kW fire.....	96
Figure 7.36. Vertical temperature profile at the corner adjacent to the vent for enclosure 2, centrally-located 300kW fire.....	97
Figure 8.1. Location of corner temperature measurement (not to scale).....	108
Figure 8.2. Plan view of the location of the thermocouple trees for enclosure 2 (not to scale).....	109
Figure 8.3. Graphical representation of Cooper et al.'s (1982) N-percent rule at time t.....	110
Figure 8.4. Gas temperature versus height plot used to derive dT/dy versus height data.....	111
Figure 8.5. An example plot of dT/dy versus height indicating a maximum at approximately 1.25m.....	112
Figure 8.6. Comparison of average upper layer temperature derived by FAST, N-percent rule, dT/dy for 330kW fire in enclosure 1.....	113
Figure 8.7. Comparison of interface height derived by FAST, N-percent rule, dT/dy for 330kW fire in enclosure 1.....	114



Figure 8.8. Comparison of average upper layer temperature derived by FAST, N-percent rule, $dT/dy$ for 430kW fire in enclosure 1.....	115
Figure 8.9. Comparison of interface height derived by FAST, N-percent rule, $dT/dy$ for 430kW fire in enclosure 1. ....	115
Figure 8.10. Comparison of average upper layer temperature derived by FAST, N-percent rule, $dT/dy$ for 500kW fire in enclosure 1.....	116
Figure 8.11. Comparison of interface height derived by FAST, N-percent rule, $dT/dy$ for 500kW fire in enclosure 1. ....	116
Figure 8.12. Comparison of average upper layer temperature derived by FAST, N-percent rule, $dT/dy$ for 300kW fire in enclosure 2.....	120
Figure 8.13. Comparison of interface height derived by FAST, N-percent rule, $dT/dy$ for 300kW fire in enclosure 2. ....	120
Figure 8.14. Comparison of average upper layer temperature derived by FAST, N-percent rule, $dT/dy$ for 600kW fire in enclosure 2.....	121
Figure 8.15. Comparison of interface height derived by FAST, N-percent rule, $dT/dy$ for 600kW fire in enclosure 2. ....	121
Figure 8.16. Comparison of average upper layer temperature derived by FAST, N-percent rule, $dT/dy$ for a centrally-located 300kW fire in enclosure 2. ....	122
Figure 8.17. Comparison of interface height derived by FAST, N-percent rule, $dT/dy$ for a centrally-located 300kW fire in enclosure 2.....	122



# List of Tables

Table 4.1. Enclosure geometry for zone modelling simulations.....	31
Table 4.2. Fire sizes and location for each simulation.....	32
Table 4.3. Example FAST input file keywords and values (for simulation 1A). .....	34
Table 4.4. Summary of steady-state upper layer gas temperatures for each enclosure.	38
Table 5.1. Effective exchange coefficients and source terms in generic transport equation for $\phi$ (reproduced from Cox (1995b))......	48
Table 5.2. Universal constants for the standard $k\sim\varepsilon$ turbulence model (Rodi, 1980).	52
Table 6.1. Grid statistics for each enclosure. ....	62
Table 6.2. Solved variables and boundary values for boundary types.....	65
Table 6.3. Molecular mass, heat of combustion, and density of volatiles for Propane and n-Heptane. ....	66
Table 6.4. Fire source definition: area, fuel type, inlet velocity and inlet Froude number. ....	67
Table 7.1. Computer run times required for the CFD simulation of the fires in enclosure 1. ....	78
Table 7.2. Computer run times required for the CFD simulation of the fires in enclosure 2. ....	97
Table 8.1. Comparison points for each enclosure. ....	108
Table 8.2. Comparisons of average upper layer gas temperature, based on two different definitions of interface height expressed as percentage of zone model results. ....	117
Table 8.3. Comparisons of temperature interface height for N-percent method and $dT/dy$ method expressed as percentage of zone model results.....	118

Table 8.4. Comparisons of average upper layer gas temperature, based on the N-percent method definition of interface height expressed as percentage of zone model results. .... 124

Table 8.5. Comparisons of temperature interface height for N-percent method and dT/dy method expressed as percentage of zone model results..... 125

# 1 Introduction

## 1.1 Zone and CFD Models

Since the introduction of New Zealand's performance-based building code in 1992 (BIA, 1992), fire engineers have had the scope to use specific design to demonstrate compliance with the performance requirements of the New Zealand Building Code. On a day-to-day basis, fire engineers now use deterministic models<sup>1</sup> to carry out specific designs rather than following traditional prescriptive-based requirements (Buchanan, 1992). The most common type of deterministic model used by consultants to simulate enclosure fires is known as a zone model.

The zone model approach assumes that two homogeneous zones are formed within an enclosure during a fire, one a relatively cold zone, the other a relatively hot layer. Zone models solve the conservation equations of mass and energy for each zone and use empirically-derived correlations to describe physical phenomena such as mass entrainment into the fire plume.

Another type of deterministic model that may be used to simulate enclosure fires is the computational fluid dynamics (CFD) model. Using a CFD model involves dividing the domain of interest into thousands of control volumes and simultaneously solving the three dimensional time dependant equations that describe the conservation of energy, mass, momentum and turbulent kinetic energy throughout the domain, taking into account the relevant boundary conditions.

---

<sup>1</sup> Deterministic models, as opposed to probabilistic models, are mathematical models that are based on physical laws, e.g., Newton's laws of motion are deterministic models (Kanury, 1987). Probabilistic models calculate the probability of an event occurring based on previous experience.

The particular strength of CFD modelling lies in the fact that it is a completely general approach, based on classical fluid dynamics theory, which does not rely on the assumptions and use of empirically-derived correlations inherent in the zone model approach.

The use of CFD techniques is not confined to fire. In fact the approach may be used in any field studying the flow of fluids undergoing combined heat and mass transfer, e.g., arterial blood flow (Rappitsch et al. (1997)).

CFD modelling is extremely difficult and expensive compared to zone modelling. In order to be able to carry out CFD simulations, high quality computing facilities must be available, the user must have sufficient funding and time to learn how to run the particular CFD code, and there must be enough time to allow the simulations to converge sufficiently. Once the simulation has finished, the data generated must then be post-processed using specific post-processing software.

## **1.2 Impetus for the Research**

It is of concern that the current trend for fire engineers in New Zealand, if not globally, is to indiscriminately use zone models without consideration of the validity of the zone model approach. The Building Research Association of New Zealand (BRANZ) has initiated this project as a sub-set of a larger project which will attempt to identify cases where it is possible to successfully use zone models to simulate fires and where it is not. The variables of interest in the BRANZ study are fire size and enclosure volume, the aim being to publish guidelines for the fire safety design of large enclosures using zone models.

Given that CFD models do not rely on empirically-derived correlations, and provide a more generalised approach to simulating enclosure fire, CFD simulation results will be used as the basis for comparison to zone model results for the BRANZ project.

## **1.3 Goals of the Research**

The goal of this research is to compare the results of zone and CFD model simulations by:

1. Simulating three different sized fires in two different sized enclosures using both zone and CFD modelling techniques.
2. Comparing the two different simulation techniques based on predicted hot/cold layer interface height, and average upper layer temperature.

Two different definitions of interface height shall be used:

- a. Cooper et al.'s (1982) N-percent method.
  - b. A height derivative of gas temperature approach where the height derivative of temperature is plotted against height and a maxima defines the interface height.
3. Highlighting cases where the zone and CFD modelling results are different.

## **1.4 Outline of this Report**

Following this introduction, chapter 2 reviews fire engineering orientated CFD literature. This is followed by a description of the BRANZ full-scale fire tests in chapter 3. Chapter 4 then describes and presents the results of the zone modelling simulations.

The CFD section of the report is covered in chapters 5-6. Chapter 5 describes the CFD code SOFIE (Welch and Rubini, 1996), including the underlying theory of computational fluid dynamics. Chapter 6 describes the methodology carried out for the CFD simulations. Chapter 7 presents the results and discussion of the CFD results.

Chapter 8 describes the method of comparison of the zone and CFD simulation results, and also presents and discusses the results.

Finally, chapter 9 will conclude this project report.

## **1.5 Limitations of this Study**

The limitations of the fire simulations carried out during this study are as follows:

- For the simulations of the domestic-sized enclosure, the height of the fuel source was at the floor level; in the full-scale fire experiments, the fuel surface was elevated 0.61m above the floor level.
- In light of the above, no comparisons of the CFD simulation results was made to the full-scale experimental data for the domestic-sized enclosure.
- The quality of the CFD simulations has not been tested using different sized grids.
- All boundaries have been assumed to be adiabatic.
- Thermal radiation has been included in the simulations by assuming that 35% of the total heat release rate is lost to the surrounding environment.



## 2 Literature Review

The purpose of this chapter is to review what work has been done with CFD models in the past. After introducing the various CFD codes, the use of CFD in the following areas will be discussed:

- Fires in domestic-sized enclosures
- Fires in large enclosures such as aircraft hangars, warehouses, shopping malls and tunnels
- Fire plumes
- CFD use in consulting engineering.

The distinction between the use of CFD techniques in consulting and other areas is that the papers reviewed present qualitative results of what sort of results are produced by CFD models . This arises because the purpose of the consulting-orientated papers is different from the research-orientated papers because they accept the particular CFD model as a tool and its use is then demonstrated with applications to commercial cases.

### 2.1 Introduction

The papers to be reviewed involve the use of three different CFD models, namely:

- **JASMINE**, developed by the Fire Research Station, United Kingdom, and having its roots in the two-dimensional, steady-state CFD code MOSIE (Kumar and Cox, 1983, and Markatos et al., 1982). The equation solver in JASMINE is PHONETICS.

- **PHONETICS**, developed by Spalding at Imperial College, United Kingdom, PHONETICS is a general purpose CFD code that includes a combustion model and the  $k\sim\varepsilon$  turbulence model<sup>2</sup>.
- **FLOW 3D**, a commercially available general-purpose CFD code that may be purchased or leased from the developers, Harwell Laboratories, United Kingdom (Stroup, 1995).

The CFD code used for this study was SOFIE (Welch and Rubini, 1996) and two papers showing SOFIE's application to simulating fires in domestic-sized enclosures will be reviewed (Lewis et al. (1997) and Moss and Rubini (1997a)).

## 2.2 Fires in Domestic-Sized Enclosures

A large amount of work has gone into the validation of CFD codes for simulating fires in domestic-sized enclosures. The most commonly used experimental dataset used for comparison purposes is that by Steckler et al. (1982); a large proportion of this comparison work has been carried out by researchers at the University of Greenwich, United Kingdom, e.g., Kerrison et al., 1994a and b.

Markatos and Cox (1984) compare Steckler et al.'s (1982) experimental results with CFD simulations using JASMINE. Comparison of the doorway mass efflux with the experimental results and the Harvard zone model show that while both models predict the general trend of increasing mass efflux with increasing heat release rate, JASMINE is a closer fit to the experimental data than the Harvard zone model.

Kumar et al. (1991) have also used JASMINE to simulate Steckler et al.'s (1982) experiments, although incorporating a six flux radiation model, the eddy

---

<sup>2</sup> The  $k\sim\varepsilon$  turbulence model (Jones and Launder, 1972) is an eddy viscosity model that solves for the turbulent eddy viscosity terms in the time-averaged Navier-Stokes equations. The  $k\sim\varepsilon$  turbulence model is the most widely used turbulence model used in CFD and the reference to the developers (Jones and Launder, 1972) is usually dropped.

breakup combustion model, and the standard  $k\sim\varepsilon$  turbulence model with buoyancy corrections by Rodi (1980).

The model's predicted temperature profiles agree well with the experimental results, and the fire plume is observed to be blown over by the inflow of air into the enclosure; this has been previously observed experimentally by Quintiere et al. (1981). Although the model predicts approximately the same mass influx and efflux as that in the experiment, the nature of the horizontal velocity profile in the doorway is totally different: the experiment has its minimum velocity at the centre of the doorway, with the maximum at the edges. The numerical simulation, however, predicts a maximum at the doorway centre and a minimum at the edges. The inclusion of radiative heat transfer is found to increase the doorway mass flow rate for fires located around the compartment's perimeter, but has no effect for fires located remote from walls. Kumar et al. (1991) feel that this is because large scale recirculation enhances the mass efflux for fires located around the enclosure periphery.

Kerrison et al. have reported comparisons of PHONETICS (1994a) and FLOW3D (1994a and 1994b) to the Steckler et al. (1982) experiments. Mawhinney et al. (1994) have also reported comparisons of PHONETICS to the same experiments. In all cases, the  $k\sim\varepsilon$  turbulence model was used with buoyancy corrections by Rodi (1980) and the total mesh size was  $8k^3$ . All boundaries were assumed to be adiabatic and radiative heat losses were ignored. Combustion was ignored and the fire source was represented as a prescribed enthalpy source.

Overall, the authors evaluated the ability of the models to predict the following parameters:

- Neutral plane height.
- Mass fluxes.

---

<sup>3</sup> This number refers to the total number of control volumes in the computational domain, the suffix refers to thousand, therefore the total number of control volumes in the computational domain was 8000.

- Average upper layer temperature.
- Doorway centre-line velocity.
- Doorway horizontal velocity profile.

The ability of the models to predict the first three parameters above was within 16% for all of the models, although PHONETICS has difficulty predicting the corner temperature stratification, with severe “smearing occurring in the predicted temperatures for the centre fire location” (Mawhinney et al., 1994). Predictions of the doorway centre-line velocity were in good agreement with the experimental results, although at the top of the door, the velocity was under-predicted. The authors feel that this was because the bi-directional probes installed in the doorway to measure the doorway velocity in Steckler et al.’s (1982) experiments were not parallel to the velocity streamlines in this location, even these probes give velocities within 10% over an angular range of  $\pm 50^\circ$  of the probe axis in any direction (Emmons, 1995).

Kerrison et al. (1994a and 1994b) investigate the issue of the different horizontal velocity profiles between numerical simulation and Steckler et al.’s (1982) experiments first raised by Kumar et al. (1991). The authors show that there is a velocity profile within the door jamb, and the nature of the horizontal velocity profile is sensitive to how the soffit above the door is modelled: if the soffit is modelled as an infinitely thin plate, it is not possible to detect the velocity profile. However, if the soffit is modelled as having a thickness of two control volumes, the horizontal velocity profile inside the edge of the jamb shows the same trend as the experimentally-derived profile.

SOFIE (Welch and Rubini, 1996) has been applied to the task of simulating fires in typically domestic-sized enclosures. However, in contrast with the other papers reviewed so far, efforts have concentrated on incorporating radiation, combustion and soot (Lewis et al. (1997) and Moss and Rubini (1997a)).

Lewis et al. (1997) show that the results of the comparisons with the Steckler et al. (1982) fire experiments are improved with the incorporation of a discrete thermal radiation model and the eddy breakup combustion model, in comparison with a simply prescribed heat source.

Moss and Rubini (1997a) present further comparisons with full-scale fire experiments in domestic-sized enclosures, including a laminar flamelet combustion model and a discrete thermal radiation model. Results show that by using the laminar flamelet combustion model, soot profiles are able to be derived throughout the enclosure with good comparisons with experimental data. Figure 2.1 shows such a soot profile derived by SOFIE.

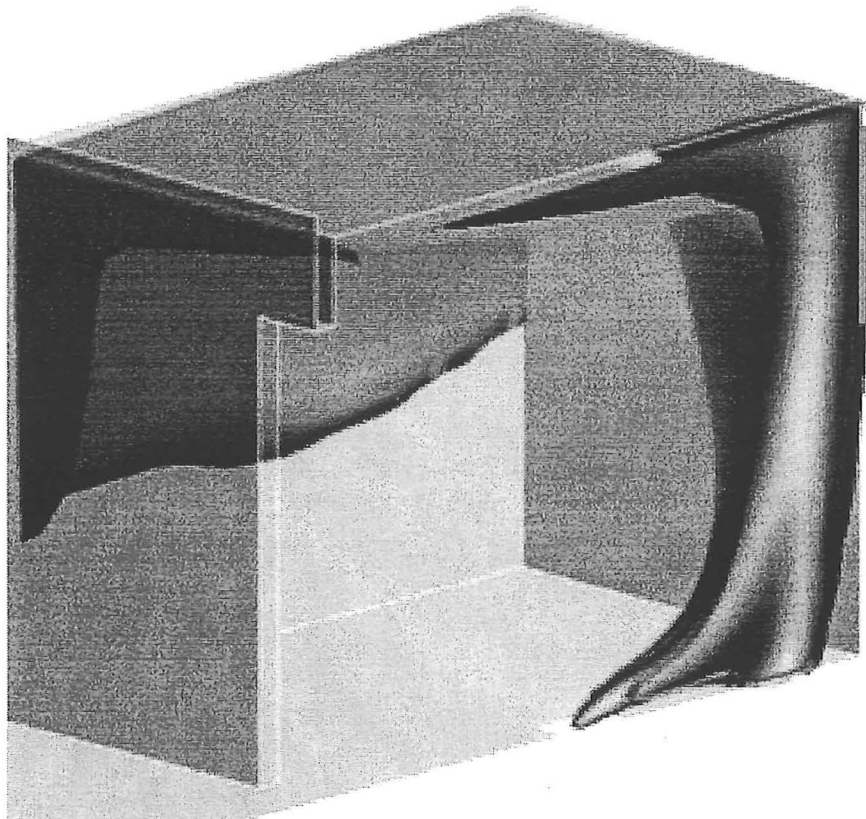


**Figure 2.1. Visualisation of 600kW methane fire in a domestic-sized enclosure showing half of the enclosure with a soot volume fraction isosurface at 0.5ppm (Moss and Rubini, 1997a).**

CFD predictions of gas temperature throughout the enclosure show that the results near the fire source compare favourably near the fire source, but the accuracy decreases with radial distance from the burner (Moss and Rubini, 1997a). Figure 2.2 shows a gas temperature profile throughout the enclosure derived by SOFIE.

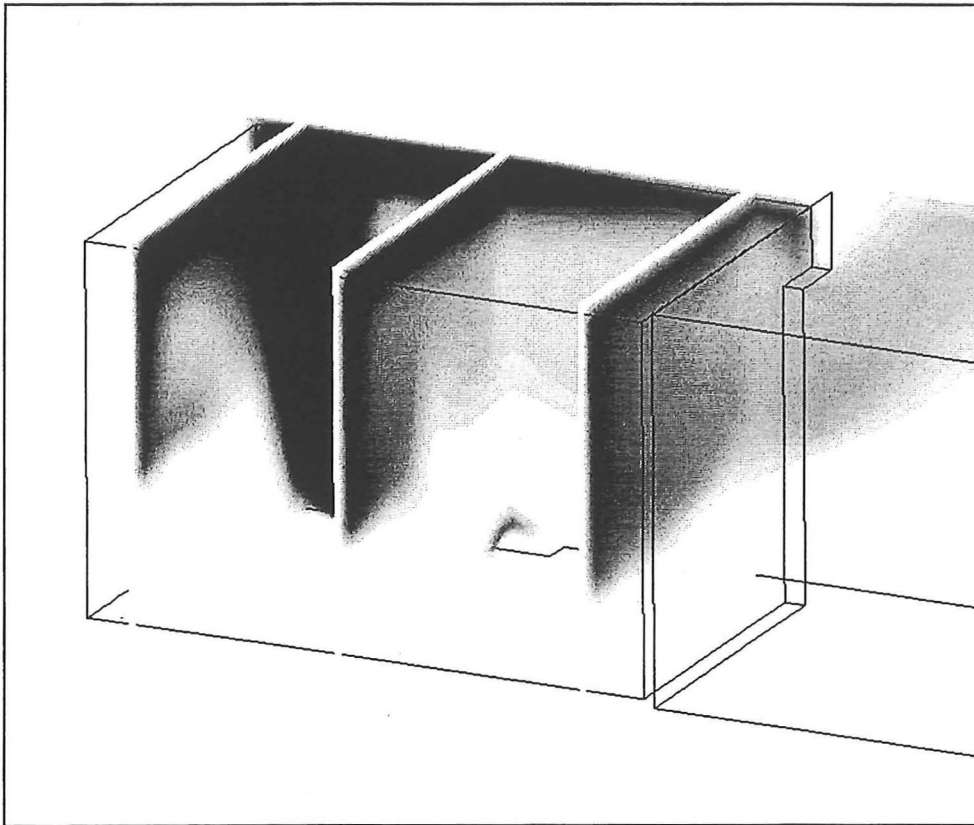


**Figure 2.2 Visualisation of smoke layer within a domestic-sized enclosure for a 600kW methane fire (Moss and Rubini, 1997a).**

## **2.3 Fires in Large Structures**

### **2.3.1 Aircraft Hangars**

#### **2.3.1.1 Introduction**

Aircraft hangars are of particular interest because in the event of a fire, rapid detection of a fire is necessary to protect any aircraft that might be stored in the hangar. Therefore, aircraft hangars represent a challenging detection design problem as there is no commonly accepted way of designing the fire protection systems necessary to protect the aircraft from fire.

The National Institute of Standards and Technology, United States, has carried out a number of full-scale experimental studies investigating fires in aircraft hangars and have compared these results to different types of deterministic fire model, FLOW3D.

#### **2.3.1.2 Notarianni and Davis (1993)**

Notarianni and Davis (1993) report on fire experiments in an aircraft hangar with a nominal height of approximately 30m. The experiments were carried out in order to calibrate the heat detection system installed in the hangar. In the first part of their report, Notarianni and Davis (1993) make comparison between the experimental gas temperatures in the hangar and those predicted by a range of computer fire models: DETACT-QS, FPETool, LAVENT and FLOW3D. In the second part of the report, the authors use FLOW3D to simulate fires in an existing room having a nominal height of approximately 27m. In all cases, computer simulations have been carried out to determine the performance of fire detection systems.

The experimental hangar used measured 389m long x 115m wide and 30m high. The hangar contained a complex ceiling structure and had draught curtains 3.7m deep and spaced approximately 12m apart. Fires were located on the floor and

at the centre of the hangar. Two tests were conducted, each with a different fire size; the fire sizes were 8.25MW and 9.9MW.

In general, all computer fire models, except FLOW3D significantly under-predicted the gas temperatures within the draught curtain area.

In their CFD simulations, Notarianni and Davis modelled the area bounded by the draught curtains. The  $k-\varepsilon$  turbulence model with buoyancy modifications was used throughout, and the fire source was modelled as a steady-state enthalpy source. The transient response of the enclosure was of interest. All boundaries, except the ceiling, were assumed to be adiabatic. The results of the CFD simulations indicate good agreement with experimental centre-line plume temperatures near the ceiling; further away from the ceiling, agreement was not so good. Also, CFD simulations yielded good agreement with the experimental temperature measurements along the ceiling indicating that the “temperature jump across the draught curtain can be qualitatively reproduced by the CFD simulation.”

In the second part of their report Notarianni and Davis (1993) have simulated 40kW, 400kW and 32MW fires in a room measuring 38m long x 27m wide x 27m high with and without laminar forced ventilation. The authors provide no information as to the location of the fires nor any background to the CFD simulations.

In the case of forced ventilation, only the larger two fires possessed enough buoyancy for the fire plume to rise to the ceiling by the time heated air was being sucked through the ventilation outlet vents.

For fires without forced ventilation, the 400kW fire was used as a base-case. The results qualitatively indicate the progress of the fire plume throughout the room and demonstrates that circulation patterns are set up within the room

### **2.3.1.3 Davis et al. (1996)**

Davis et al. (1996) compare the results of fire experiments held in an aircraft hangar measuring 98m long x 74m wide x 15m (maximum) high with three different class of deterministic fire models:

1. Correlations for plume and ceiling jet temperature and velocity.



2. Zone models CFAST, FPETool, and LAVENT.

3. CFD models FLOW3D and NIST-LES (a large eddy simulation model).

Results for two different fire sizes: 500kW and 2.7MW, are compared for two cases where the fire is located in an area with and without draught curtains.

Regarding the CFD modelling, the computational grid was comprised of approximately 34k cells, even though only one quarter of the real-life volume was simulated due to symmetry. All boundaries were assumed to be adiabatic no-slip boundaries, except for the ceiling where heat conduction to the outside was accounted for. Radiative heat transfer was dealt with by assuming that 35% of the total heat release rate was radiated to the enclosure environment.

Regarding the large eddy simulation, in this type of CFD model, no turbulence model is used to simulate the sub-grid fluid motion. Instead, the large eddies are simulated directly and the sub-grid fluid motion suppressed (Karlsson, 1997). In this case the number of cells in the computational domain was increased to 885k.

In their comparison, Davis et al. (1996) compare experimental centre-line plume temperatures, radial temperatures from the plume centre, ceiling jet temperature profiles, ceiling jet velocity, draught curtain filling time, draught curtain spilling time, temperature difference across the draught curtain and smoke detector activation time with the deterministic fire models.

Considering their extensive results, Davis et al. (1996) concluded that the “performance of the CFD models in some comparisons is better than the zone models but in other comparisons no advantage was gained by using the CFD models”. Notwithstanding this conclusion, for the 500kW fire, the atrium model of FPETool over-predicted centre-line plume temperatures by 50% (FLOW3D predicted results within the experimental uncertainty, and NIST-LES over-predicted results by 45%). For the 2.7MW fire, the atrium model of FPETool under-predicted the centre-line plume temperatures by 300%; DETACT and NIST-LES were the only other models outside the experimental error with errors of  $\pm 25\%$ .

For the 500kW fire, the radial temperatures from the plume centre predicted by all models fall within the experimental error. For the 2.7MW fire, CFAST, FPETool, DETACT, LAVENT, and NIST-LES all fall outside the experimental error.

For the other comparisons, FLOW3D predicted results outside the experimental error for the ceiling jet velocity of the 2.7MW fire (-25%), and the draught curtain spilling time for both fire sizes (+50%).

#### **2.3.1.4 Gott et al. (1997)**

Gott et al. (1997) document several full-scale fire experiments held in two aircraft hangars, one in Hawaii measuring 97.8m long x 73.8m wide x 15m high and the other in Iceland measuring 73.8m long x 45.7m wide x 22m (maximum) high. Computer modelling is also briefly documented in the report; modelling was used to determine the experimental fire sizes, and to indicate particular locations within the enclosures that would require additional instrumentation.

The tests and modelling carried out on the Hawaiian enclosure has previously been reviewed in the document by Davis et al. (1996), therefore, it will not be discussed any further here.

The Iceland hangar was barrel-shaped, and as a consequence, the impact of this curved ceiling on smoke and heat flow is not easily established. Gott et al. (1997), using FLOW3D, simulate jet fuel fires with and without draught curtains in the hangar. Results of simulations for two fire sizes (32MW and 40MW) are included and show the temperature at the ceiling and the effect of a wind blowing into the hangar.

At the end of their report Gott et al. (1997) compare the ability of Heskestad's (Heskestad, 1995) plume correlation, DETACT (Alpert's ceiling jet correlation (Alpert, 1972)), and FPETool (Alpert and Ward's ceiling jet correlation (Alpert and Ward, 1983)) to predict the temperature at the ceiling as a function of fire size and wind effects.

For the closed door tests, the correlations over-predict for small fires, but as the fire size increases, the correlations substantially under-predict the ceiling temperature. The difference between the predictions and the experiments is less for the open door cases; however, the lower experimental ceiling temperatures are due to wind effects, i.e., factors unaccounted for in the models, therefore, this result is considered “favourable” by Gott et al. (1997).

Gott et al. (1997) forward three possible explanations for the poor performance of the correlations. In conclusion, Gott et al. (1997) argue:

- that the **fixed radiative fraction** of 30% assumed in the correlations is significantly more than is the case in the experiment, as the radiative fraction of a large pool fire drops due to the volume becoming optically thick. Therefore, the convective heat transfer is actually less in the experiment than assumed in the model which causes the over-predictions, and
- Gott et al. (1997) question the **validity of the plume correlations** with respect to the experimental setup (ceiling temperature measurements too close to the combustion zone) and to large fire sizes where a hot smoke layer develops rapidly.

Overall, FPETool (Alpert and Ward’s plume correlation) predicts the highest ceiling temperatures, and DETACT (Alpert plume correlation) predicts the lowest ceiling temperatures. This may be because of the conservatism built into the models as FPETool is concerned with predicting structural damage, while DETACT is concerned with detector activation.

### 2.3.2 Tunnel Fires

Initial CFD simulations of tunnel fires were carried out by Cox et al. (1985), where they applied JASMINE to simulating a 200 litre petrol pool fire in a tunnel measuring 390m long x 5m wide x 4m high. Results show good agreement with experimental results except near the fire source where the combined effects of ignoring radiative heat transfer, a coarse grid and a simple combustion model are thought to cause the errors in the simulations.

Perhaps the most high profile use of CFD techniques was in the post fire investigation of the Kings Cross underground fire (Simcox, et al., 1992). In this investigation, Harwell Laboratories were commissioned to simulate the flows that were caused by the fire in the underground subway complex; and particularly to investigate if there were any three-dimensional flow effects that might have influenced the fire spread.

In their simulation of the fire, the Harwell team utilised the standard  $k-\epsilon$  turbulence model with buoyancy corrections by Rodi (1980). Radiation heat transfer and combustion were not modelled, the fire source was modelled as a transient enthalpy source, and all external boundaries were treated as adiabatic. The spreading of the fire was approximated by the time varying source; Simcox et al. (1992) acknowledge the crudeness of this assumption.

The key result of the investigations was that the hot gases in the “buoyant plume” lay along the floor of an escalator leading from one of the platforms to the main ticket hall. This phenomena has become known in the fire engineering community as the “trench effect” and its occurrence was later confirmed by a series of scale experiments (Moodie and Jagger, 1992).

Recently, the most significant contribution regarding simulation of fires in tunnels is that of Woodburn and Britter (1996). Woodburn and Britter have carried out sensitivity studies of CFD simulations of a full scale experiment in a longitudinally ventilated tunnel, particularly investigating the results near the fire source and the area downstream of the fire.

Woodburn and Britter (1996) used FLOW3D to simulate the fires and find that near the fire source, the length of the upstream propagating smoke layer length is sensitive to the ventilation velocity, the ventilation velocity profile, the turbulence model used and the heat input rate. Downstream of the fire, the results of the simulations were most sensitive to natural convective heat transfer, radiative heat transfer and wall roughness. Other parameters investigated include the downstream boundary position, slope and turbulence model.

Regarding the sensitivity of the results near the fire source to the turbulence model, the authors investigated the differences between the standard  $k\sim\varepsilon$  turbulence model with and without buoyancy modifications by Rodi (1980). The use of the different turbulence models caused a significant change in the simulation results; the standard  $k\sim\varepsilon$  model caused the results to grossly under-predict the upstream propagation of the hot layer. The differences in the results predicted by the two turbulence models were much greater than the initial difference in the shear stress calculated by each model.

### 2.3.3 Other

Markatos and Cox (1984) have used JASMINE to simulate a fire in a L-shaped shopping mall complex. The fire was located within a shop measuring 4m long x 8m wide x 3m high, which is connected to a mall measuring 16m long x 6m wide x 3m high. Qualitative results were presented showing the effect of the inclusion of a smoke screen at the far end of the mall and of the transient smoke movement throughout the complex.

Simulation of transient fires in a hospital ward with ambient natural convection, using JASMINE, have been reported by Cox, et al. (1985), and Kumar, et al. (1985). The hospital ward measured 7.3m long x 7.9m wide x 2.7m high.

In all cases radiative heat transfer was ignored, combustion was modelled by the eddy breakup model and all boundaries were treated as no-slip and adiabatic. Numerical simulations showed that there was poor agreement with experimental results near the fire source, which improved with distance away from the source. As was the case with Cox et al.'s (1985) tunnel simulations, the poor results were blamed on ignoring radiative heat transfer, a coarse grid and a simple combustion model.

Miles and Cox (1996) have applied JASMINE to simulate the fire emissions from a warehouse measuring 70m long x 30m wide x 8m high. The effect of wind strength and direction was investigated. The warehouse had 16 vents, automatically opened by heat detectors, installed on its flat roof. The standard  $k-\epsilon$  turbulence model with buoyancy corrections by Rodi (1980) was used, combustion was modelled by the eddy breakup model and all boundaries were considered non-adiabatic. Radiative heat transfer was included in the simulations by using JASMINE's six flux radiation model. 88k cells were included in the computational grid.

The results of the simulations show:

1. It is possible to numerically simulate this scenario using CFD.

2. The quantity of fire emissions through the roof vents is not highly sensitive to the strength and direction of wind.
3. No significant difference is obtained in the transient simulation results by reducing the timestep from 1 second to  $< 1$  second.

## 2.4 Simulation of Fire Plumes

Initial investigations using PHONETICS concentrated on the study of “unbounded fire plumes” and specifically the turbulence-induced structures within the plume. Markatos et al. (1986) approach the problem numerically by simulating the turbulent diffusion flames as two interspersed fluids, one being the oxidant (air), and the other containing pyrolyzed fuel, products of combustion and entrained oxidant. Prandtl’s mixing-length model is used to evaluate the turbulent diffusion within each fluid, and simulations were run as steady-state. Combustion in the second fluid is accounted for by the eddy breakup combustion model.

Markatos et al. (1986) compare the performance of their model with the experiments of Cox and Chitty (1982), and mixture temperature and velocity are reported for five downstream locations. Comparison with experiments indicate that the model is qualitatively realistic, providing temperatures and velocities that fall within the experimental range.

As part of a larger project devoted to simulating the interaction of fire and sprinkler spray, Nam and Bill (1993) have used PHONETICS to simulate the flow field induced by pool heptane spray fires. The authors primarily concentrated on modifications to the standard  $k\sim\varepsilon$  turbulence model to include the effects of buoyancy generated turbulent kinetic energy. Results obtained from this modified turbulence model showed good agreement with experimental results for pool diameters between 0.7m and 1.2m, corresponding to heat release rates of 164kW and 295kW.

In the first example of the application of FLOW3D to simulating plumes, Sinai and Owens (1995) have simulated the flame geometry around a 20m kerosene pool fire subject to a cross-wind, and compared these results to experimental results. The predicted flame shape compares well with the experimental observations.

In their numerical simulations, Sinai and Owens (1995) use the  $k\sim\varepsilon$  turbulence model with buoyancy corrections (Rodi, 1980), and model combustion using the eddy break-up combustion model. The work investigates the influence of



pool shape, the bund and the level of ambient atmospheric turbulence on the geometry of the flame. No allowance has been made for radiative heat transfer in the current work, although a convective heat release rate equal to 75% of the total heat release rate was used in defining the fire source.

Sinai and Owens (1995) state that although good agreement is evident for a circular pool fire between the numerical simulations and the experiments, their work highlights the fact that there are significant difference in the aerodynamics of round and square pool fires. Finally, it is felt that numerical simulations were not handicapped by the deficiencies in the turbulence and combustion models for this class of problem, provided the analyst is aware of the deficiencies that are present in the technique, such as, applying the modified  $k\sim\varepsilon$  turbulence model to highly non-isotropic flows.

Figure 2.3 shows temperature contours at  $y = 5.5\text{m}$  for a square kerosene pool fire burning at  $11\text{kg/s}$ , by Sinai and Owens (1995).

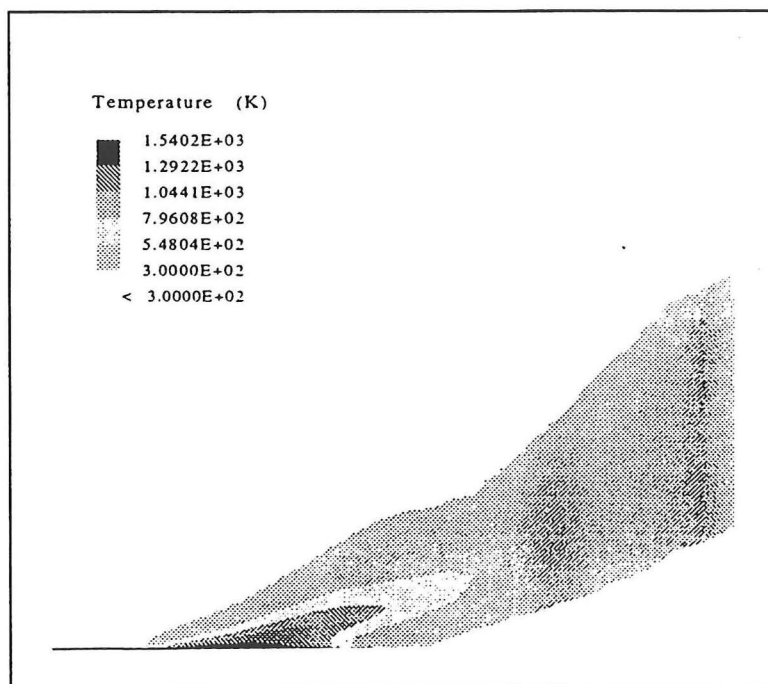


**Figure 2.3. Temperature contours at  $y = 5.5\text{m}$  for a square kerosene pool fire burning at  $11\text{kg/s}$  (Sinai and Owens, 1995).**

## **2.5 CFD in Consulting Engineering**

Waters (1985 and 1989) applied the Phonetics code to the simulation of fire-induced smoke movement in a large (300m long x 200m wide x 12m high) uncomparted enclosure. Waters approaches the problem from a design standpoint and considers that the generality of the CFD simulation approach to be superior to zone modelling approaches for such large enclosures.

## **2.6 Other**

A recent example of the application of CFD codes to fire engineering problems is the four year project being carried out by the National Institute of Standards and Technology in the United States, where FLOW3D is being used in a parametric study of fire detection (Davis et al., 1997). Preliminary results indicate that the use of CFD codes has the potential to greatly improve the technical basis for the siting of fire detectors, particularly in complex geometries.

To date in New Zealand, the only example of CFD use in fire engineering is Kardos's (1996) investigation of transient gravity currents.

## **2.7 The Future of CFD in Fire Engineering**

The use of CFD models in fire engineering will only increase with future developments of faster computers. While none of the researchers working in the field admit to being content with the current state of the art, it is evident that the solving algorithms are available and work must now continue on refining the imbedded sub-models such as radiative heat transfer, combustion, and turbulence (Bilger, 1994).

For experimental fire researchers, the emphasis will now turn to specifically designing experiments with sufficient instrumentation so that more extensive validation of CFD codes can be carried out.

## 2.8 Summary

Considering the CFD-related articles reviewed here, a number of key points may be summarised:

1. CFD codes have been applied to a large number of different cases, including domestic-sized enclosures, large enclosures, and plumes.
2. Numerical prediction of fires in domestic-sized enclosures and the NIST aircraft hangar experiments generally fall within the experimental error.
3. The  $k\sim\varepsilon$  turbulence model with buoyancy corrections by Rodi (1980) is the most commonly used turbulence model, however, further modifications to the  $k\sim\varepsilon$  model may be necessary to simulate plumes sufficiently.
4. Previously, the performance of the CFD codes near the fire source has been restricted by the crude assumptions made in dealing with radiative heat transfer, and combustion, although progress is being made in incorporating thermal radiation and combustion into the CFD codes.
5. Few examples of the use of CFD in consulting are available due to the large expense associated with the use of the techniques in a commercial environment.
6. The future for CFD is positive, especially given that faster computers will become available with time. Research will continue on the improvement of the imbedded sub-models contained in the CFD codes and on the development of experimental datasets suitable for CFD comparison/validation.



# 3 Full-Scale Fire Experiments

The purpose of this chapter is to briefly introduce one set of full-scale fire experiment that will be compared to the CFD simulation results. The fire experiments conducted by the Building Research Association of New Zealand in their industrial-sized enclosure (Collier, 1997) will be qualitatively compared to the CFD simulation results.

The fire experiments by Dembsey et al. (1995) in the domestic-sized enclosure will not be compared with the results of the CFD simulations because of a different fuel height was used in the CFD simulations from that of the full-scale experiments.

## 3.1 Collier (1997)

Three full-scale fire experiments were conducted in a test enclosure measuring 41m x 11m x 11m (Collier, 1997) by the Building Research Association of New Zealand. The aim of these experiments was to gather a data set suitable for comparison with CFD simulation results.

Two different fire sizes were used for these experiments: 300 and 600kW and two thermocouple trees were fitted inside the enclosure - each with 8 thermocouples spaced vertically at approximately 1.25m intervals.

As the fire experiments progressed, a uniform interface was visible along the length of the enclosure. This interface descended in height as each experiment progressed (Collier, 1997).

### **3.1.1 Issues Arising**

There a number of experimental issues that need to be considered before any comparisons are made of the results form these tests to the CFD results, namely:

1. The unsteady nature of the heat output from the fire source.
2. The experimental method in general

Firstly, the experimental fire source were hydrocarbon pool fires. These fires resulted in an unsteady release of heat into the enclosure during the test.

Secondly, Collier (1997) states that the pre-ignition ambient conditions were “confused by solar heating of the air apace”. In an attempt to equalise temperatures over the height of the enclosure, ceiling extraction fans were turned on for a time period of between 5 and 10 minutes prior to ignition. This action is likely to have caused large-scale recirculation of the ambient air that would have disturbed the smoke flow throughout the enclosure once the fire was ignited.

Also regarding the experimental method, the test facility contained large amounts of equipment at the time of the tests (test furnaces, etc.) which, in addition to displacing smoke, also introduce local disturbances to the smoke flow throughout the enclosure.

By comparison, the CFD simulations used a steady heat release rate into the enclosure. The ambient conditions of the air inside the enclosure was such that it was still and had a uniform temperature distribution with height. Also, the enclosure did not have any other objects placed within that could disturb the smoke flow.

### **3.1.2 Conclusion**

In light of the above, it is likely that temperature comparisons between the CFD simulations for this enclosure will not be a true comparison and therefore have not been carried out. However, a qualitative comparison between the full-scale fire experiments and the CFD simulations, based on the visual observation of a layer interface during the experiments, is possible, and will be made.

# 4 Zone Modelling Simulations

This chapter details the zone modelling that was carried out as part of this project. The aims, methodology, and results of the exercise will be given, along with some theoretical background to the model used for the simulations.

In later sections of this report, the results of the zone modelling simulations will be compared with the results of the CFD modelling simulations for the same fire scenarios.

## 4.1 Aims

The following were aims of the zone modelling simulations:

1. Derive results for comparison with the CFD modelling, namely: enclosure temperature history, and interface height.

## 4.2 Theoretical Background to FAST

This section will cover some of the theoretical background to FAST version 3 beta 2 (Peacock et al., 1997). Quintiere (1989) provides an excellent theoretical presentation of compartment fire zone modelling in general.

### 4.2.1 Introduction

FAST version 3 beta 2 (Peacock et al., 1997) is the latest version of the CFAST (Peacock et al., 1993) family of zone model, developed by the National Institute of Standards and Technology in the United States. The main difference between FAST and previous versions of CFAST is that FAST has a graphical user interface; FAST contains the same theory and numerical solution methods as

previous versions of CFAST with some enhancements as outlined in the user's guide (Peacock et al., 1997).

#### 4.2.2 The Equation Set

All zone models solve a mixture of differential and algebraic equations for each zone or control volume. These equations are developed from conservation laws of mass, energy and momentum, in addition to the ideal gas law and relationships defining density (Peacock et al., 1993).

Dividing the fire enclosure in to two zones (see figure 4.1), one a relatively hot upper layer, including the fire plume, and another relatively cooler layer, is the first, most fundamental assumption made in developing the theory for a two zone model. It is assumed that properties such as temperature, density and chemical species take constant values throughout each zone. Also, the fire plume is assumed to be buoyancy-driven (i.e., Froude number much less than 1) and to have negligible volume compared to the gas layer (Quintiere, 1989). Two further assumptions reduce the computational expense of solving the equations, namely:

- Momentum is ignored within an enclosure<sup>4</sup>.
- Pressure is taken as approximately uniform within the enclosure.

The second assumption is applied in the conservation equations and Peacock et al. (1993) argue that pressure differences over the height of the enclosure will always be insignificant compared to the atmospheric pressure.

All other assumptions made in the development of a zone model are covered by Quintiere (1989).

---

<sup>4</sup> At vents such as doors and windows, the Bernoulli equation is used to calculate the flow. The pressure within the enclosure is assumed to be hydrostatic; the pressure difference between the inside and outside of the enclosure is what "drives" the flow.

Momentum is also implicitly included in the conservation of energy equation in the fire plume.



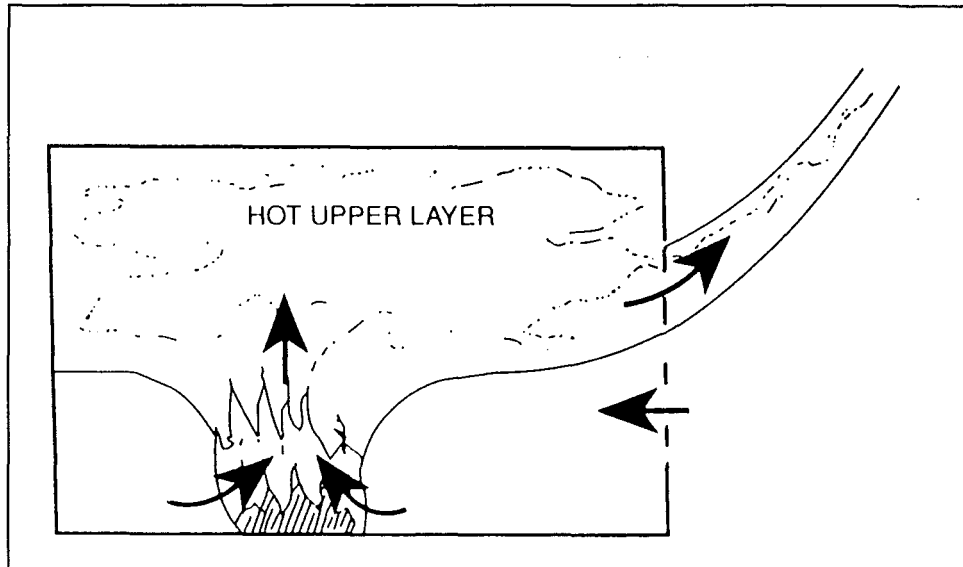


**Figure 4.1. The two zone model with no mass exchange between the zones except the plume (Walton, 1995).**

By dividing the enclosure into two zones, mass, internal energy, density, temperature and volume can be defined for each zone. By applying the first law of thermodynamics (internal energy + work = enthalpy) to a zone, differential equations for the time derivative of pressure, layer volume, temperature and density can be derived. In total, FAST solves four different differential equations for each zone, namely: the time derivative of pressure, zone volume, upper layer temperature, and lower layer temperature. The initial pressure and temperature of the system must be defined.

### **4.2.3 Empirical Relationships**

The form of the differential equations expressing the conservation laws for each zone is such that the physical phenomena occurring during a fire are treated as source terms. These source terms may be quantities such as the fuel mass loss rate, the mass flux from the fire into the upper layer, or the quantity of mass entrained from one layer into another layer in the case of a vent flow (Cox, 1995b). Thus, in order to close the equation set, values must be available for the particular source terms.

Due to the simplified nature of the zone model formulation, it is not possible to solve for the source terms from a first principle basis. Therefore, it is necessary for

zone models to rely on empirically-derived correlations to describe these phenomena where a first principles theoretical-type approach is not possible or computationally efficient. Such empirical correlations are derived from dimensional analysis of experimental data (i.e., “curve fitting”).

Due to the fact that empirically-derived correlations are present in zone models, there are cases where the empirical correlations are not applicable. The limits of applicability arise because it is not possible to derive empirical correlations that will cover the complete range of possible cases. Thus, the range of applicability of the correlations is then transferred to the zone models that incorporate the them.

Currently, there are three types of physical phenomena that are missing from zone models. These phenomena are all governed by the conservation of momentum which is ignored within the zone model formulation. These three features are (Quintiere, 1995):

- Vent flames,
- transient smoke flows in corridors, and
- shaft flows.

Due to the absence of the above phenomena from zone models, it would not be appropriate for a zone model to be applied to cases where these phenomena might be significant.

### 4.3 Method

The effects of three different sized fires were simulated for each of the two different sized enclosures using FAST version 3.0 beta 2 (Peacock et al., 1997). The geometry for each enclosure is listed in table 4.1:

**Table 4.1. Enclosure geometry for zone modelling simulations.**

Enclosure	Enclosure Geometry			Vent Geometry	
	Width (m)	Depth (m)	Height (m)	Height (m)	Width (m)
1	2.5	3.7	2.5	2.0	0.76
2	41	11	11	11	0.30 <sup>5</sup>

The fire sizes and location within the enclosure for all simulations are listed in table 4.2. Enclosure 1 was chosen to be simulated because the experiments by Dembsey et al. (1995) were considered to represent a high quality experimental data set. Enclosure 2 was chosen because the sponsors of this project, the Building Research Association of New Zealand, had conducted full-scale fire experiments in this sized enclosure. The heat release rates for each enclosure were as per the particular set of full-scale experiments.

---

<sup>5</sup> The vent width corresponds to a leakage area ratio of approximately 1.5 times the “very loose” construction leakage area defined by Klote and Milke (1992).

**Table 4.2. Fire sizes and location for each simulation.**

<b>Enclosure</b>	<b>Reference</b>	<b>Fire size (kW)</b>	<b>Fire location</b>
1	1A	330	Centre
	1B	430	Centre
	1C	500	Centre
2	2A	300	4m from end wall
	2B	300	Centre
	2C	600	4m from end wall

### **4.3.1 Other modelling notes**

#### **4.3.1.1 Fuel Type, and Location**

For enclosure 1, the fuel was taken to be propane gas, having a heat of combustion equal to 46.36MJ/kg (DiNenno, 1995), which is consistent with the experiments of Dembsey et al. (1995). In enclosures 1, the fuel was placed in the centre of the enclosure (see table 4.2).

For enclosure 2, the fuel used in the experiments by Collier (1997) was Pegasol A, a liquid alkane. Therefore, for consistency, the fuel was assumed to be n-Heptane, having a heat of combustion equal to 44.56MJ/kg (DiNenno, 1995). Fuel was placed in two different locations for the three different tests; 300kW fire at the centre of the enclosure, and 300 and 600kW fires on the enclosure's centre line, 4m from one end.

The height of the fire source was taken as being at floor level for all of the enclosures, i.e., the fuel surface is at the floor level.

In all cases, a radiative fraction of 35% of the total heat release rate was assumed and the fire was defined as being "constrained" by the amount of oxygen available for combustion (FAST keyword LFBT in table 4.3).

#### **4.3.1.2 Thermal Boundaries**

All boundary walls, floors and ceiling elements were assumed to be adiabatic.

**Table 4.3. Example FAST input file keywords and values (for simulation 1A).**

<b>Keyword</b>	<b>Description</b>	<b>Input values</b>
VERSN	FAST version number	3
TIMES	Time step control of output	1800, 0, 10, 10, 0
TAMB	Ambient conditions inside	290, 101300, 0
EAMB	External ambient conditions	300, 101300, 0
HI/F	Absolute height of the compartment floor	0
WIDTH	Width of the compartment	2.5
DEPTH	Depth of the compartment	3.7
HEIGHT	Height of the compartment	2.5
CEIL	Name of ceiling descriptor	OFF
WALLS	Name of walls descriptor	OFF
FLOOR	Name of floor descriptor	OFF
HVENT	Specify horizontal vent	1,2, 1, 0.76, 2.0, 0,0
CVENT	Opening/closing parameter	1, 2, 1, 1.0, 1.0, 1.0
CHEMI	Miscellaneous chemical kinetics	0, 0, 10, 4.63E+7, 290, 400, 0.35
LFBO	Compartment of fire origin	1
LFBT	Type of fire	2
FPOS	Fire position	-1.25, -1.75, 0
FTIME	Points of time on fire timeline	1.0, 1800
FMASS	Pyrolysis rate	0, 0.00712743, 0.00712743
FQDOT	Heat release rate	0, 330000, 330000
CJET	Ceiling jet	OFF
HCR	Hydrogen/carbon fuel mass ratio	0, 0, 0

## 4.4 Results

Upper layer gas temperatures (figures 4.2, and 4.4) and interface height (figures 4.3, and 4.5) derived from the zone modelling will be presented for each case.

### 4.4.1 Enclosure 1

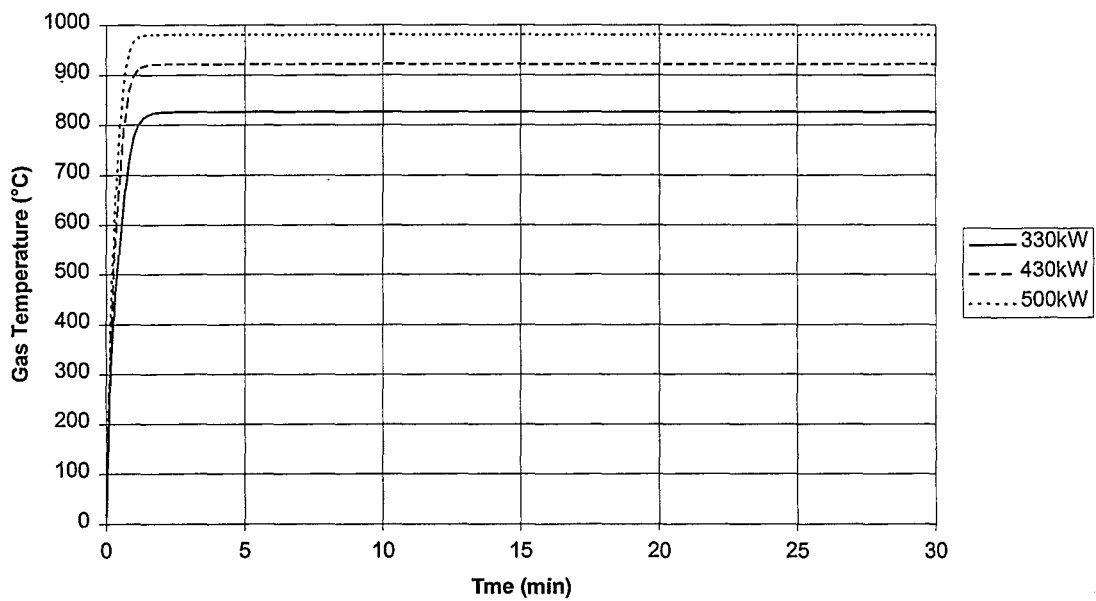


Figure 4.2. Upper layer gas temperature history for enclosure 1.

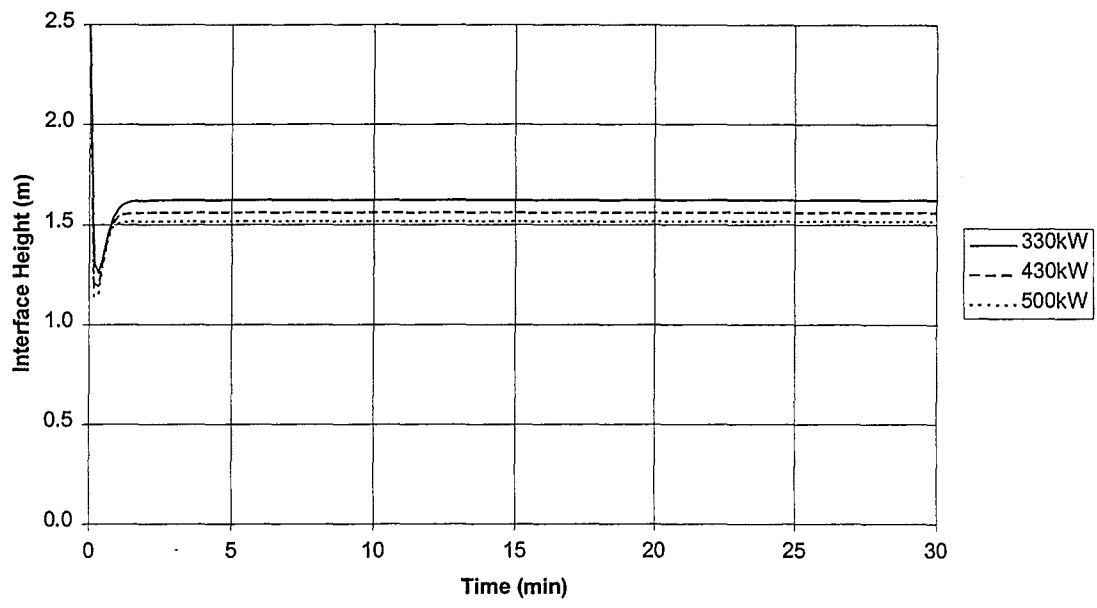


Figure 4.3. Interface height history for enclosure 1.



## 4.4.2 Enclosure 2

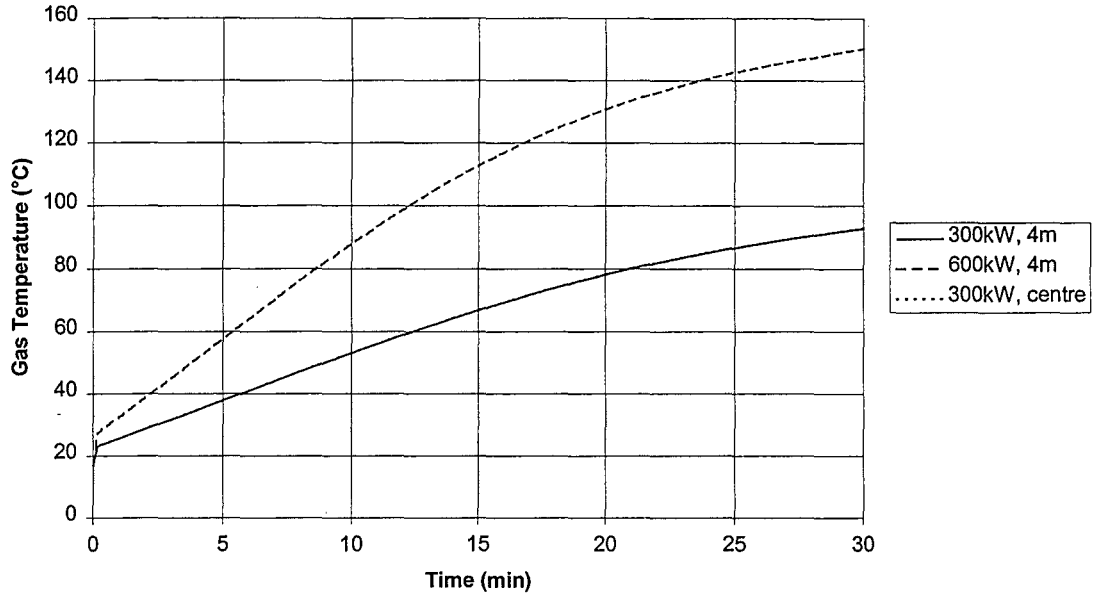


Figure 4.4. Upper layer gas temperature history for enclosure 2.

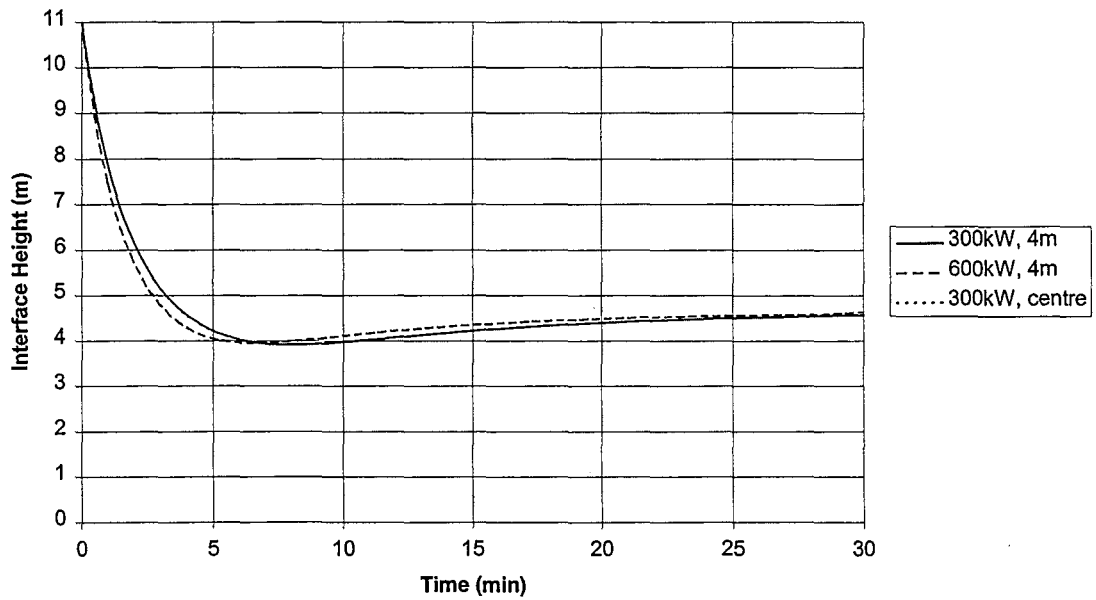


Figure 4.5. Interface height history for enclosure 2.

### 4.4.3 Summary

Table 4.4. Summary of steady-state upper layer gas temperatures for each enclosure.

Reference	Steady-state upper layer gas temperature (° Celsius)	Time to reach steady-state (minutes)
1A	826	2.3
1B	921	1.8
1C	980	1.7
2A	93	*
2C	93	*
2B	150	*

\* The upper layer gas temperatures for these cases did not reach a steady-state, therefore, the upper layer gas temperature at 30 minutes is reported.

## **4.5 Discussion**

The results (particularly upper layer gas temperature history) for each enclosure will be briefly commented on. Following this, more general comments will be made regarding the outcomes of the zone modelling simulations.

### **4.5.1 Enclosure 1**

Upper layer gas temperatures for enclosure 1 are between approximately 800 and 1000°C (see table 4.4); well in excess of the 600°C upper layer gas temperature normally associated with the onset of flashover (Walton and Thomas, 1995). From table 4.4, the upper layer gas temperatures reach a steady-state very quickly (within 3 minutes) for all fire sizes.

### **4.5.2 Enclosure 2**

Upper layer gas temperatures do not reach a steady-state within the 30 minute fire duration. However, referring to figure 4.5, we see that the interface heights appear to be at a steady-state for all cases of approximately 4 metres.

The different location for the 300kW fires has no effect on the upper layer gas temperature history. This is because the fire location, for a fixed vertical elevation, within an enclosure has no bearing on the upper layer gas temperature in a zone model.

### **4.5.3 General**

Considering the upper layer gas temperature histories for enclosure 1, the ability of a zone model to simulate fires in enclosures with adiabatic boundary conditions is questioned. The results for this enclosure show that very high upper layer gas temperatures are reported for relatively low heat release rates. The results from the full-scale fire experiments by Dembsey et al. (1995) show average upper layer temperatures for the 330, 430 and 500kW fires were 370, 462, and 505°C respectively, these results were far less than the zone model results.

Given that the fuel height was placed lower than Dembsey et al.'s (1995) full-scale experiments, and assuming that the adiabatic boundary assumption in the zone model was valid, the zone model temperatures should be less than the experimental results because of the increased entrainment length available for cooling of the fire plume. The boundaries used in the full-scale experiments by Dembsey et al. (1995) were constructed of combinations of ceramic fibreboard, gypsum wallboard, and plywood in an attempt to approximate adiabatic behaviour.

Computer run times were of the order of 3 to 5 minutes to simulate these cases using FAST (Peacock et al., 1997).

# 5 SOFIE - Simulation of Fires in Enclosures

The purpose of this chapter is to introduce the CFD model used throughout the course of this project - SOFIE version 2.06 (Welch and Rubini, 1996).

SOFIE, an acronym for “simulation of fires in enclosures” is a fire-specific CFD code developed through a coordinated collaboration between VTT (Finland), SP Boras (Sweden), FRS (United Kingdom), CSTB (France), Lund University (Sweden), Cranfield University (United Kingdom), HSE (United Kingdom), and the Home Office (United Kingdom) (Moss and Rubini, 1997b). Cranfield University, United Kingdom is primarily responsible for planning SOFIE’s development.

An overview of all of the background theory to SOFIE will be provided that is relevant to the problem under consideration.

## 5.1 SOFIE Structure

SOFIE is a console (text only), command-oriented fire-specific CFD software package that may be run interactively by entering commands and data at the command-line prompt, or by running sets of commands stored in script files. A script file is a file that may be created in a text editor that contains the commands that would otherwise be typed in at the command line. The script file, once completed, may be then executed within SOFIE.

Figure 5.1 shows the top level of SOFIE’s command interface. To move to the file level, one would type file.

```
<Menu>: Sofie: Available items are :-  
  
file      setup    run      print    control  quit     end
```

**Figure 5.1. The top level of SOFIE's command interface.**

During a simulation, SOFIE is required to “read in” material and fuel data, depending on the nature of the problem being simulated. The three files that contain this data are: Density.coe, Conductivity.coe, and SpecificHeat.coe. These files contain a large amount of data and act as databases of information. Additional data may be added to them if required, e.g., to define the material properties of a specific boundary type that is not included in the databases.

During a simulation, SOFIE creates data for each solved variable at each time step. This data is saved in the respective problem directory. However, before the data can be viewed with a separate post-processing software package, the unformatted ascii data that SOFIE creates must be specifically exported in a format that the post-processor will accept. For the purpose of this project, the post-processor used was Fieldview for Windows, a commercially available post-processor developed by Intelligent Light, United States of America.

Figure 5.2 shows graphically the general structure of SOFIE.

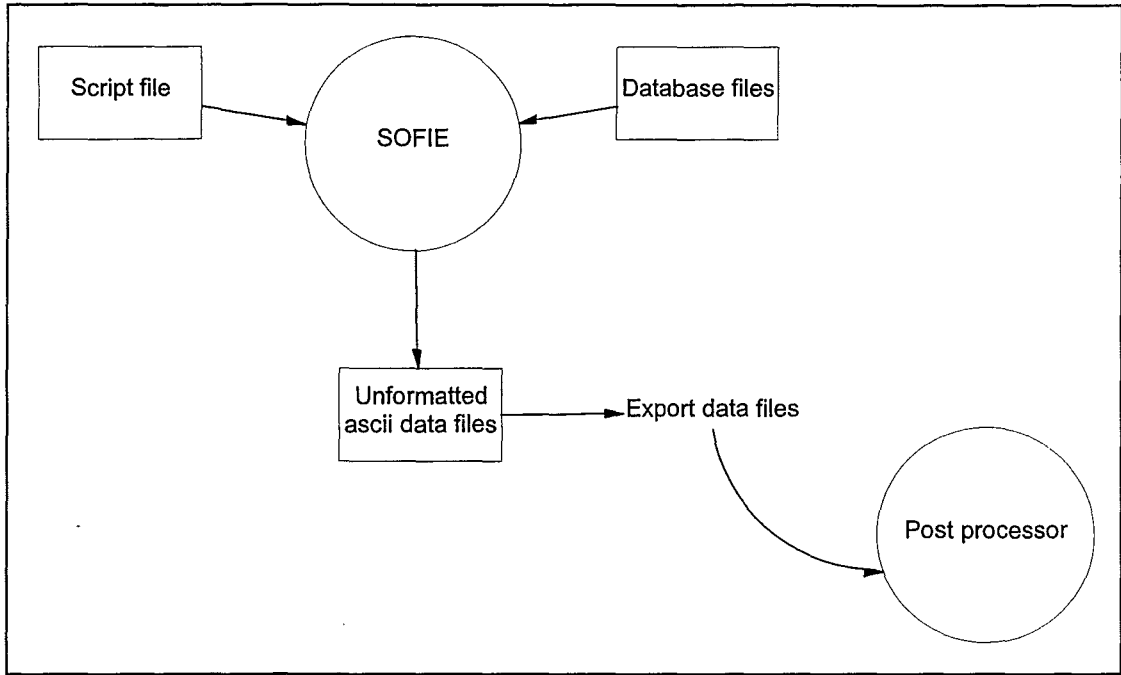


**Figure 5.2. Graphical representation of the elements of the SOFIE CFD package system.**

## 5.2 Governing Equations of Fluid Flow

The purpose of this section is to give an introduction to the conservation equations, excluding the turbulence equations, that SOFIE solves simultaneously throughout the domain during a CFD simulation. The relevant equations will be presented and explained without proof, the aim being to develop familiarity with the equations.

General reference has been made to the work of Hinze (1957), Patankar (1980), Hunt (1995) and Cox (1995a); further in-depth development is available from these sources, particularly Hinze (1957).

### 5.2.1 Conservation of Mass Equation

The general conservation of mass equation states that the rate of mass storage within a given control volume, due to density changes, is balanced by the net rate of inflow, by convection, of mass across the control volume boundaries. In the case of a steady flow situation, the conservation of mass equation states that what flows into the control volume must flow out.

The conservation of mass equation in Cartesian-tensor notation is written as:

$$\frac{\partial \rho}{\partial t} + \frac{\partial}{\partial x_j}(\rho u_j) = 0 \quad (5.1)$$

### 5.2.2 Conservation of Momentum Equation

The Navier-Stokes equations describe the conservation of momentum for an element of fluid. A derivation is provided in Hinze (1957) and is developed from Newton's second law of motion that states that the sum of the forces acting on a fluid volume is equal to its rate of change of momentum. The Navier-Stokes equations can be written as:

$$\frac{\partial}{\partial t}(\rho u_i) + \frac{\partial}{\partial x_j}(\rho u_j u_i) = -\frac{\partial p}{\partial x_i} + \frac{\partial \tau_{ij}}{\partial x_j} + g_i \quad (5.2)$$



The left hand side of equation 5.2 represents the local rate of change of momentum for a small volume element travelling with the fluid. The right hand side represent the forces acting on the small volume element; including surface force terms (the first two) acting on the fluid within the control volume and a volumetric body force term associated with forces acting outside the control volume. In fires, the body force term is the most important as it represents the influence of buoyancy in the system.

Assuming Newtonian fluid behaviour, the viscous stress tensor is given by:

$$\tau_{ij} = \mu \left( \frac{\partial u_i}{\partial x_j} + \frac{\partial u_j}{\partial x_i} \right) - \frac{2}{3} \mu \frac{\partial u_k}{\partial x_k} \delta_{ij} \quad (5.3)$$

The viscous stress tensor is the stress acting on the surface of an element perpendicular to  $i$  and in the direction of  $j$  and it causes deformation in the fluid elements. It is possible to relate the stresses  $\tau_{ij}$  to the spatial variations in  $\partial u_i / \partial x_j$  of the velocity field  $u_j$  (Hinze, 1957).

### 5.2.3 Conservation of Energy Equation

The energy equation in its most general form contains a large number of variables, most of which are application specific. The equation itself can be written in a variety of ways depending on what variable is chosen as the primary variable.

Quoting from Cox (1995a), the conservation of energy equation describes “the balance between the rate of energy accumulation within the control volume, including both internal and kinetic energy, and the energy influx due to convection, conduction, radiation, the interdiffusion of species together with the net rate of work done on the gases by viscous stresses and body forces.”

For fires and other applications where velocities are usually low, a number of simplifications can be made:

- The viscous dissipation of enthalpy is neglected,
- the mixture kinetic energy is considered small compared to mixture enthalpy,

- mechanical work due to buoyancy forces is considered small compared to the thermal energy exchange,
- heat fluxes caused by concentration gradients (the Dufour effect) are neglected, and
- a Lewis number of unity is assumed.

The conservation of energy equation, in terms of the mixture static enthalpy, can be written as:

$$\frac{\partial}{\partial t}(\rho h) + \frac{\partial}{\partial x_j}(\rho u_j h) = \frac{\partial p}{\partial t} + \frac{\partial}{\partial x_j} \left[ \frac{k}{c_p} \frac{\partial h}{\partial x_j} - \dot{q}_j^R \right] \quad (5.4)$$

The mixture static enthalpy,  $h = c_p T + \sum_{\alpha} Y_{\alpha} H_{\alpha}$  and  $H_{\alpha}$  is the heat of reaction for the species  $\alpha$ . For a fluid mixture at constant pressure, the specific heat is given by:

$$c_p = \sum_{\alpha} Y_{\alpha} c_{p,\alpha} \quad (5.5)$$

#### 5.2.4 Chemical Species Conservation

In the presence of a velocity field,  $u_j$ , the conservation of the mass fraction,  $Y$ , of a chemical species,  $\alpha$ , is given by:

$$\frac{\partial}{\partial t}(\rho Y_{\alpha}) + \frac{\partial}{\partial x_j}(\rho u_j Y_{\alpha}) = \frac{\partial}{\partial x_j} \left( \rho D \frac{\partial Y_{\alpha}}{\partial x_j} \right) + S_{\alpha} \quad (5.6)$$

The source term,  $S_{\alpha}$ , is caused by chemical reactions. Thus,  $S_{\alpha}$  can be positive or negative depending on whether the reaction produces or destroys chemical species. In the case of non-reacting species,  $S_{\alpha}$  would be zero.

$D$  is a diffusion coefficient for the species  $\alpha$  and is given by Fick's law of diffusion, where  $J_{\alpha}$  is the diffusion flux:

$$J_{\alpha} = -D \left( \frac{\partial Y_{\alpha}}{\partial x_j} \right) \quad (5.7)$$

Equation 5.6 states that the time rate of storage of the chemical species,  $\alpha$ , is balanced by the net rate of flow of  $\alpha$  into the control volume due to convection and diffusion in addition to the production (or destruction) of  $\alpha$  within the control volume.

### 5.2.5 General Conservation Equation

With reference to equations 5.1, 5.2, 5.4, and 5.6, it is clear that all the dependant variables presented here obey the same sort of general conservation principle. Therefore, it is convenient to express the time-averaged dependant variable as  $\phi$  and write one general differential equation:

$$\underbrace{\frac{\partial}{\partial t}(\rho\phi)}_{\text{unsteady}} + \underbrace{\frac{\partial}{\partial x_j}(\rho u_j \phi)}_{\text{convection}} = \underbrace{\frac{\partial}{\partial x_j} \left( \Gamma_\phi \frac{\partial \phi}{\partial x_j} \right)}_{\text{diffusion}} + \underbrace{S_\phi}_{\text{source}} \quad (5.8)$$

The dependant variable  $\phi$  may stand for a variety of different quantities, such as mass fraction of chemical species  $Y_\alpha$ , temperature, components of velocity, turbulent kinetic energy and so on. Table 5.1 lists what values of exchange coefficient and source term take on for different transport variables.

The density appearing in equation 5.8 above can be related to temperature (or other variables) via an equation of state:

$$p = p(\rho, T) \quad (5.9)$$

For an ideal gas mixture:

$$p = \rho R_o T \sum_\alpha \frac{Y_\alpha}{M_\alpha} \quad (5.10)$$

where  $R$  is the gas constant specific to the mixture:

$$R = R_o \sum_\alpha \frac{Y_\alpha}{M_\alpha} \quad (5.11)$$

**Table 5.1. Effective exchange coefficients and source terms in generic transport equation for  $\phi$  (reproduced from Cox (1995b)).**

Transport of	$\phi$	$\Gamma_\phi$	$S_\phi$
Mass	1	0	0
Momentum	$u_i$	$\mu_{eff}$	$-\frac{\partial p}{\partial x_i} + \frac{\partial}{\partial x_j} \left( \mu_{eff} \frac{\partial u_j}{\partial x_i} \right) + g_i$
Enthalpy	$h$	$\frac{\mu_{eff}}{\sigma_h}$	$\frac{\partial p}{\partial t} + S_{h,rad}$
Turbulent kinetic energy	$k$	$\frac{\mu_{eff}}{\sigma_k}$	$G_K + G_B + \rho\varepsilon$
Rate of dissipation of turbulent kinetic energy	$\varepsilon$	$\frac{\mu_{eff}}{\sigma_\varepsilon}$	$\frac{\varepsilon}{k} \left[ (G_K + G_B) (1 + C_3 R_f) C_1 - C_2 \rho \varepsilon \right]$
Mixture fraction	$f$	$\frac{\mu_{eff}}{\sigma_f}$	0
Mixture fraction fluctuations	$\overline{f'^2}$	$\frac{\mu_{eff}}{\sigma_{f'^2}}$	$C_{g1} \mu_{eff} \left( \frac{\partial f}{\partial x_i} \right)^2 - C_{g2} \rho \frac{\varepsilon}{k} \overline{f'^2}$
Fuel mass fraction	$Y_f$	$\frac{\mu_{eff}}{\sigma_Y}$	$S_f$

where  $G_K = \mu_t \left( \frac{\partial u_i}{\partial x_j} + \frac{\partial u_j}{\partial x_i} \right) \frac{\partial u_i}{\partial x_j}$

$$G_B = -\beta g \frac{\mu_t}{\sigma_t} \frac{\partial T}{\partial x_j}$$

$$\mu_{eff} = \mu + \mu_t$$

$$\mu_t = C_\mu \rho \frac{k^2}{\varepsilon}$$

and  $C_{g1} = 2.8$ ,  $C_{g2} = 2.0$ , and  $\sigma_t = \sigma_h = \sigma_f = \sigma_Y = \overline{\sigma_{f'^2}} = 0.7$ . All other constants are listed in section 5.3 and will be discussed in relation to turbulence modelling.

## 5.3 Physical Models

SOFIE contains three specific physical models:

- $k\sim\varepsilon$  turbulence model,
- eddy breakup combustion model, and
- radiative heat transfer model.

These physical models will be detailed in this section.

### 5.3.1 Turbulence Modelling

SOFIE incorporates the industry-standard (Woodburn, 1995) two equation  $k\sim\varepsilon$  turbulence model.

#### 5.3.1.1 General

A turbulent flow can be described as one that is in a random (chaotic) and unstable state. At a micro-scale, the flow contains many vortices of different sizes and intensities, while at the macro-scale the flow continues to be controlled by its environment. Turbulence is initiated by a disturbance that causes instability that continues to be amplified as time increases. The Reynolds number is a type of stability parameter and represents the ratio of inertial forces to viscous forces; turbulent flows are classified by large Reynolds number. The mathematical details of the transition from laminar flow to turbulent flow is poorly understood (Tennekes and Lumley, 1972).

Turbulence causes increased rates of momentum, heat and mass transfer in the flow; this is referred to as the diffusivity of turbulence (Tennekes and Lumley, 1972).

Turbulent flows are always dissipative. This is explained by considering an element of fluid- viscous stress forces perform work on the element which causes deformation and an increase in internal energy. These energy losses must be made up

with additional turbulent kinetic energy or else the turbulence will decay. In the case of fire, the energy is provided by the fire source in the form of buoyancy forces.

### 5.3.1.2 The Requirement for a Turbulence Model

Time-averaging of the Navier-Stokes equations presented in section 5.2, introduces unknown relationships between fluctuating velocities, and between velocity and scalar functions. A turbulence model is required to solve for these unknowns because turbulence occurs on a much smaller length scale than the grid scale used in a typical CFD simulation, thus preventing their direct solution. Turbulence models solve for these variables using differential equations for the turbulence variables.

The version of the  $k\sim\varepsilon^6$  turbulence model presented here is not the only turbulence model available. There exist a large number of different “one equation”, “two equation” and more complicated turbulence models that can be used to describe turbulent flow. Of these other models, the “Reynolds-stress” models (e.g., Chou, 1945) seem to be the only type of turbulence models that perform better than the  $k\sim\varepsilon$  “two equation” model (Launder and Spalding, 1974). This type of model, however, is significantly more complex in nature (requiring the solution of between 9 and 17 differential equations (Launder and Spalding, 1972)) and is, therefore, not preferred in practice.

### 5.3.1.3 The Standard $k\sim\varepsilon$ Turbulence Model

The  $k\sim\varepsilon$  turbulence model is a robust and simple model that gives good results for free shear flows. The deficiencies of the model occur when effects such as strong streamline curvature, or body forces such as rotation or buoyancy, act on the fluid (Woodburn, 1995). The  $k\sim\varepsilon$  turbulence model detailed here is restricted to high-

---

<sup>6</sup> The  $k\sim\varepsilon$  turbulence model is attributed to Jones and Launder (1972), however, the model is so universally known and used that the reference to Jones and Launder is usually dropped.

Reynolds number flows and is not applicable to the viscous sub-layer near walls (Rodi, 1980).

The  $k\text{-}\varepsilon$  model is an eddy viscosity model, the basis for which, quoting Kumar (1983) is “that the turbulent eddies are thought of as lumps of fluid, which, like molecules, collide and exchange momentum, obeying the kinetic theory of gases.” Therefore, turbulent stresses are assumed to be proportional to the mean velocity gradients. Thus, similar to the viscous stress tensor (equation 5.3), the Reynolds (turbulent) stresses are modelled according to:

$$-\overline{u'_i u'_j} = \nu_t \left( \frac{\partial \bar{u}_i}{\partial x_j} + \frac{\partial \bar{u}_j}{\partial x_i} \right) - \frac{2}{3} k \delta_{ij} \quad (5.12)$$

Note that  $\nu_t$  is referred to as the turbulent or eddy viscosity which unlike the kinematic viscosity,  $\mu$ , is not a fluid property; the turbulent viscosity is a function of the local state of the turbulence and varies significantly between locations within the flow field (Kumar, 1983). The turbulence is assumed to be isotropic. The turbulent viscosity,  $\nu_t$ , is given by:

$$\nu_t = \frac{\mu_t}{\rho} = C_\mu k^{1/2} l \quad (5.13)$$

where  $l$  is a characteristic mixing length of the flow and  $C_\mu$  is an empirically-derived constant. Turbulent kinetic energy,  $k$ , is given by:

$$k = \frac{\overline{u'_i u'_j}}{2} \quad (5.14)$$

The model is completed by two differential equations for  $k$  and  $\varepsilon$ :

$$\frac{\partial}{\partial t}(\bar{\rho}k) + \bar{u}_i \frac{\partial}{\partial x_i}(\bar{\rho}k) = - \frac{\partial}{\partial x_i} \left[ \left( \frac{\mu_t}{\sigma_k} + \mu \right) \frac{\partial k}{\partial x_i} \right] - \underbrace{\mu_t \left( \frac{\partial \bar{u}_i}{\partial x_j} + \frac{\partial \bar{u}_j}{\partial x_i} \right) \frac{\partial \bar{u}_i}{\partial x_j}}_P - \underbrace{\beta g \frac{\mu_t}{\sigma_k} \frac{\partial \bar{T}}{\partial x_i}}_G - \rho \varepsilon \quad (5.15)$$

where the right hand side terms bracketed by P and G represent the turbulence production terms due to shear and buoyancy respectively. The G term is a modification to the standard form of the  $k\text{-}\varepsilon$  turbulence model proposed by Rodi

(1980) and is an attempt to improve the performance of the standard  $k\sim\varepsilon$  for buoyant flows. This is how the  $k\sim\varepsilon$  turbulence model is modified for buoyancy in SOFIE (Welch and Rubini, 1996).

$\beta$  is given by:

$$\beta = -\frac{1}{\rho} \left( \frac{\partial \bar{\rho}}{\partial T} \right)_p \quad (5.16)$$

The differential equation for  $\varepsilon$  is written as:

$$\underbrace{\frac{\partial}{\partial t}(\bar{\rho\varepsilon})}_{\text{derivative}} + \underbrace{\bar{u}_i \frac{\partial}{\partial x_i}(\bar{\rho\varepsilon})}_{\text{convection}} = - \underbrace{\frac{\partial}{\partial x_i} \left[ \left( \frac{\mu_i}{\sigma_\varepsilon} + \mu \right) \frac{\partial \varepsilon}{\partial x_i} \right]}_{\text{diffusion}} + \underbrace{C_1 \frac{\varepsilon}{k} (G_K + G_B) - C_2 \bar{\rho} \frac{\varepsilon^2}{k}}_{\text{production-destruction}} \quad (5.17)$$

where  $C_1$ ,  $C_2$ , and  $\sigma_\varepsilon$  are all empirically-derived constants (see table 5.2) and  $G_K$  and  $G_B$  are shear and buoyancy source terms respectively.

**Table 5.2. Universal constants for the standard  $k\sim\varepsilon$  turbulence model (Rodi, 1980).**

$C_\mu$	$C_1$	$C_2$	$C_3$	$\sigma_k$	$\sigma_\varepsilon$
0.09	1.44	1.92	-	1.0	1.3

Some formulations of the  $k$ -equation (equation 5.15) include a  $C_3 R_f$  term in the production-destruction term, where  $R_f$  is the Richardson number  $= -G_B/G_K$  and  $C_3$  is an empirically derived constant (e.g., Cox, 1995b). The inclusion of the  $C_3 R_f$  term is to account for buoyancy effects on the production (or destruction) of turbulence; the constant  $C_3$  takes a value of unity for horizontal layers and zero in vertical shear layers (Cox, 1995b). SOFIE, however, does not include the Richardson number term because it is not clearly defined for flows where both plumes and stratified layers may exist (Rubini, pers. comm.).



### 5.3.2 Eddy Breakup Combustion Model

SOFIE models combustion by the standard form of the eddy breakup combustion model with no Arrhenius terms included (Magnussen and Hjertager, 1976). The model assumes that the rate of combustion is controlled by the minimum of the rate at which oxidant or fuel arrives at the combustion site by turbulent mixing of the fluid.

The eddy breakup combustion model assumes a single, one step combustion reaction:



where  $F$ ,  $O$  and  $P$  refer to the masses of fuel, oxidant and products.

The rate of combustion is then defined as (Cox, 1995b):

$$S_f = -C\rho \frac{\varepsilon}{k} \min \left[ Y_f, \frac{Y_o}{s}, Y_f Y_o B \exp\left(\frac{-E}{RT}\right) \right] \quad (5.19)$$

where  $s$  is the stoichiometric oxidiser/fuel ratio, and  $Y_f$ ,  $Y_o$ , and  $Y_p$  are the mass fractions of fuel, oxidant and products respectively, and  $C$  is a constant defined as:

$$C = 23.6 \left( \frac{\nu \varepsilon}{k^2} \right)^{1/4} \quad (5.20)$$

### 5.3.3 Heat Transfer

SOFIE models thermal radiation using the discrete transfer radiation model<sup>7</sup> (Lockwood and Shah, 1981). This method uses a ray tracing procedure to solve the radiative transfer equation is solved along a finite number of ray paths. The net balance between emission and absorption for all rays traversing that control volume then defines the change in radiative flux across an individual control volume. Summation of the final intensity at the end of a line of sight in all directions then yields the incident flux upon the boundary face.

---

<sup>7</sup> Radiative heat transfer was not modelled in this study.

## 5.4 Numerical Solution Procedure

Given a computational domain, numerical methods treat, as the unknowns, discrete values of the dependant variable at individual grid points throughout the domain. The task of numerical methods is to provide a set of algebraic equations for the unknown values of the dependant variable and prescribe a suitable algorithm for solving these equations.

This section will introduce the methods by which SOFIE discretises the general conservation equation (5.8), determines the value of the dependant variable at each cell face, solves the equation set, and corrects the velocity and pressure fields.

### 5.4.1 Discretisation Methods

SOFIE uses a “finite control volume” discretisation method to discretise the general conservation equation (equation 5.8). Given a computational domain divided into a number of control volumes, so that each grid point is surrounded by one control volume, the general equation is discretised by integrating over the control volume. This integration yields a linear algebraic equation for the dependant variable at each grid point. Referring to figure 5.3, integrating the dependant variable,  $\phi$ , over the shaded control volume would yield a linear equation of  $\phi$  at P.

The “finite control volume” discretisation method has the advantage that it expresses an exact solution of the dependant variable at each grid point; even for coarse grids, it still represents an exact solution.

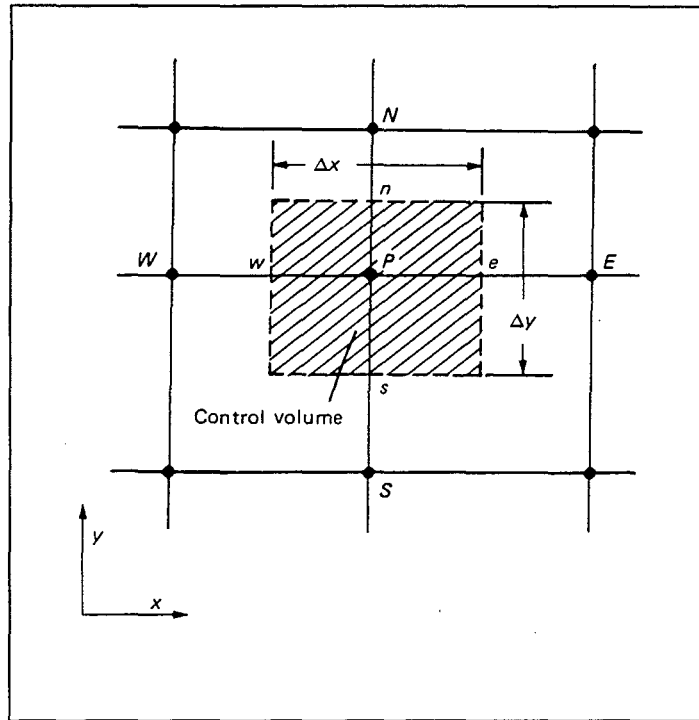


**Figure 5.3. A two-dimensional control volume surrounding a grid point P (Patankar, 1980).**

The most common method of discretising the general equations is usually by a truncated Taylor-Series approximation (Patankar, 1980).

## 5.4.2 Interpolation Methods

SOFIE uses a number of different interpolation schemes for determining the value of the dependant variable on each cell face. The schemes SOFIE uses include: upwind, hybrid, and the second order upwind (Welch and Rubini, 1996). The central difference method is not used by itself because can result in physically unrealistic results<sup>8</sup>.

The hybrid difference scheme is a combination of the central and upwind schemes; identical to the central scheme when  $-2 \leq Pe \leq 2$ , where  $Pe$  is the Peclet number defined as the ratio of convective to diffusive fluxes across a cell face. The

---

<sup>8</sup> The coefficients of the discretised form of the general equation using a central difference scheme can take on negative values, thus implying that it is possible that a point by point solution of the discretised equations might diverge.

hybrid scheme becomes the upwind scheme when  $Pe > 2$  (Patankar, 1980). The truncation error for the hybrid scheme depends on which scheme is being used (a function of  $Pe$ ) -  $\Delta x^2$  for the central difference scheme, and  $\Delta x$  for the upwind scheme.

Comprehensive details of various interpolation methods employed by SOFIE are available in a standard text such as Patankar's (1980).

### 5.4.3 Algebraic Equation Solver

Once the values of the dependant variable have been substituted into the discretised equation, the linearised algebraic form of the general conservation equation is solved by the use of the tri-diagonal matrix algorithm (TDMA), named because all of the non-zero coefficients align themselves along three diagonals. This algorithm has the advantage of only requiring computer storage and computer processing time proportional to  $N$ , where  $N$  is the number of grid points, rather than to  $N^2$  or  $N^3$  as some other algebraic solution methods (Patankar, 1980).

Non-linearity in the linear algebraic equations might arise where a boundary condition, for example, is a function of the dependant variable. In such cases, successive iterations are carried out while solving the equations until a converged solution is reached. The rate at which the dependant variable changes from iteration to iteration is controlled by the over and underrelaxation factors. Underrelaxation is used to slow down the changes between iterations in highly non-linear problems and enhances the likelihood of a converged solution. There are no accepted methods for finding the correct underrelaxation factor, as it is a function of the nature of the problem, the number of grid points, the grid spacing and the iterative procedure.

## **5.4.4 Calculating the Flow Field**

### **5.4.4.1 Pressure Correction Methods**

In addition to the generalised equations, SOFIE also applies a pressure correction to the pressure and velocity field to ensure that local and overall continuity is satisfied. The SIMPLEC algorithm, developed by Van Doormaal and Raithby (1984) which is based on Patankar and Spalding's (1972) SIMPLE algorithm is used by SOFIE.

The SIMPLEC pressure correction technique is widely used in incompressible flow computer codes, where it has been found to be stable and suitable for transient simulations (Welch and Rubini, 1996). The other advantages of the technique is that it forces mass conservation at each time step/iteration which is important when the flow may be undergoing chemical reactions.

### **5.4.4.2 Velocity Calculation**

SOFIE uses a non-staggered velocity storage arrangement, where all variables are stored at the central node of the control volume. This can cause the velocity and pressure fields to become de-coupled which can cause the pressure field to oscillate (known as checkerboarding). SOFIE attempts to remove oscillations in the pressure field by adding a fourth power pressure derivative term to the continuity equation. This term has no effect in areas of smooth pressure gradients, and only acts to smooth unrealistic pressure oscillations (Rubini and Welch, 1996).



# 6 CFD Simulation Methodology

The purpose of this chapter is to detail the methodology adopted in setting up and carrying out the CFD simulations; covering computer hardware and software, enclosure geometry and fire details, and script file construction. Reference to the previous chapter discussing SOFIE may be required. An example script file for each enclosure is appended in Appendix A.

## 6.1 Introduction

A total of 6 CFD simulations have been carried out in two different sized enclosures. The results of these simulations are to be compared with the results of the zone modelling discussed previously.

The nature of the fire and enclosure simulated using CFD are exactly as presented in the zone modelling chapter.

## 6.2 Computer Hardware and Software

The CFD software used to simulate the fires was SOFIE version 2.06 (Welch and Rubini, 1996).

Fieldview version 2, a commercially available post-processing software package developed by Intelligent Light, United States of America was used to process the data generated by SOFIE.

All simulations were carried out on Intel Pentium II 233MHz personal computers running the Windows NT operating system. The PCs all had 32MB of RAM.

### **6.2.1 Solution Type**

The solution type is selected according to the physical problem being studied and the type of model being used for the solution. SOFIE has a default setting of steady state iso-thermal laminar flow.

The solution type used in all simulations was transient, turbulent (with buoyancy modifications to the  $k\sim\epsilon$  turbulence model (Rodi, 1980)), buoyant fluid flow undergoing heat transfer. Combustion was modelled using the eddy breakup model (Magnussen and Hjertager, 1976).

Heat transfer did not include the effects of radiation, and only solves for convection and diffusion of enthalpy in the fluid.

### **6.2.2 Grid Generation**

CFD techniques require the domain of interest to be divided into a computational grid. SOFIE, being a cell-centred scheme, solves for property values at the centre of each cell; the lines of the computational grid representing the edges of the cells.



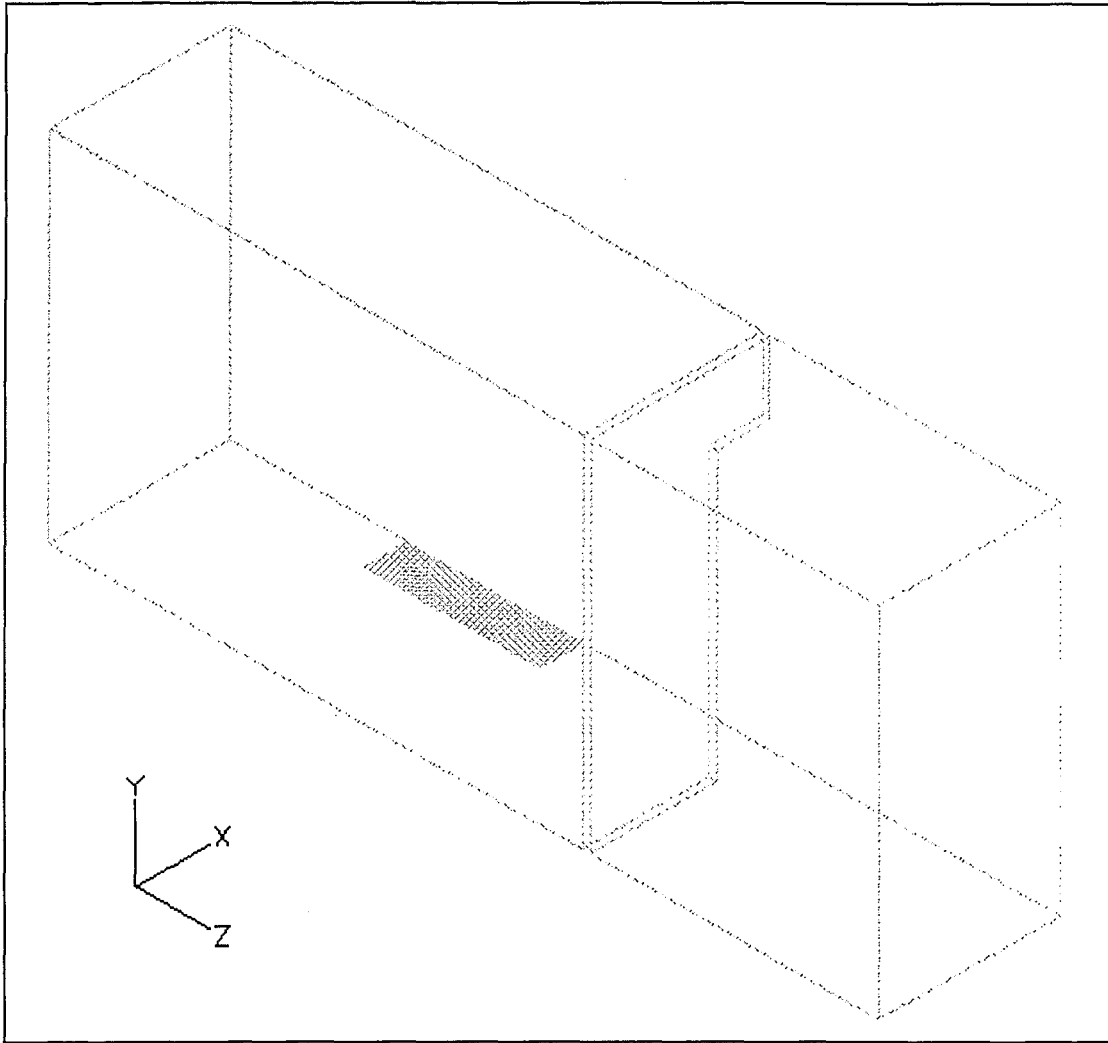


**Figure 6.1. The domain for enclosure 1, the shaded region indicates the fuel source. Note: a mirror line boundary exists down the doorway centre-line and the boundary in the x-y plane outside the doorway is the static pressure boundary.**

The grid generated in all cases was 3-dimensional Cartesian coordinate grid (see figures 6.1 and 6.2).

In order to set up the grid, the grid parameters in each coordinate axis are defined independently and then the grid is generated. Each coordinate axis is divided into a number of different regions, each containing a user-specified number of control volumes over a fixed length; the number of control volumes for each enclosure is tabulated in table 6.1.

In addition to the number of regions and the number of control volumes, two further parameters that govern the grid-line spacing must be defined. The grid stretch point, and grid stretch power define whether the grid lines are uniform, expanding or contracting for a particular region.

**Table 6.1. Grid statistics for each enclosure.**

Enclosure	Number of control volumes in each direction <sup>9</sup>			Total number of control volumes
	x	y	z	
1	15	19	47	13 395
2	14	15	50	10 500

---

<sup>9</sup> These figures do not include extra “dummy” cells created by SOFIE.

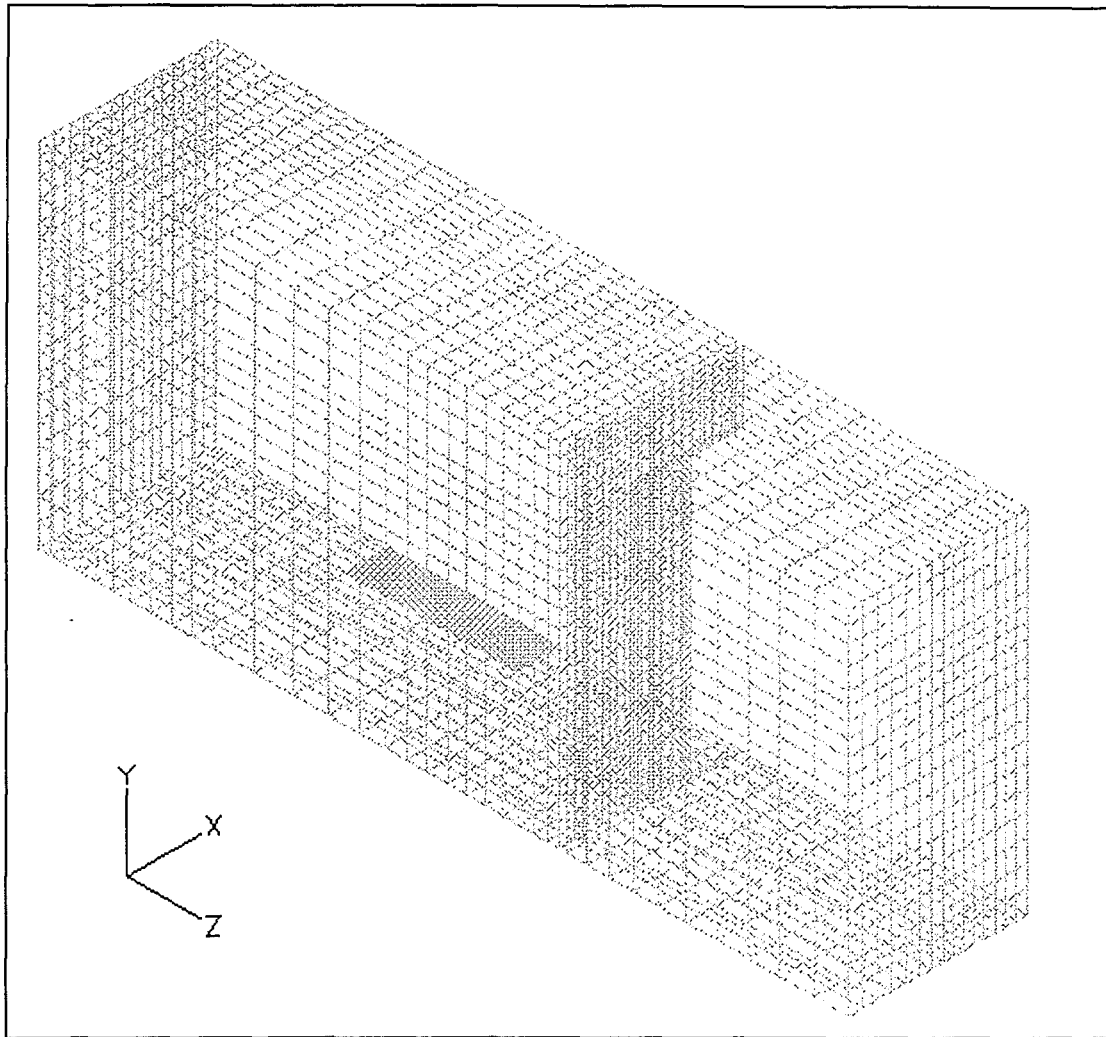


**Figure 6.2. The computational grid for enclosure 1.**

### **6.2.3 Blockages**

Blockages represent an obstruction in the fluid flow, and are applied to sections of the grid to represent boundaries and objects within the domain. By applying a blockage to the grid, the cells are taken out of the fluid flow calculations.

Inactive blockages, meaning the cells do not conduct heat, were used to define enclosure walls. This was achieved by blocking a section of grid and deleting the blocked off cells where vents occurred along the wall. All blockages were 2 cells in depth because SOFIE requires one cell-depth adjacent to each fluid region. Even though inactive blockages were defined, the thickness of the blocked region was taken as what the wall thickness would be in reality.

## 6.2.4 Boundary Types

Two different classes of boundary type are allowed in SOFIE: fluid and thermal. Fluid boundary types were used throughout to represent walls, a mirror plane and a pressure boundary.

The boundary type 'wall', which is a sub-set of the 'fluid' boundary type mentioned above, defines a solid boundary that prevents fluid flow between cells; the enclosure walls, ceiling and floor were defined as a 'wall' boundary type.

A line of symmetry about the centre-line of the enclosure vent was used in all cases. This was achieved by defining the centre-line as a 'mirror' boundary type (see figure 6.2).

A static pressure boundary was created 2m outside the vent of each enclosure in order to avoid the specification of the flow condition at the vent. In this case, at the vent flows are calculated from Bernoulli's equation assuming a hydrostatic pressure gradient in the doorway.

## 6.2.5 Boundary Values

Boundary values are the numerical values of face variables which are used in the calculation. Each solved variable must have a boundary value specified. Boundaries such as walls were defined as smooth and did not have a velocity set.

The boundary values specified are the same for each enclosure, and are listed in table 6.2.

**Table 6.2. Solved variables and boundary values for boundary types.**

Boundary Type	Solved Variable	Boundary Value
Mirror line of symmetry	Turbulent kinetic energy intensity on face	1%
	Turbulent dissipation rate on face	0.1m
Static pressure boundary	Turbulent kinetic energy intensity on face	1%
	Turbulent dissipation rate on face	0.1m
All interior fluid cells	Temperature	290K

The fire source is defined as a velocity inflow based on the burning rate of a hydrocarbon pool fire with heat release rate,  $Q$ , such that:

$$u = \frac{Q}{H_c \rho A} \quad (6.1)$$

$\rho$ , the density of the volatiles was calculated assuming ideal gas behaviour at an ambient temperature,  $T$ , of 290K:

$$\rho = \frac{Mp}{RT} \quad (6.2)$$

where  $M$  = the molecular mass of the fuel,  $p = 101\,325\text{Pa}$  = the atmospheric pressure,  $R = 8.314\text{J/K.mol}$  = the Universal gas constant. Table 6.3 lists the molecular mass, heat of combustion, and density of the volatiles for Propane and n-Heptane.

**Table 6.3. Molecular mass, heat of combustion, and density of volatiles for Propane and n-Heptane.**

<b>Fuel</b>	<b>Molecular Mass (kg/mol)</b>	<b>Heat of Combustion (MJ/kg)</b>	<b><math>\rho</math> (kg/m<sup>3</sup>)</b>
Propane	0.0441	46.36	1.85
n-Heptane	0.1002	44.56	4.21

Table 6.4 lists all details of the fire source definition, including total heat release rate, fire area, fuel type, inlet velocity and inlet Froude number.

The Froude number is given by:

$$Fr = \frac{u^2}{gD} \quad (6.3)$$

where  $D$  is the characteristic dimension of the fuel pan and was taken as being the diameter of an equivalent area circular pan.

Equation 6.3 expresses the ratio of momentum forces to buoyancy forces; a Froude number less than 1 indicates the flow is “buoyancy-driven”. Thus, all fire sources in table 6.4 are “buoyancy-driven”.

A fixed fraction of 35% of the total heat release rate was assumed to be lost to the surrounding enclosure via thermal radiation.

**Table 6.4. Fire source definition: area, fuel type, inlet velocity and inlet Froude number.**

<b>Reference</b>	<b>Total Heat Release Rate (kW)</b>	<b>Fire Area (m<sup>2</sup>)</b>	<b>Fuel Type</b>	<b>Velocity (m/s)</b>	<b>Froude number (--)</b>
1A	330	0.74	Propane	3.38E-03	1.20E-06
1B	430	0.74	Propane	4.40E-03	2.03E-06
1C	500	0.74	Propane	5.12E-03	2.75E-06
2A	300	0.18	n-Heptane	5.77E-03	7.09E-06
2B	600	0.36	n-Heptane	5.77E-03	7.09E-06
2C	300	0.18	n-Heptane	5.77E-03	7.09E-06

The fire area defined in table 6.4 is the total surface area of the fuel source. These areas were taken as close as practically possible to the size of the fire source used in the experiments by Dembsey et al. (1995) and Collier (1997). The fire area is represented graphically in figures 6.1 and 6.2 as the shaded region.

### **6.2.6 Convergence Limits and Numerical Solution**

Simulation convergence was defined by the mass residual error. This was set to 0.005 kg/s (0.5%). The mass error parameter represents the mass errors, at each iteration, for each control volume summed over the whole solution domain and normalised by the mass flow into the domain.

The maximum number of iterations per time step was set to 200. This means that SOFIE moves onto the next time step after 200 iterations regardless of the mass residual error, and consequently, simulation run times are shorter. This method can bring about problems with conservation of mass within the solution.

## **6.2.7 Running the Simulation**

Once the above procedure has been followed, the simulation may now be started. The 'run' command, followed by the number of transient time periods that are to be simulated is all that is required to start the simulation.

## **6.2.8 Result File Exporting**

At any point in the simulation, a result file may be generated and exported to post-processing software. This has to be done manually and involves halting the simulation (if it is still running), writing the current solution and exporting the solution in ascii format to the post-processing software.

The above procedure may be completed interactively by working through control line prompts or through reading in additional lines from a script file.



# 7 CFD Results and Discussion

The purpose of this chapter is to present the results of the CFD simulations. The results presented will include post-processor generated graphics of the temperature profile throughout the enclosures, and plots of vertical temperature profiles at specific locations within the enclosures. To construct the vertical temperature profiles, the gas temperature is generated, using the post-processor, at vertical intervals of 0.25m.

The post-processor generated graphics use temperature units of Kelvin. There is a region of cooler fluid present at the edge of the flow domain indicated in the post-processor generated images. This cooler fluid represents the “dummy cells” created by Sofie in order to carry out the simulation and does not represent fluid cells within the enclosure.

In addition to the temperature profile results, the computer run times required for each simulation will also be presented and discussed.

Following the presentation of the results, discussions will follow.

## 7.1 Enclosure 1

Three different sized fires were simulated in enclosure 1: 330kW, 430kW, and 500kW. For each of these cases, the following results will be presented:

- Post-processor generated visualisation of the temperature profile throughout the enclosure at 20 minutes.
- Vertical temperature profiles at 5 minutes and 20 minutes at the centre-line of the fire source, the doorway centre-line and the corner adjacent to the doorway.

### 7.1.1 330kW

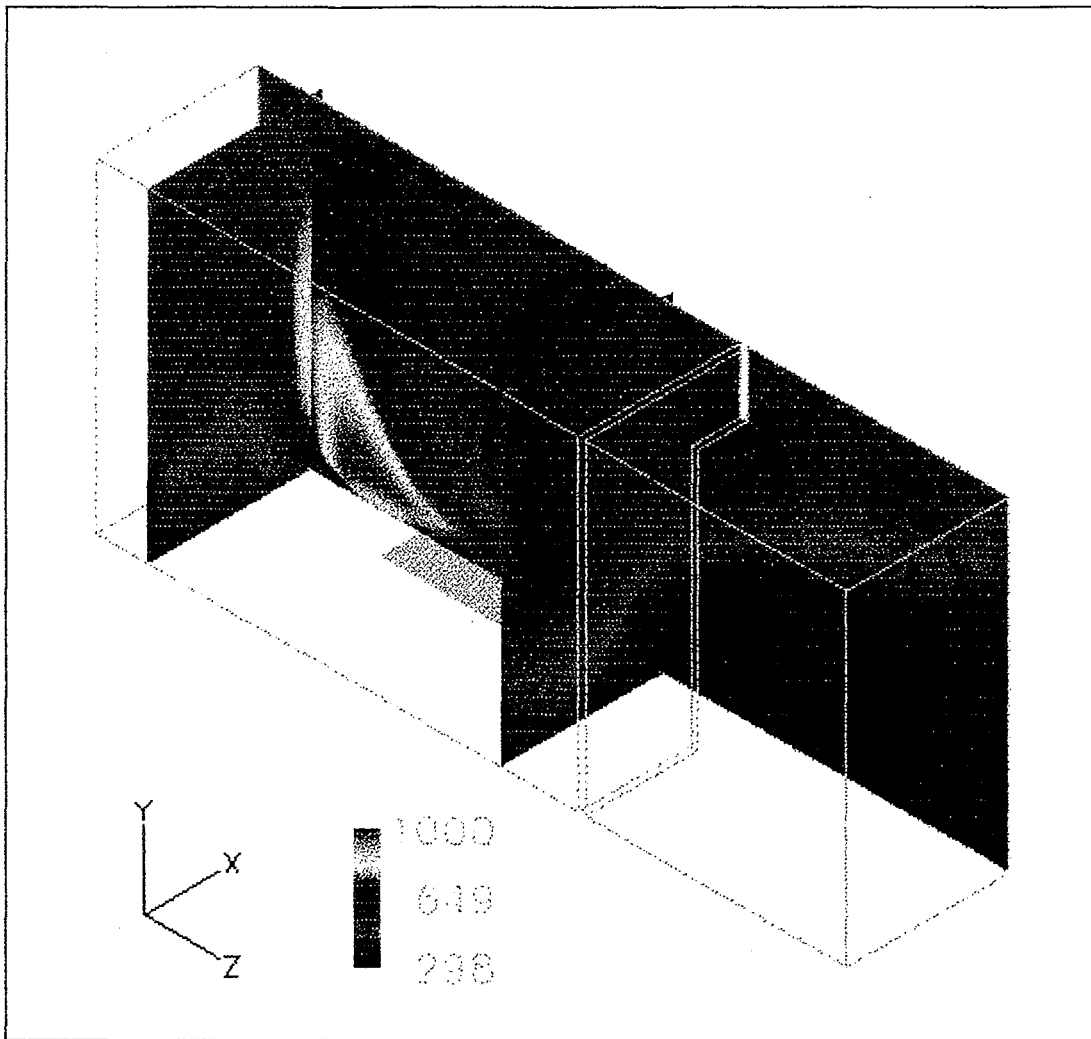


**Figure 7.1. Gas temperature profile throughout enclosure 1, 330kW fire at 20 minutes.**

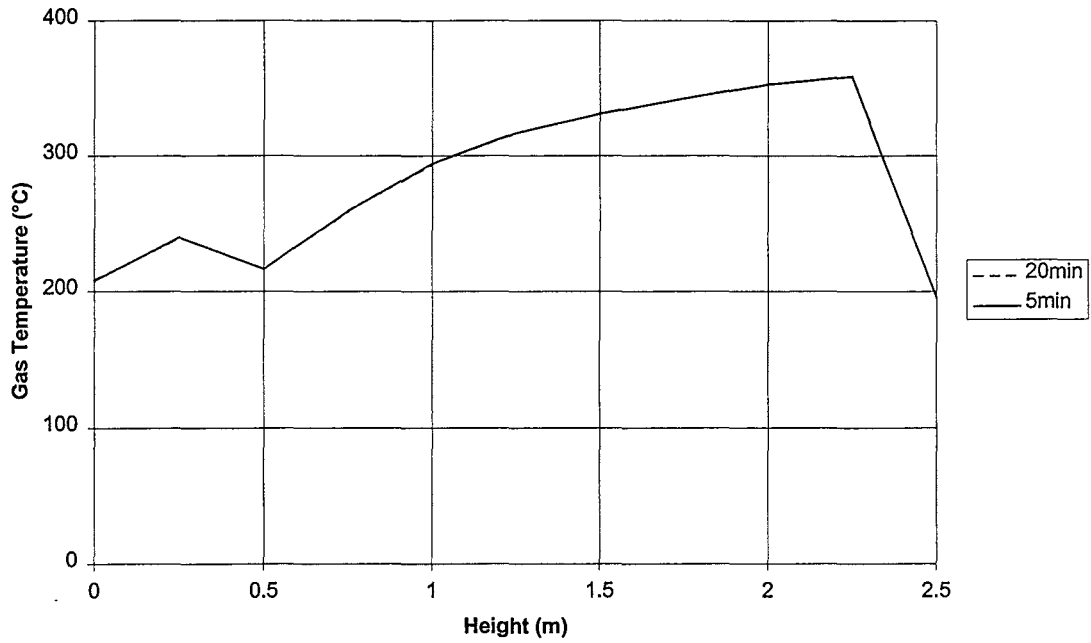


**Figure 7.2. Vertical temperature profile at the fire source centre-line for enclosure 1, 330kW fire.**

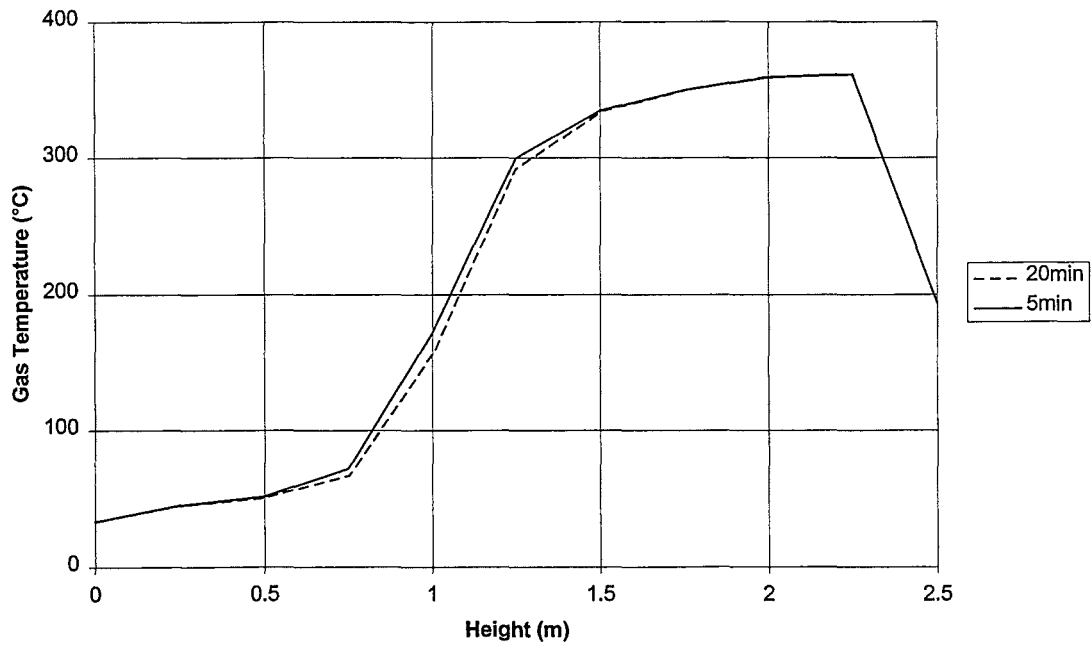


**Figure 7.3. Vertical temperature profile at the doorway centre-line for enclosure 1, 330kW fire.**

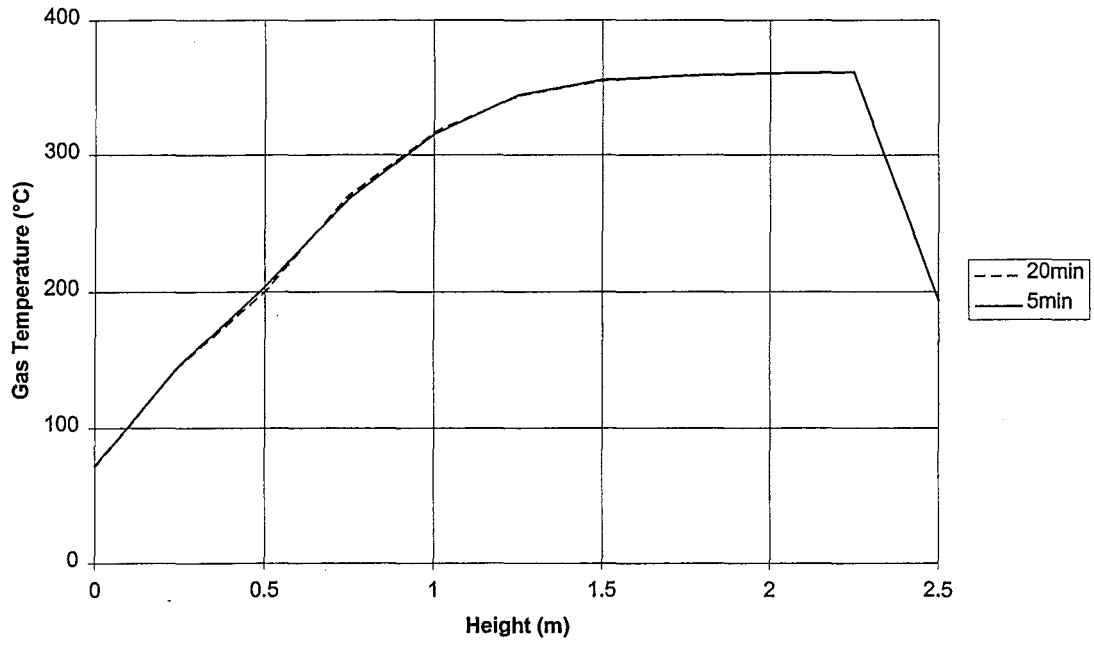


**Figure 7.4. Vertical temperature profile at the corner adjacent to the doorway for enclosure 1, 330kW fire.**

### 7.1.2 430kW

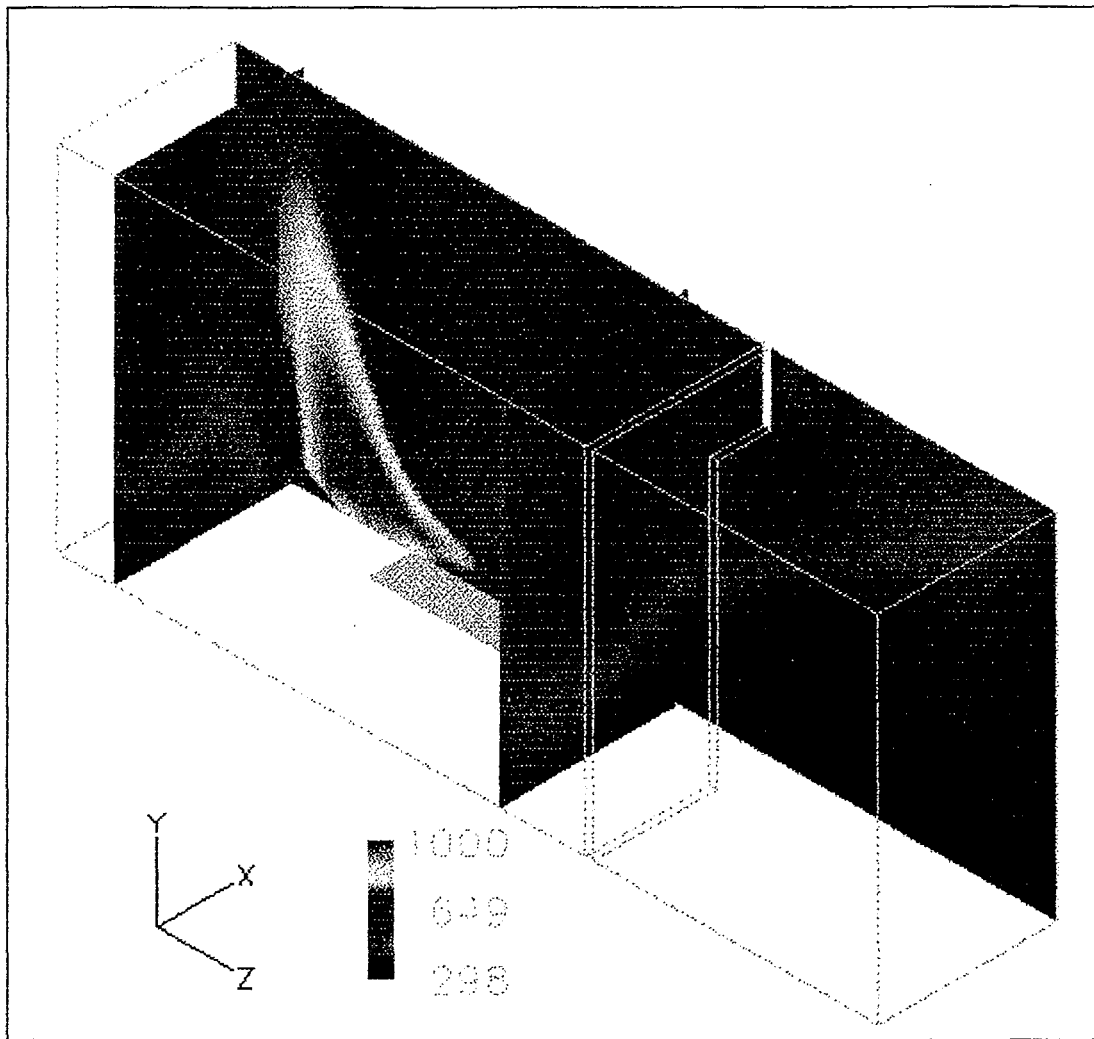


**Figure 7.5. Gas temperature profile throughout enclosure 1, 430kW fire at 20 minutes.**

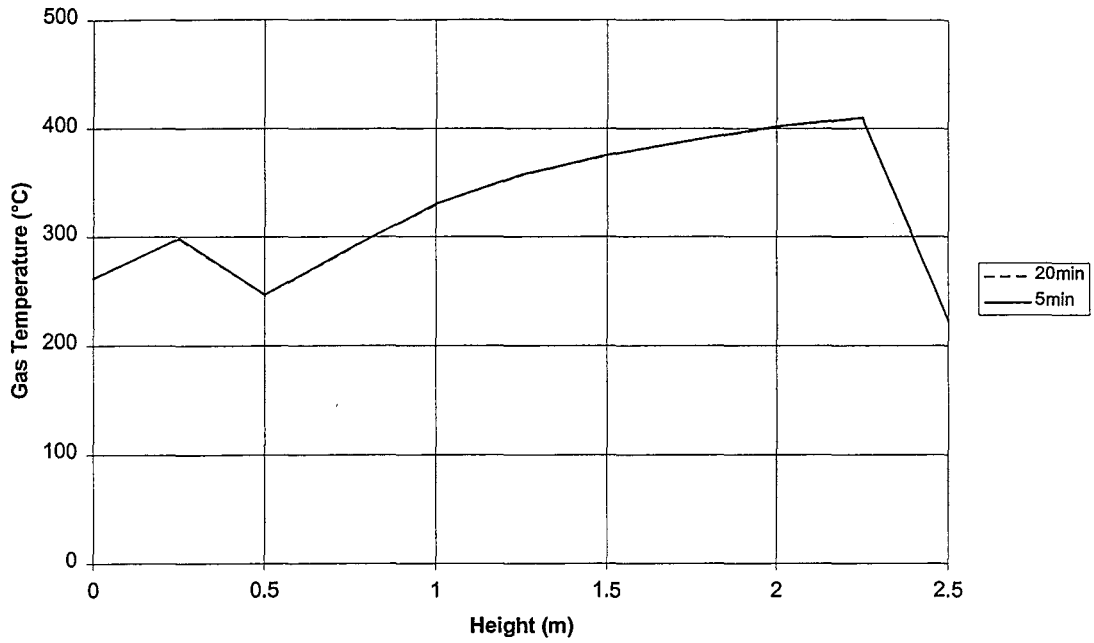


**Figure 7.6. Vertical temperature profile at the fire source centre-line for enclosure 1, 430kW fire.**

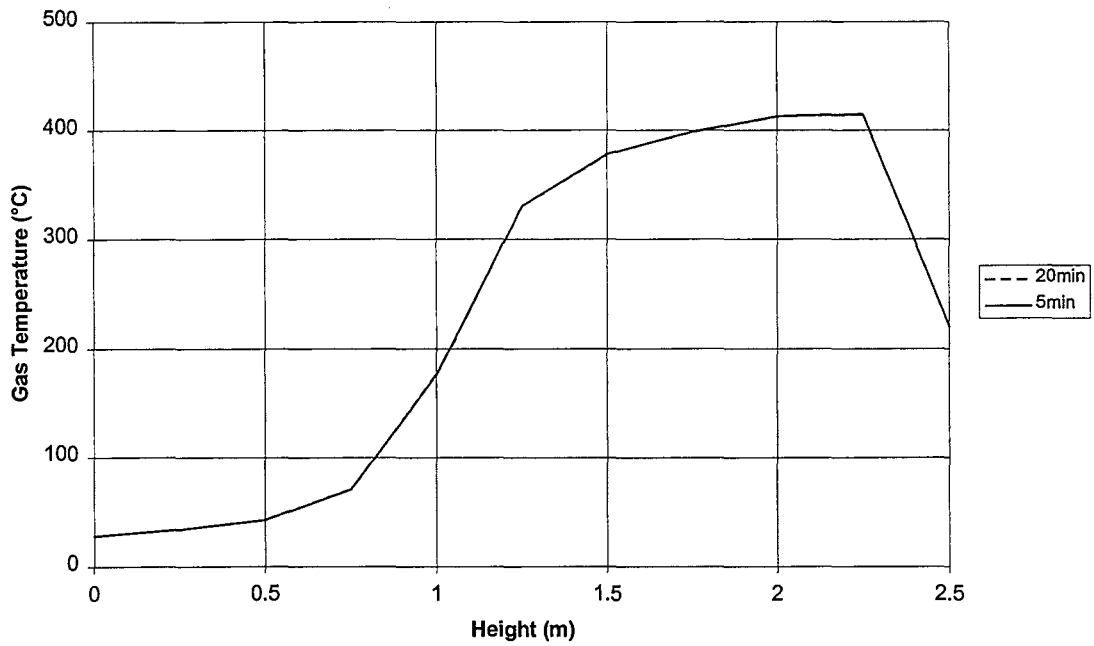


**Figure 7.7. Vertical temperature profile at the doorway centre-line for enclosure 1, 430kW fire.**

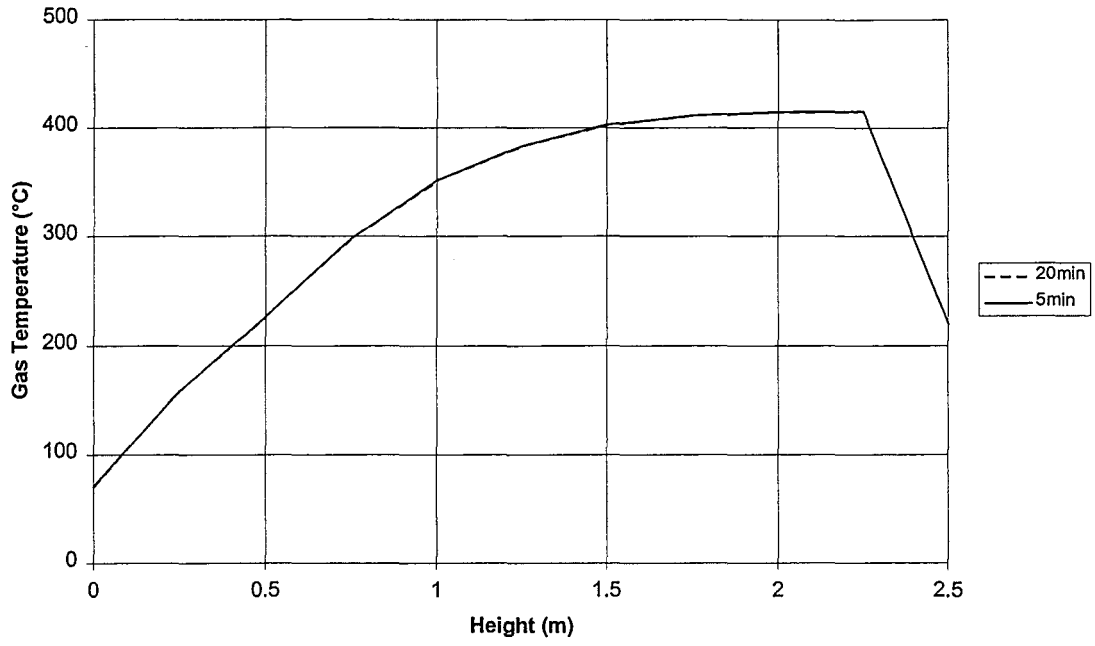


**Figure 7.8. Vertical temperature profile at the corner adjacent to the doorway for enclosure 1, 430kW fire.**

### 7.1.3 500kW

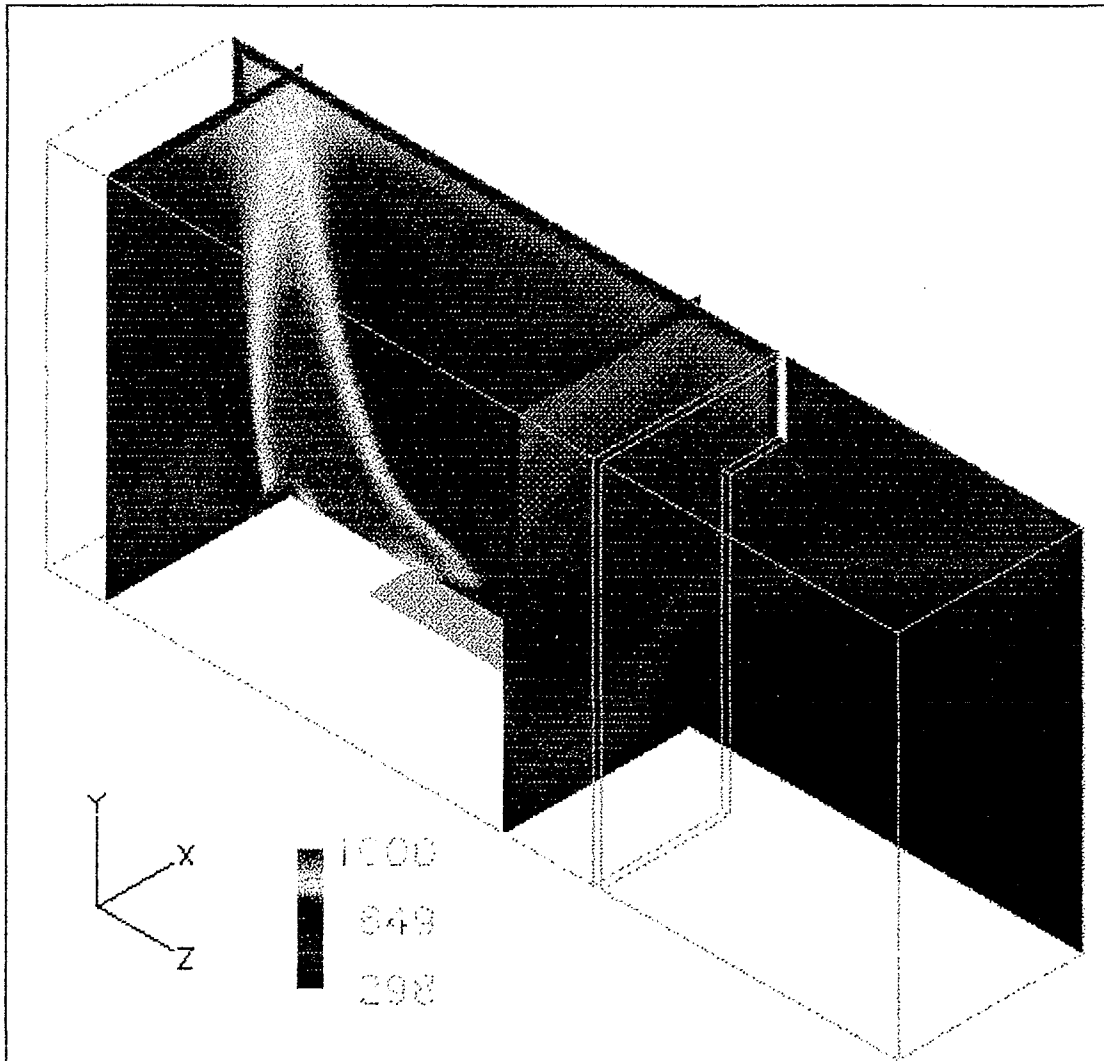


**Figure 7.9. Gas temperature profile throughout enclosure 1, 500kW fire at 20 minutes.**



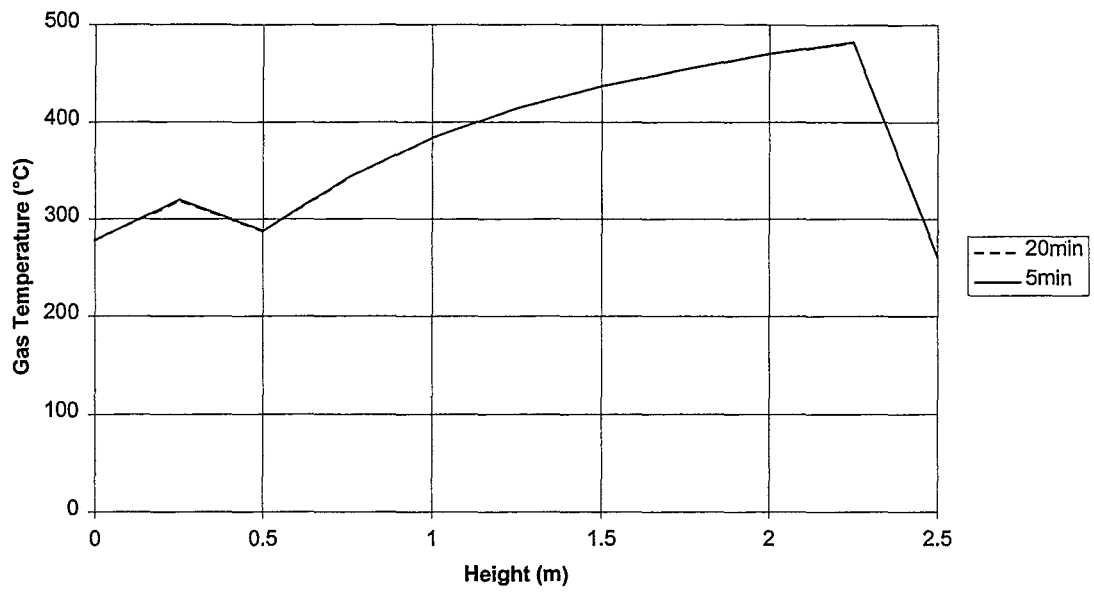


**Figure 7.10. Vertical temperature profile at the fire source centre-line for enclosure 1, 500kW fire.**

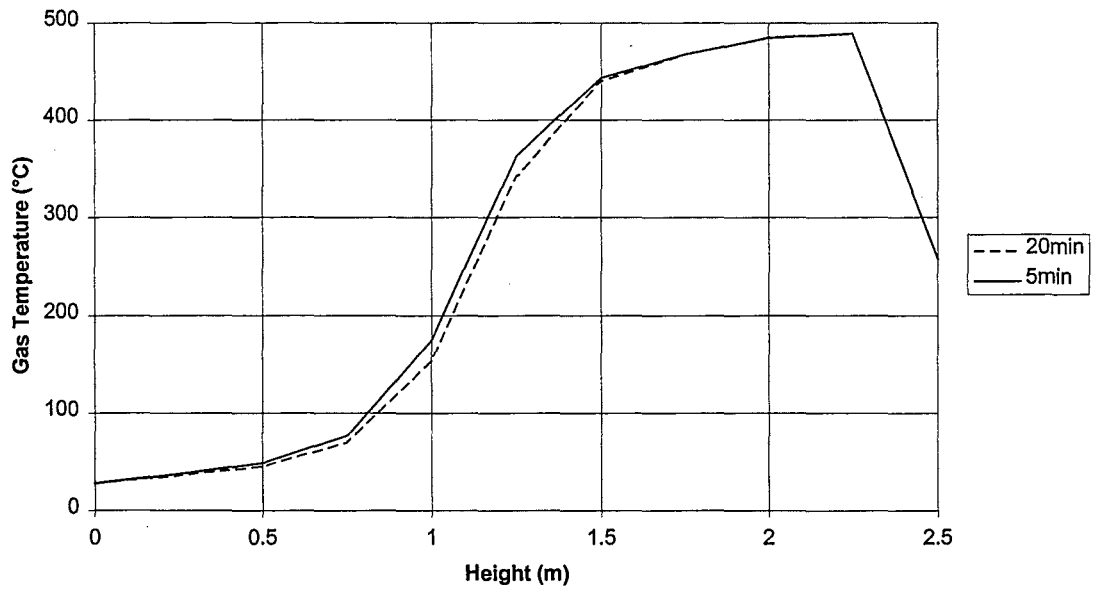


**Figure 7.11. Vertical temperature profile at the doorway centre-line for enclosure 1, 500kW fire.**

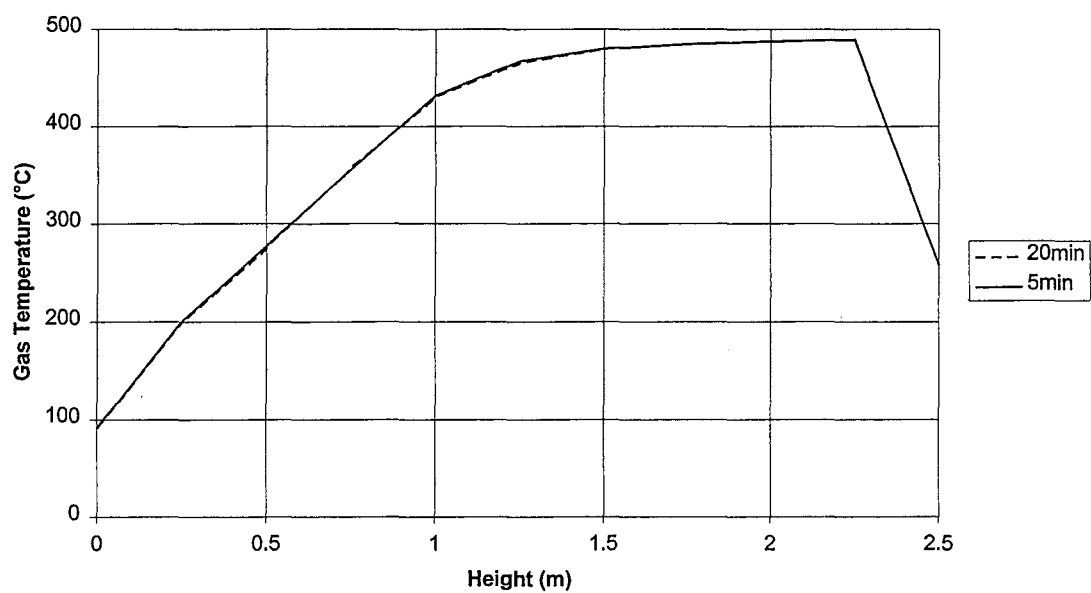


**Figure 7.12. Vertical temperature profile at the corner adjacent to the doorway for enclosure 1, 500kW fire.**

**Table 7.1. Computer run times required for the CFD simulation of the fires in enclosure 1.**

Heat Release Rate (kW)	Computer Run Time (hours:minutes)
330	17:44
430	16:52
500	15:33

#### 7.1.4 Remarks for Enclosure 1

Results for the CFD simulation of three different sized fires have been presented for enclosure 1. These results include post-processor generated visualisation of the temperature profiles throughout the enclosure for each simulation (figures 7.1, 7.5, and 7.9). These visualisations indicate:

1. An **inclination of the fire plume** away from the cool air flowing into the enclosure through the open doorway.
2. An **interface** between relatively hot and cool fluid.
3. With **increasing heat release rate**, the **temperatures** in the enclosure **increase**.

In addition to the temperature visualisations, temperature profiles are presented for three different locations throughout the enclosure:

- The plume centre-line.
- The doorway centre-line.
- The corner adjacent to the doorway.

These temperature profiles indicate:

1. A **steady-state temperature field** in the enclosure.
2. An **increase in gas temperature above the fire source with increasing height**.
3. An **increase in temperatures with increasing heat release rate**.
4. An area of **rapidly changing temperature with height at the doorway centre-line** indicating an interface between two layers - one with relatively low temperatures and the other with relatively high temperatures.

Table 7.1 indicates that it took between 15 and 17 hours to complete each 30 minute (real-time fire duration) simulation in this enclosure.

## 7.2 Enclosure 2

Three different sized fires were simulated in enclosure 2: 300kW, 600kW, and 300kW centrally-located. For each of these cases, the following results will be presented:

- Post-processor generated visualisation of the temperature profile throughout the enclosure at 10, 20 and 30 minutes.
- Vertical temperature profiles at 10, 20, and 30 minutes at the centre-line of the fire source, the two thermocouple locations (per the BRANZ experiments), the vent centre-line, and the corner adjacent to the vent.

### 7.2.1 300kW

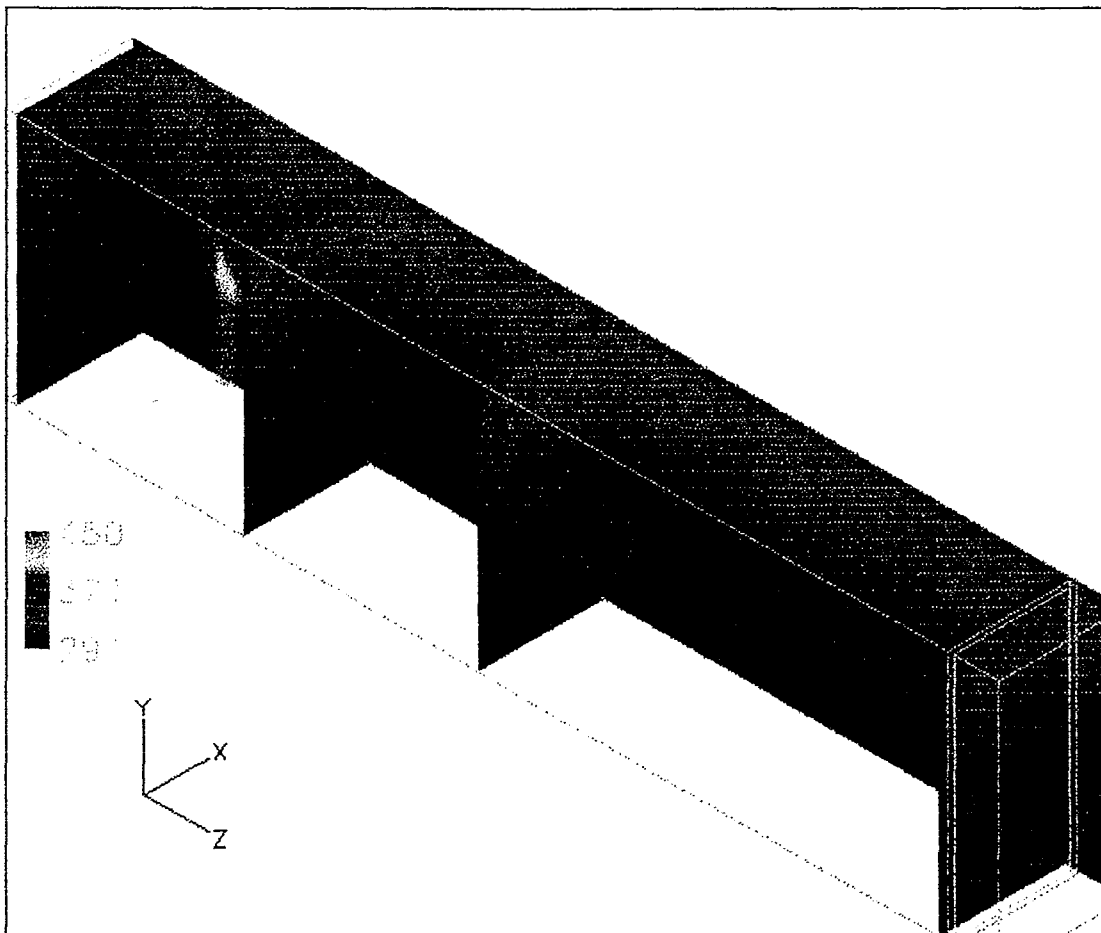


**Figure 7.13. Gas temperature profile throughout enclosure 2, 300kW fire at 10 minutes.**

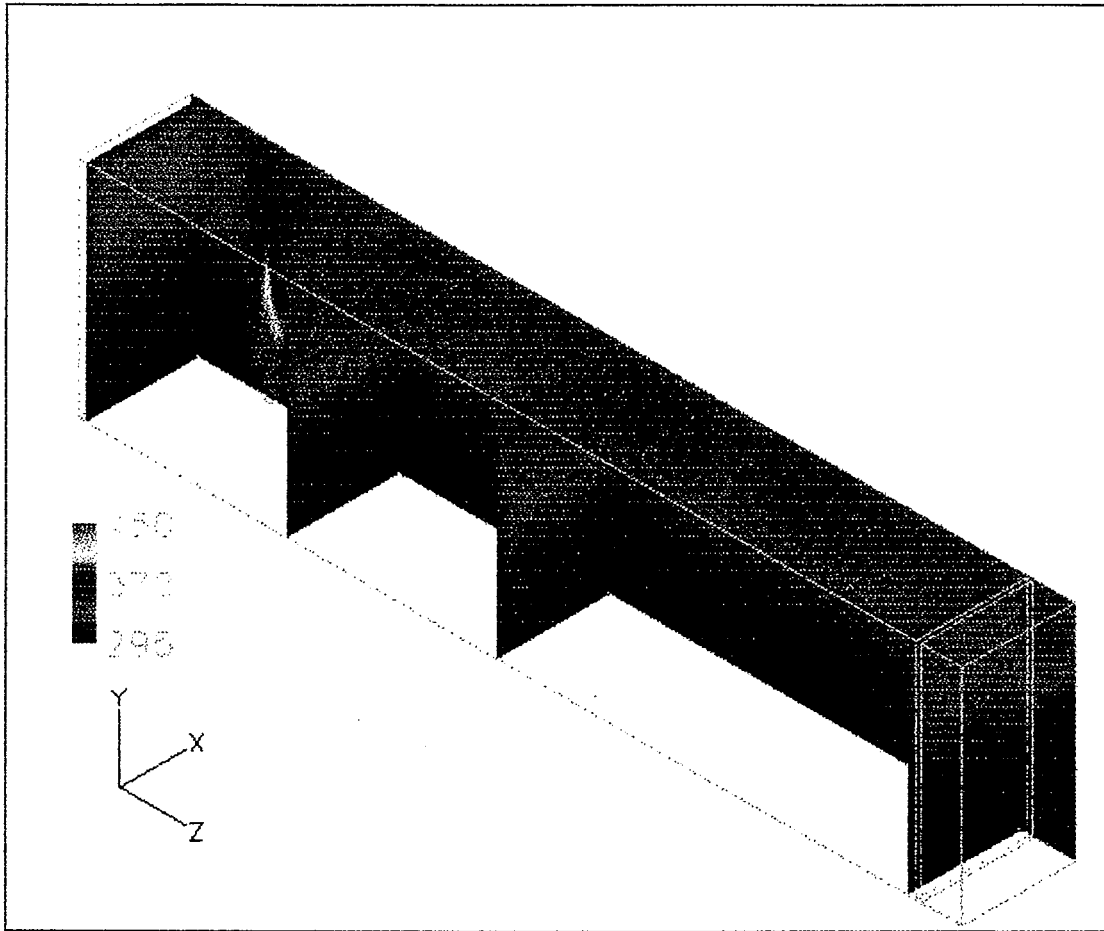


**Figure 7.14. Gas temperature profile throughout enclosure 2, 300kW fire at 20 minutes.**

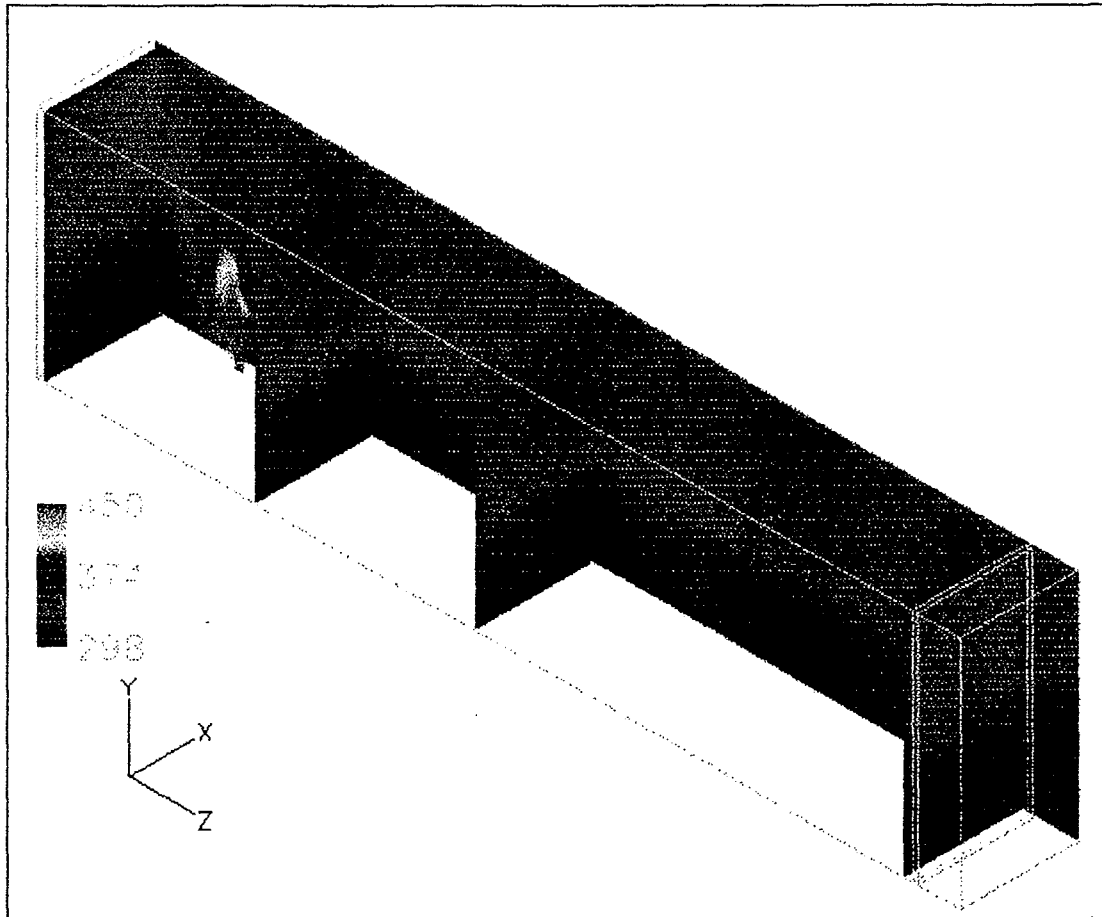


**Figure 7.15. Gas temperature profile throughout enclosure 2, 300kW fire at 30 minutes.**

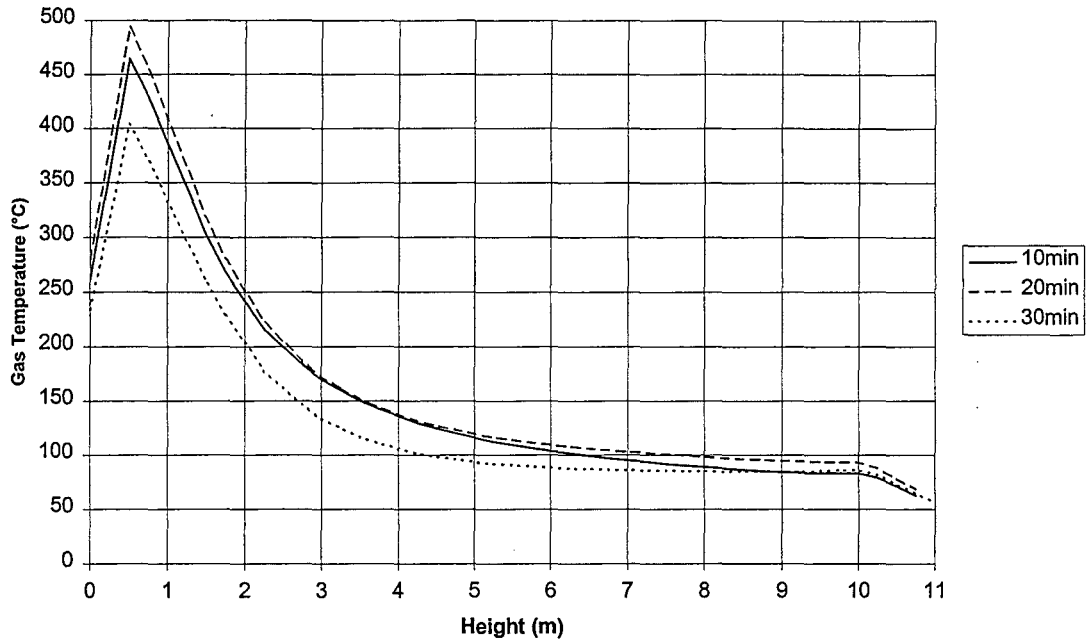


**Figure 7.16. Vertical temperature profile at the fire source centre-line for enclosure 2, 300kW fire.**

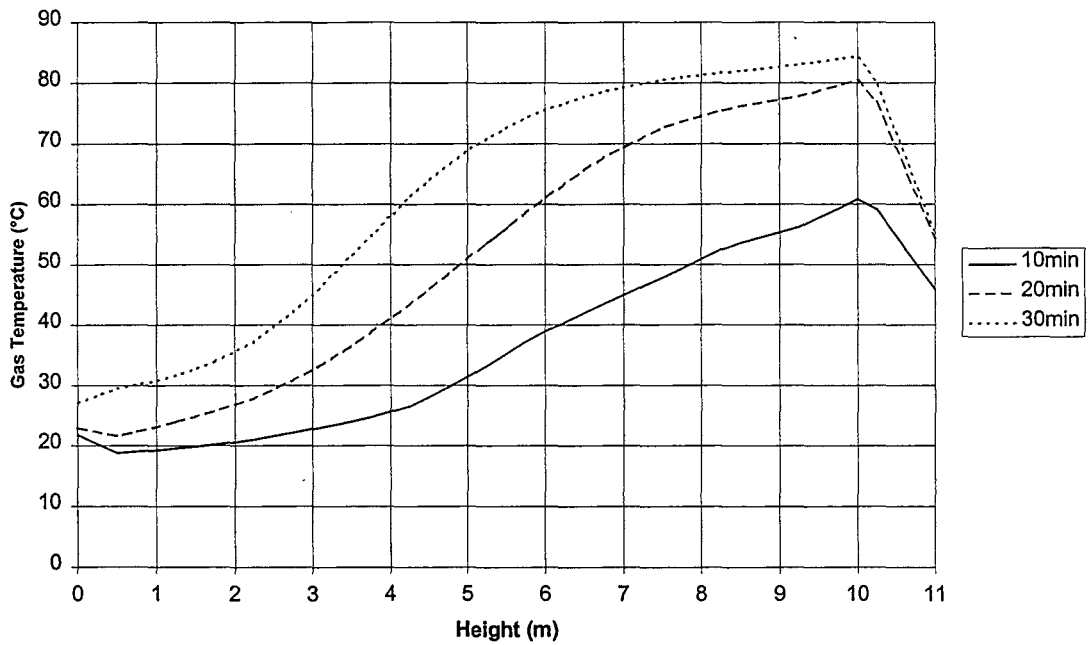


**Figure 7.17. Vertical temperature profile at thermocouple 1 for enclosure 2, 300kW fire.**

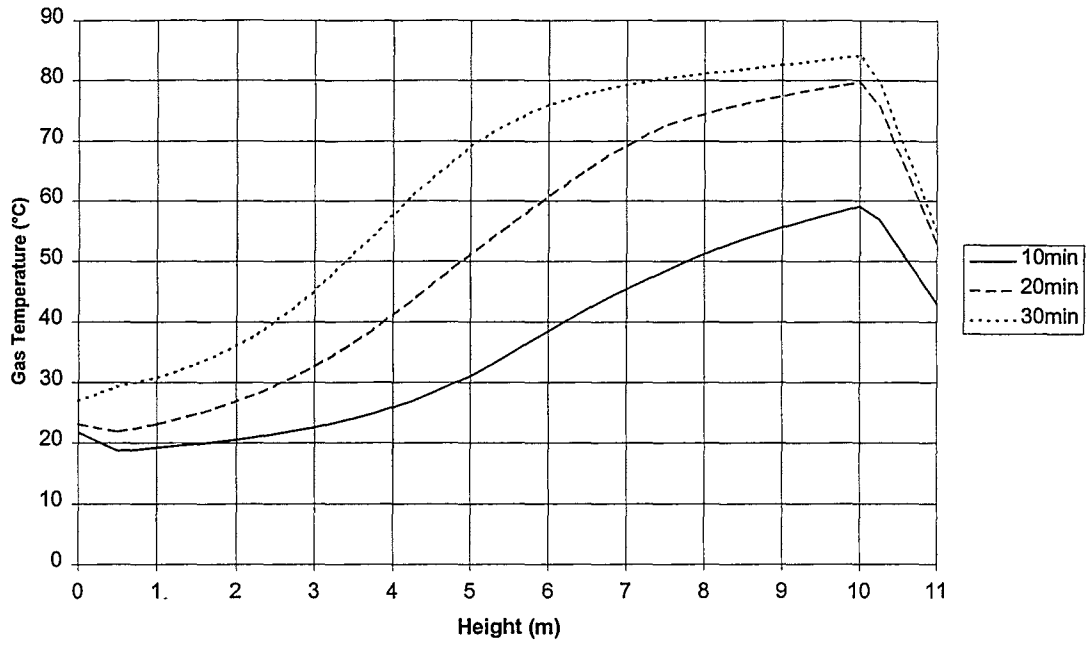


**Figure 7.18. Vertical temperature profile at thermocouple 2 for enclosure 2, 300kW fire.**

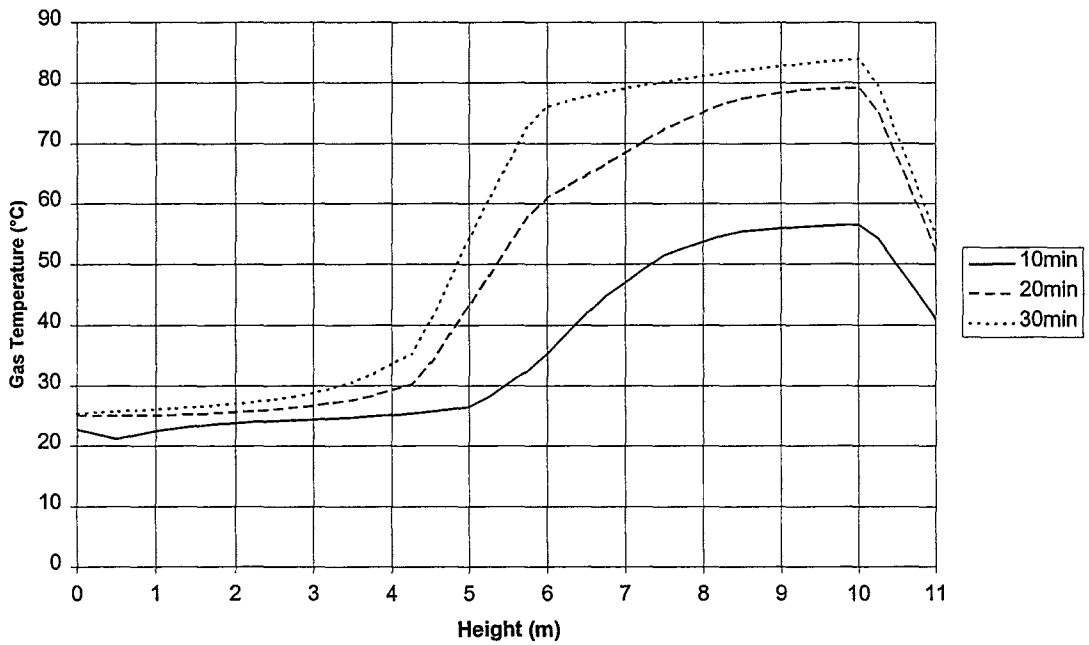


**Figure 7.19. Vertical temperature profile at the vent centre-line for enclosure 2, 300kW fire.**



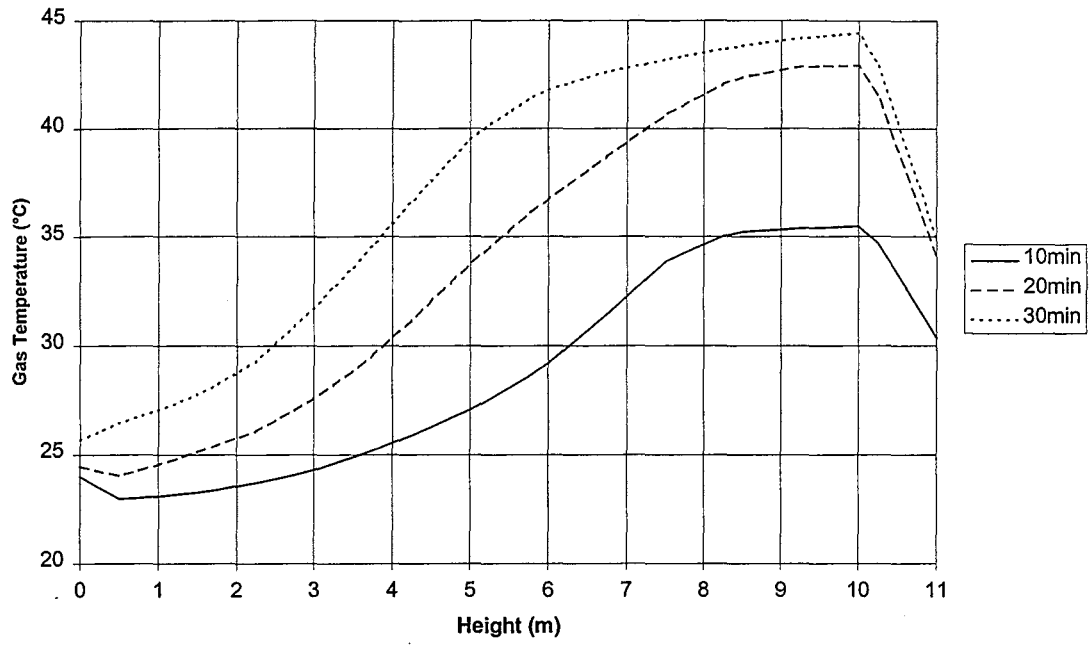


**Figure 7.20. Vertical temperature profile at the corner adjacent to the vent for enclosure 2, 300kW fire.**

## 7.2.2 600kW

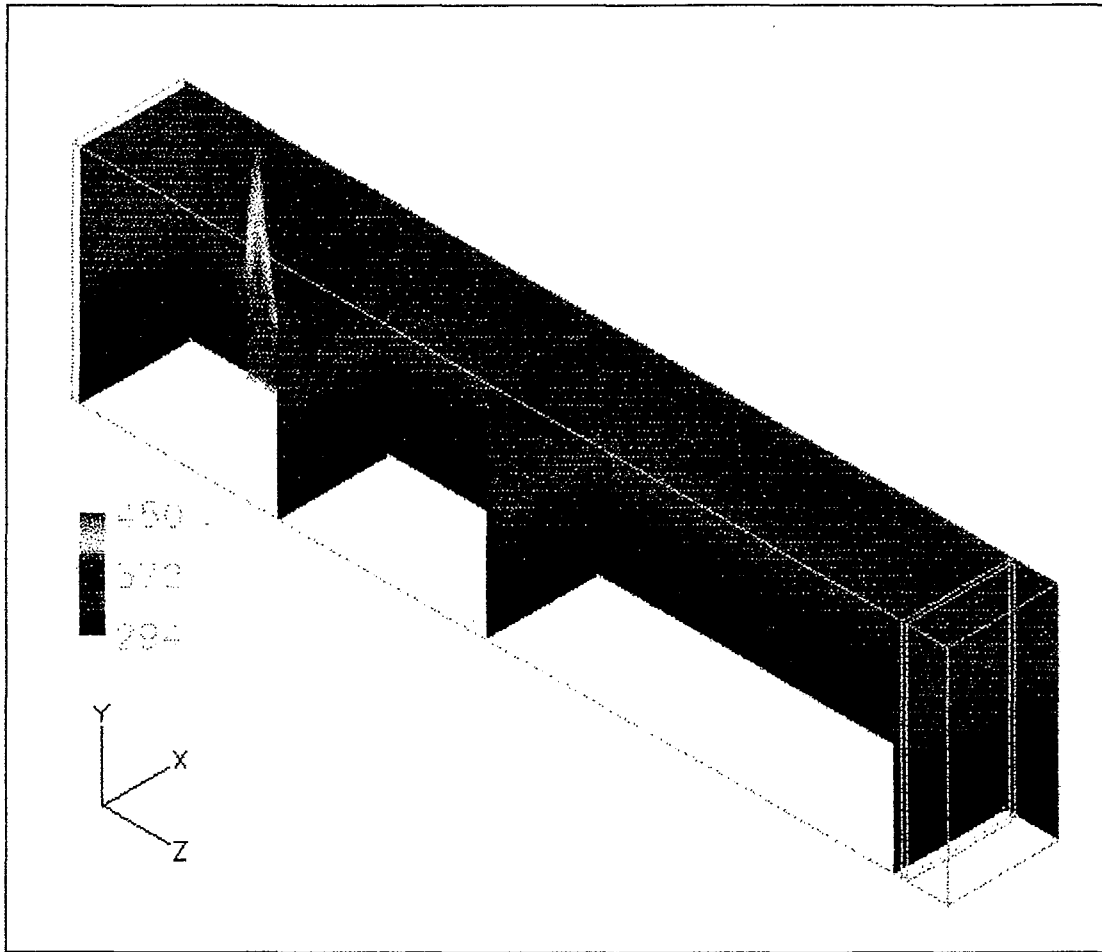


**Figure 7.21. Gas temperature profile throughout enclosure 2, 600kW fire at 10 minutes.**

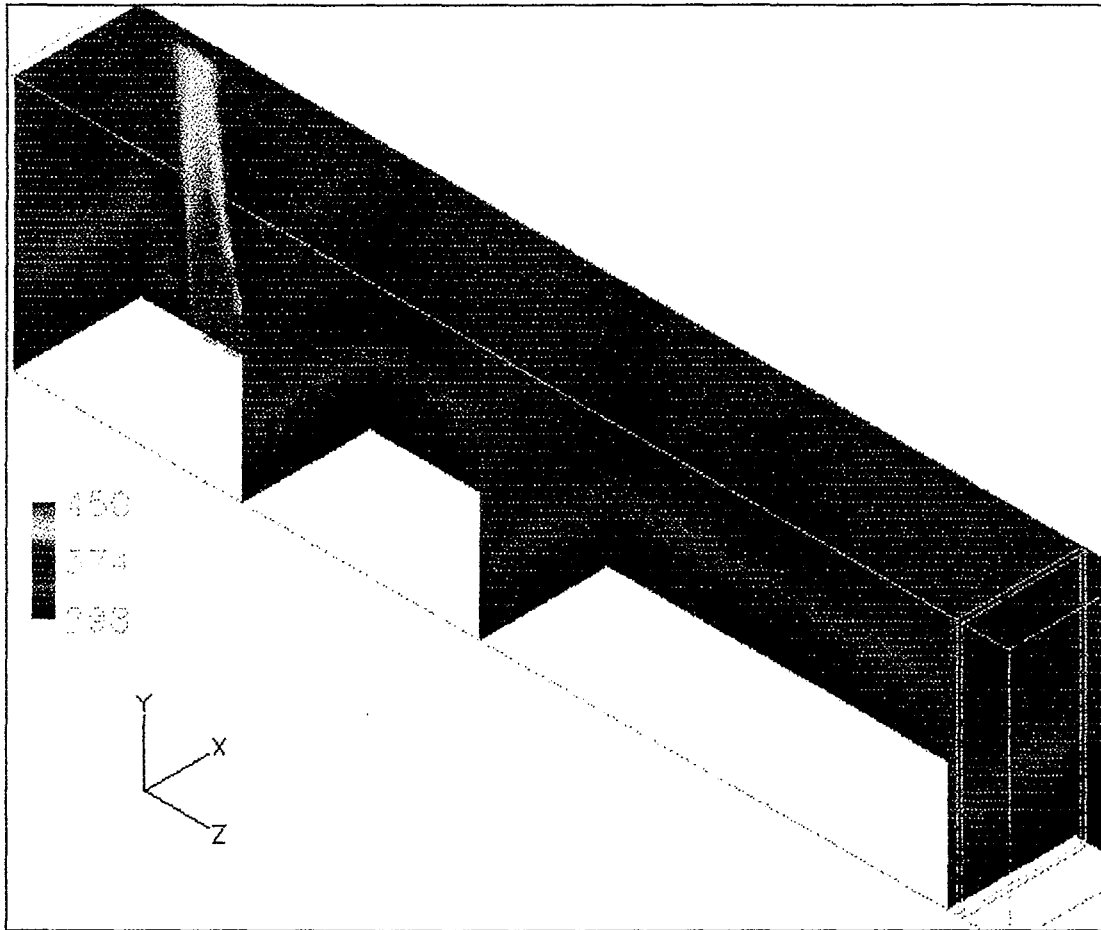


**Figure 7.22. Gas temperature profile throughout enclosure 2, 600kW fire at 20 minutes.**

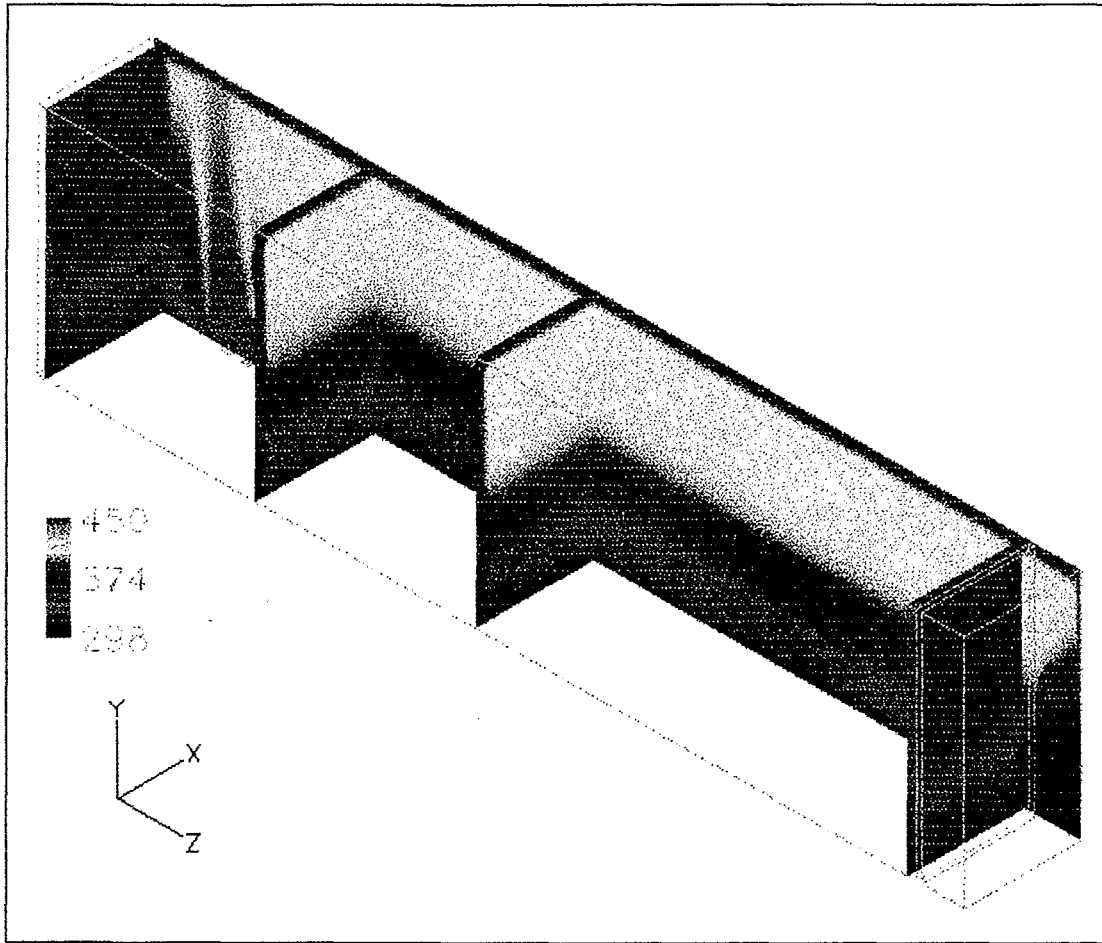


**Figure 7.23. Gas temperature profile throughout enclosure 2, 600kW fire at 30 minutes.**

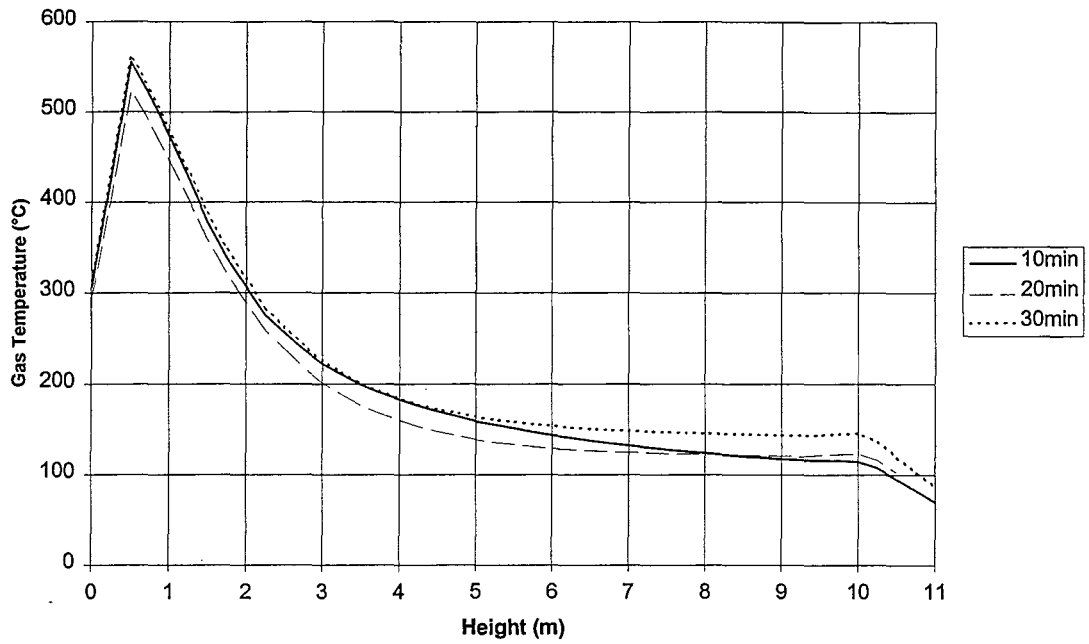


**Figure 7.24. Vertical temperature profile at the fire source centre-line for enclosure 2, 600kW fire.**

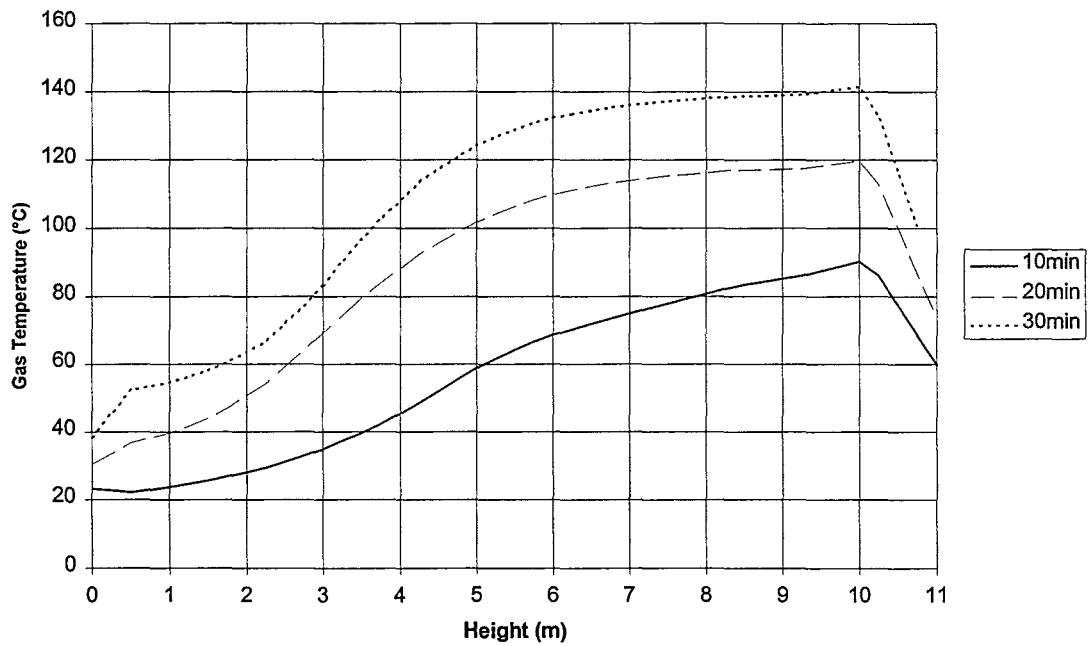


**Figure 7.25. Vertical temperature profile at thermocouple 1 for enclosure 2, 600kW fire.**

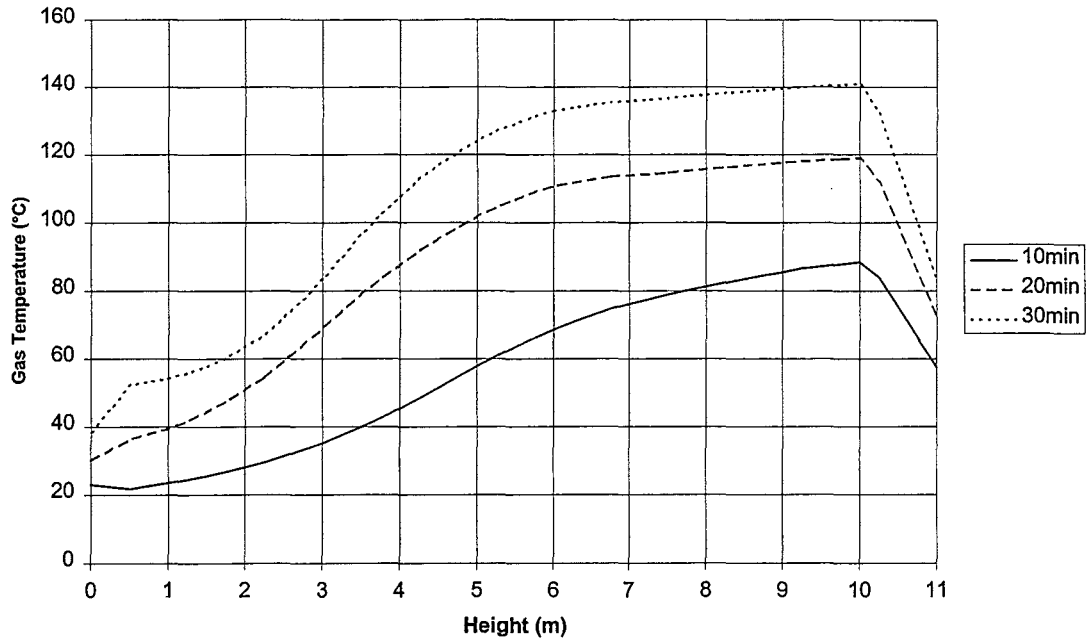


Figure 7.26. Vertical temperature profile at thermocouple 2 for enclosure 2, 600kW fire.

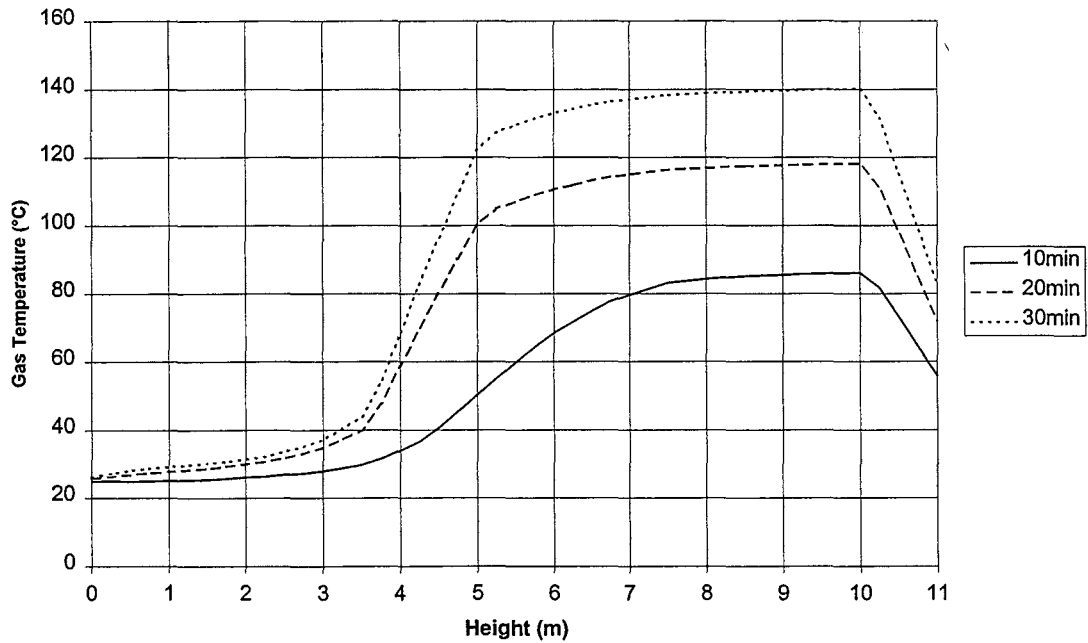
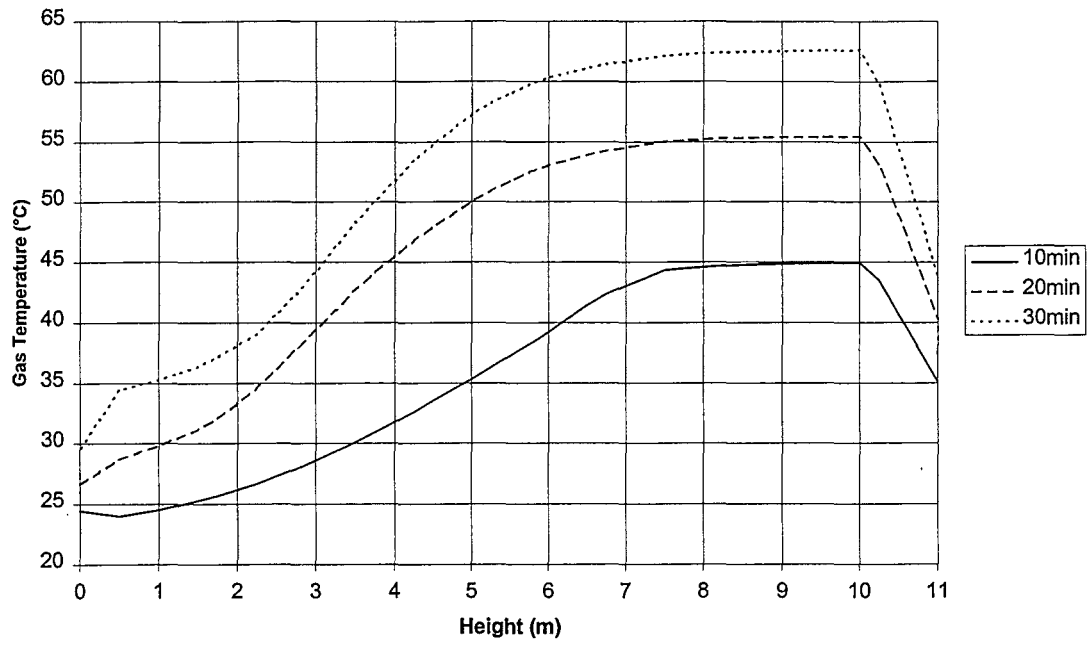


Figure 7.27. Vertical temperature profile at the vent centre-line for enclosure 2, 600kW fire.



**Figure 7.28. Vertical temperature profile at the corner adjacent to the vent for enclosure 2, 600kW fire.**

### 7.2.3 300kW - central location

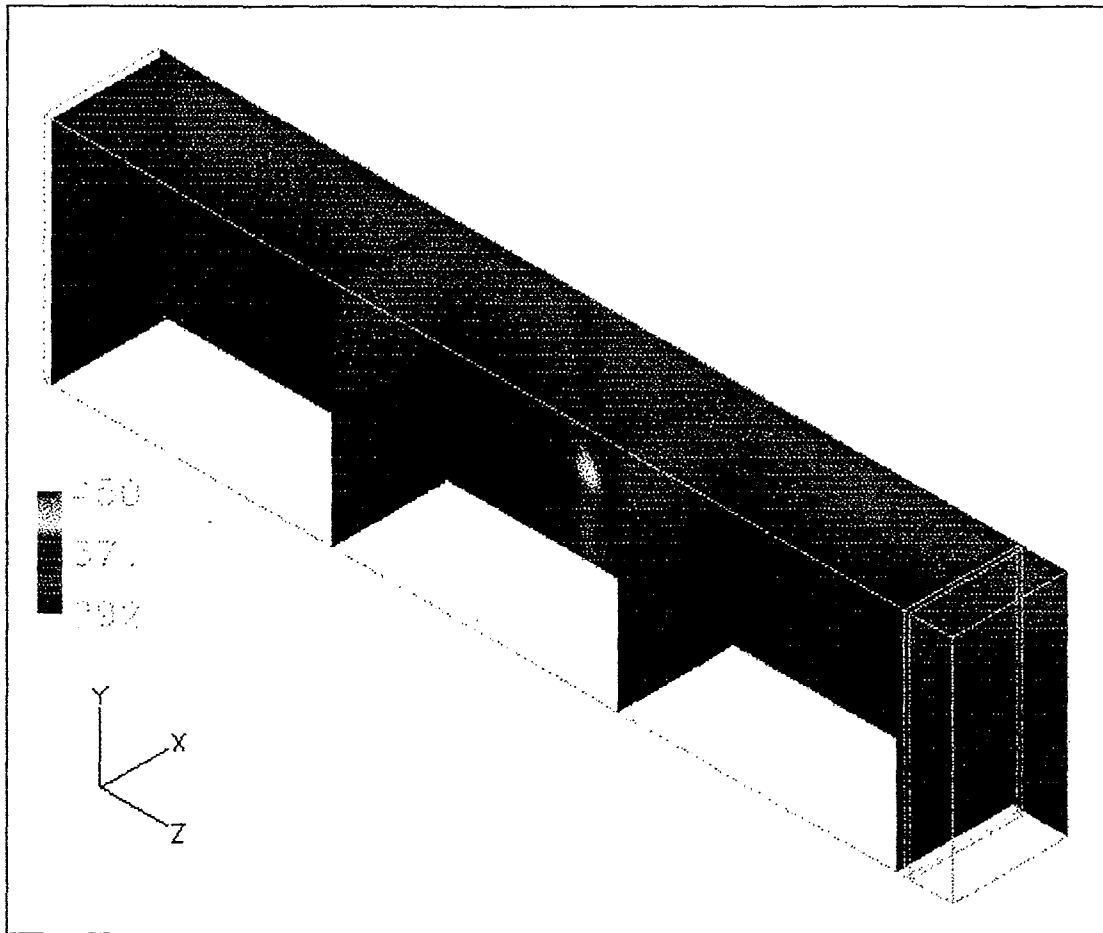
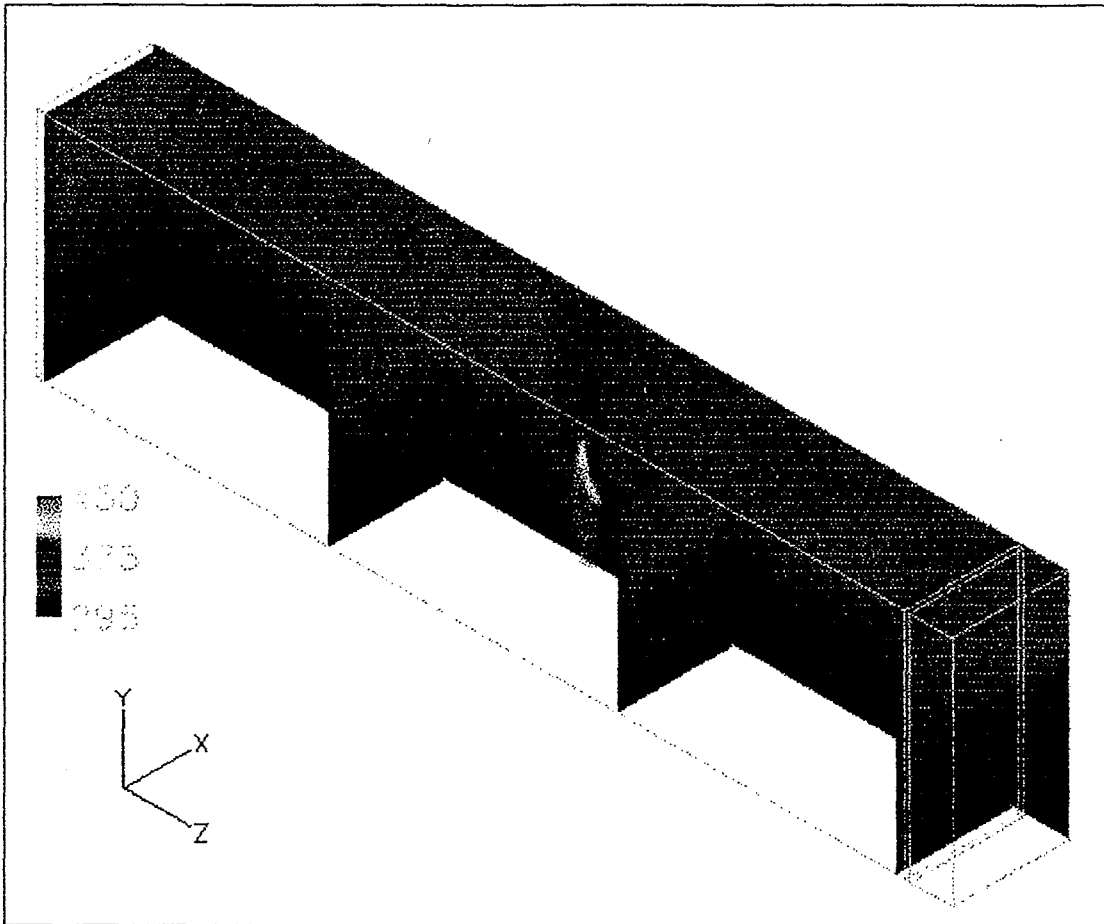
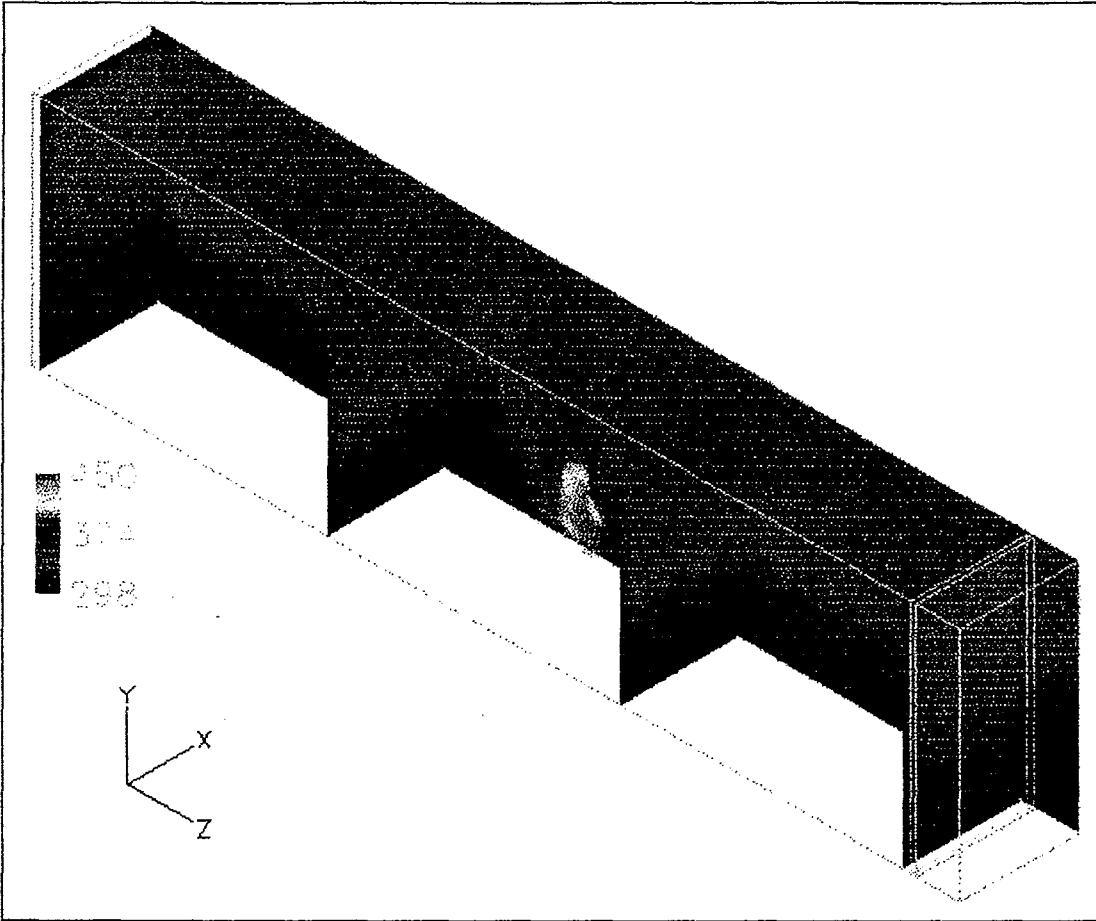


Figure 7.29. Gas temperature profile throughout enclosure 2, centrally-located 300kW fire at 10 minutes.





**Figure 7.30. Gas temperature profile throughout enclosure 2, centrally-located 300kW fire at 20 minutes.**



**Figure 7.31. Gas temperature profile throughout enclosure 2, centrally-located 300kW fire at 30 minutes.**

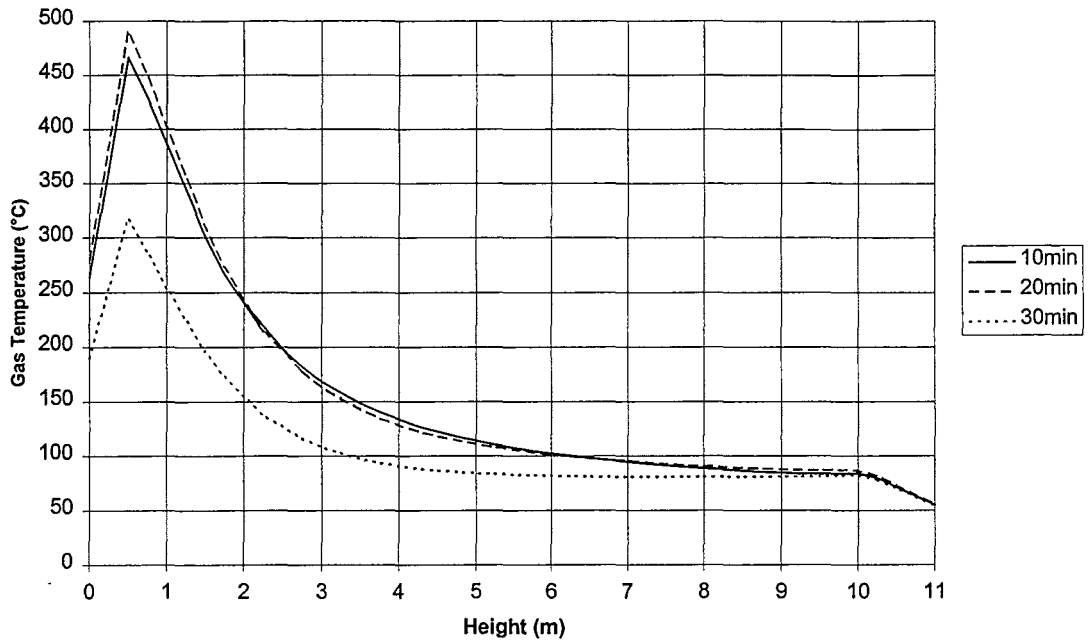


**Figure 7.32. Vertical temperature profile at the fire source centre-line for enclosure 2, centrally-located 300kW fire.**

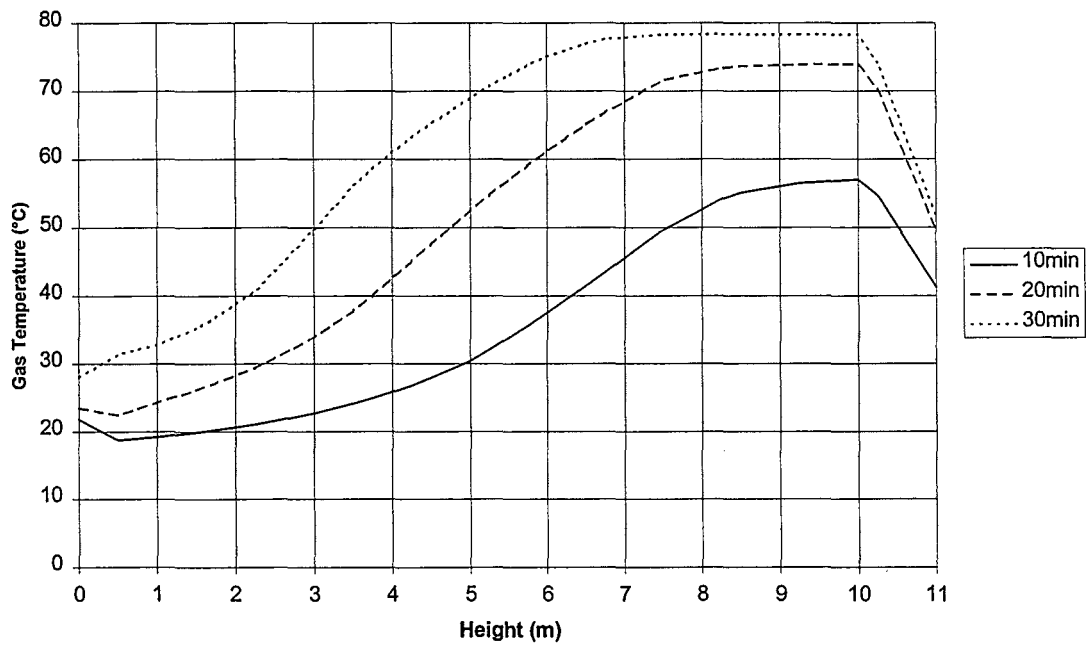


**Figure 7.33. Vertical temperature profile at thermocouple 1 for enclosure 2, centrally-located 300kW fire.**

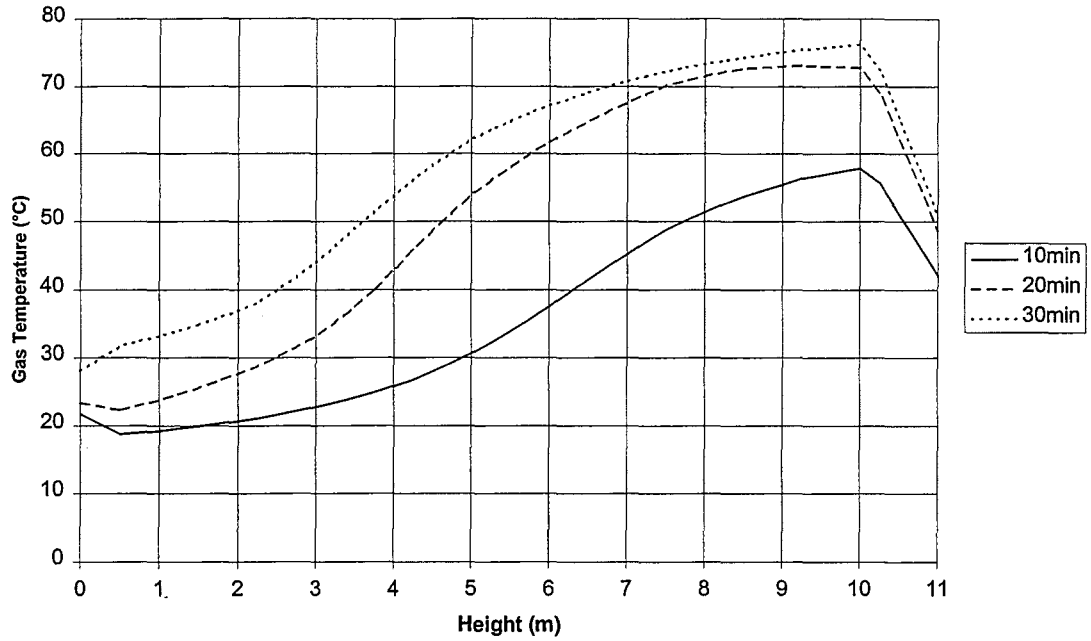


**Figure 7.34. Vertical temperature profile at thermocouple 2 for enclosure 2, centrally-located 300kW fire.**

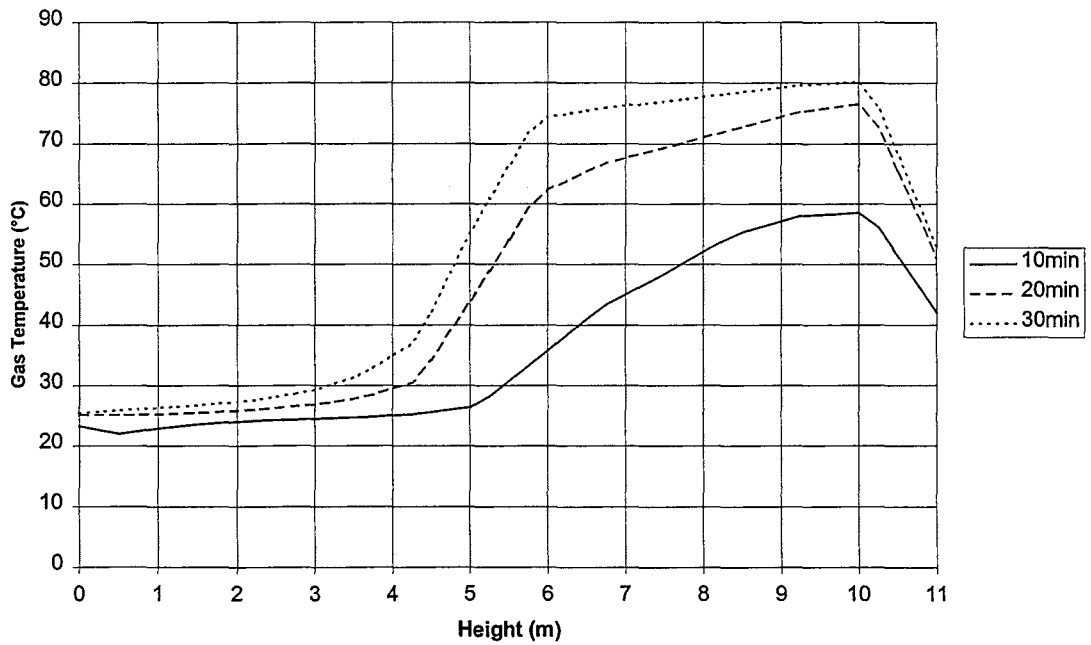


**Figure 7.35. Vertical temperature profile at the vent centre-line for enclosure 2, centrally-located 300kW fire.**

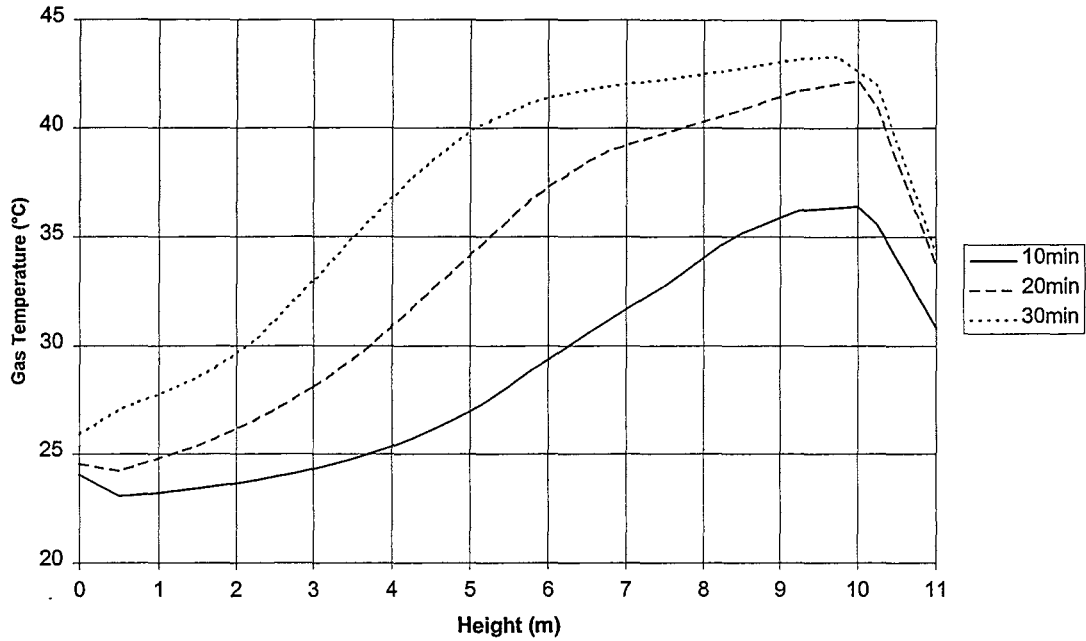


**Figure 7.36. Vertical temperature profile at the corner adjacent to the vent for enclosure 2, centrally-located 300kW fire.**

**Table 7.2. Computer run times required for the CFD simulation of the fires in enclosure 2.**

Heat Release Rate (kW)	Computer Run Time (hours:minutes)
300	114:39
600	122:23
300 - centrally located	144:38

## 7.2.4 Remarks for Enclosure 2

Results for the CFD simulation of three different sized fires have been presented for enclosure 2. These results include post-processor generated visualisation of the temperature profiles throughout the enclosure for each simulation (figures 7.13-7.15, 7.21-7.23, and 7.29-7.31). These visualisations indicate:

1. A **reduced inclination of the fire plume** away from the cool air flowing into the enclosure.
2. A **uniform interface** between relatively hot and cool fluid.
3. A changing or **unsteady-state temperature field with time**.
4. With **increasing heat release rate**, the **temperatures** in the enclosure **increase**.

In addition to the temperature visualisations, temperature profiles are presented for five different locations throughout the enclosure:

- The plume centre-line.
- Two thermocouple locations.
- The doorway centre-line.
- The corner adjacent to the doorway.

These temperature profiles indicate:

1. An **unsteady-state temperature field** in the enclosure.
2. An high gas temperature above the fire source height, followed by a **decrease in gas temperature with increasing height** as cooling of the plume gasses by entrained air occurs.
3. An **increase in temperatures with increasing heat release rate**.
4. The **temperature profiles** at the two thermocouple locations **do not indicate an area of rapidly changing temperature with height**.

Table 7.2 indicates that it took between 114 and 144 hours to complete each 30 minute (real-time fire duration) simulation in this enclosure.

## 7.3 Discussion

### 7.3.1 Enclosure 1

#### 7.3.1.1 Temperature Visualisations

Figures 7.1, 7.5, and 7.9 show the gas temperature profiles throughout half of enclosure 1 after the respective fires have been burning for 20 minutes. There are three key features identifiable in these images, namely:

1. The lying over of the fire plume.
2. Areas of cooler fluid around the edges of the fire plume indicating the entrainment of ambient air into the fire plume.
3. The changing, or non-linear temperature profile throughout the enclosure.

Firstly, the fire source was defined as a velocity inflow of pyrolyzates in the CFD simulations. As the fire burns, a fluid recirculation pattern is developed that causes air to enter the enclosure at the doorway. This air entering the enclosure effectively blows the pyrolyzated fuel away from the fuel source before it is burned and causes both the displacement of the fuel from the fire source and the leaning over of the plume. This phenomena has been previously observed experimentally (Quintiere et al., 1981) and has been investigated numerically (Kumar et al., 1991).

Secondly, as the warm fluid in the fire plume rises due to buoyancy differences with the surrounding fluid, the surrounding fluid is entrained into the plume. This is apparent in the gas temperature profiles (figures 7.1, 7.5, and 7.9) because there are regions surrounding the fire plume with colours signifying lower temperatures.

Thirdly, there does not appear to be a uniform temperature-height relationship throughout the enclosure for the different sized fires (figures 7.1, 7.5, and 7.9), which would thus signify a uniform “hot layer” height. The reason for this is that for this small-sized enclosure, there are large changes in temperature (and fluid density) with small distances away from the fire source.

### 7.3.1.2 General Trends

There are three trends indicated in figures 7.1, 7.5, and 7.9 for the CFD simulations of enclosure 1, namely:

1. The temperature profiles at 5 minutes are very close if not exactly the same as the 20 minute profiles, thus indicating a steady-state situation.
2. The gas temperatures at the locations considered increase with increasing heat release rate.

The fire plume temperature profiles (figures 7.2, 7.6, and 7.10) show that the temperature increases above the fire source, with a maximum temperature occurring at approximately 2.25m. There is no decrease in the gas temperature with height because the amount of air entrained over the height of the enclosure is not sufficient to cool the plume gases.

The centre-line doorway temperature profiles (figures 7.3, 7.7, and 7.11) show that there is an area where the temperature is changing rapidly (the slope of the plot is a maximum (positive) slope) with height. This area of rapid temperature change with height indicates an interface between a lower layer having a relatively constant low gas temperature and an upper layer having a relatively high gas temperature.

The corner temperature profiles (figures 7.4, 7.8, and 7.12) show an almost linear increase in gas temperature with height until a maximum temperature is reached. This maximum temperature remains constant to a height of approximately 2.25m. The temperature then decreases rapidly as the distance to the ceiling decreases. The corner temperature gradients from the floor to ceiling of the enclosure are smaller than for the centre-line doorway location.

Table 7.1 show that it took between 15 and 17 hours of computer processor time to run the simulations for enclosures 1.



## 7.3.2 Enclosure 2

### 7.3.2.1 Temperature Visualisations

Figures 7.13-7.15, 7.21-7.23, and 7.29-7.31 show the gas temperature profiles throughout half of enclosure 2 after the respective fires have been burning for 10, 20, and 30 minutes respectively. There are three key features identifiable in these images, namely:

1. Reduced “lying over” of the fire plume.
2. Areas of cooler fluid around the edges of the fire plume indicating the entrainment of ambient air into the fire plume.
3. The relatively uniform vertical temperature profile throughout the enclosure, and the decrease in layer height with time.

Firstly, because the fire source is not located close to the vent, the air entering the enclosure does not blow the plume over as was observed in enclosure 1.

Secondly, areas of lower fluid temperature are observed near the fire source, indicating entrainment of surrounding air into the plume.

Thirdly, except for near the fire source, there appears to be a uniform temperature-height relationship throughout the enclosure for the different sized fires (see figures 7.13 to 7.15 for example), which would signify a uniform “hot layer” height. The reason for this is that for this sized enclosure, as the distance from the fire source increases, the temperature and density differences are not as significant as near the fire source. The height of this layer decreases as time progresses, and is indicated in figures 7.13-7.15, 7.21-7.23, and 7.29-7.31 by the higher temperatures at decreased heights as time progresses.

The full-scale tests held in this enclosure (Collier, 1997) showed that there was clearly a uniform layer throughout the enclosure, therefore, in terms of the presence of a uniform layer, the CFD simulations qualitatively agree with the full-scale results.

### 7.3.2.2 General Trends

There are four trends indicated in figures 7.13-7.15, 7.21-7.23, and 7.29-7.31 for the CFD simulations of enclosure 2, namely:

1. The temperature profiles at 10, 20, and 30 minutes are different, thus indicating an unsteady-state situation.
2. The gas temperatures at the locations considered increase with increasing heat release rate.
3. The temperature profiles at thermocouple 1, thermocouple 2 and in the corner do not show an area of rapidly changing temperature with height (no clear hot/cold layer interface).

The fire plume temperature profiles (figures 7.16, 7.24, 7.32) show that the temperature increases to a maximum above the fire source, then decreases with increasing height. The decrease in temperature with height is because the entrained air cools the plume gases. In this case, the ceiling height is 11m which provides a large entrainment length over which this cooling can occur.

The centre-line vent temperature profiles (figures 7.19, 7.27, 7.35), as was the case with enclosure 1, show that there is an area where the temperature is changing rapidly (the slope of the plot is a maximum (positive) slope) with height. This area of rapid temperature change with height indicates an interface between a lower layer having a relatively constant low gas temperature and an upper layer having a relatively high gas temperature.

Regarding the temperature profiles for thermocouple 1, 2 and at the corner (figures 7.17, 7.18, 7.20, 7.25, 7.26, 7.28, 7.33, 7.34, and 7.36) there appears to be smearing in the CFD results which prevent the determination of an area where the temperature profile indicates the presence of a layer interface.

Table 7.2 shows that it took between 114 and 144 hours of computer processor time to run the simulations for enclosure 2.

### 7.3.3 Computer Run Time

Tables 7.1 and 7.2 show the computer processor time taken to run the simulations for enclosures 1 and 2 respectively. These tables show that it took between 12 and 17 hours of computer processor time to simulate a 30 minute fire in enclosure 1 and between 114 and 144 hours for enclosure 2.

When these simulation times are compared to the time taken to run the same duration fire in the same enclosures using a zone model is of the order of 2-3 minutes, the time taken to run the CFD model is extremely long.

The run times for enclosure 1 are shorter than for enclosure 2 because the flow field in enclosure 1 reaches a steady-state early in the simulation. The flow field for enclosure 2, by comparison, remains changing throughout the complete simulation which requires a more iterations to converge the solution at each time step.

The amount of time taken for CFD simulations to run is a continuing concern in the CFD community because if CFD simulation techniques are to be ever adopted by the consulting fire engineer, then the run times must decrease to the order of hours, rather than tens or hundreds of hours. Even if CFD does represent a more general and theoretically sound approach to simulating fires, if the computer run time required to reach a solution do not improve, it will be uneconomical for consultants to use.

There is cause for optimism that with further developments in computers, as faster computers with more memory become available, computer run times for CFD simulations will decrease. However, it is impossible, due to the number of calculations performed in a simulation, to hope that CFD run times will ever approach the run times of zone models for the same simulation scenario.

### 7.3.4 Limitations

There are significant limitations in the current CFD analysis which are the combined result of the incomplete explanation of the relevant chemical and physical phenomena within the SOFIE and the trade-off that exists between computer processing time and a more complete model.

The limitations can be grouped together under two headings:

1. Physical sub-model issues.
2. Computational grid issues.

Firstly, the absence of suitable sub-models to quantify physical phenomena is a major limitation of the current analysis and CFD techniques in general. The two main phenomena considered here are thermal radiation and combustion.

Thermal radiation has been dealt with in the current analysis by assuming that 35% of the total heat release rate is lost by the fire, via thermal radiation, to the surrounding environment. This is a crude estimate of the complex processes actually occurring in a fire, but was chosen instead of one of the radiation sub-models available in SOFIE because this is the way that thermal radiation is incorporated into a zone model. This assumption would ease comparisons between the two modelling methods. The absence of a thermal radiation model is most likely to effect the quality of the solution near the fire source because radiation will be the dominant mode of heat transfer in this area where temperatures are high.

The eddy breakup combustion model was adopted in the current analysis, and is, at best, a crude assumption of the combustion process. Therefore, these simulations are subject to the same limitations of the eddy breakup model.

Secondly, “smearing” of the vertical temperature profile can occur when the vertical resolution of the grid is too large to ensure detailed vertical temperature resolution and causes the temperatures to be averaged over the cell height. Should this cell height be large, it is possible that changes in the real temperature profile are not reflected in the averaged temperature profile generated by the CFD code. The fact

that no sensitivity studies of the solution's dependence on grid size is a significant limitation of this work.

Considering the smearing of the vertical temperature profiles for enclosure 2, it is reasonable to assume that if the simulation was re-run using a computational grid having twice the number of cells as the one used for these simulations, the smearing of the vertical temperature profiles would be removed from the solution, and an interface height would be able to be interpreted from the results.



# 8 Comparisons

The purpose of this chapter is to detail the comparisons between the CFD and zone modelling simulations. Comparison will be on the basis of an interface height and the average gas temperature of the upper layer.

## 8.1 Aim

The aim of this chapter is the following:

1. Present the basis and method for comparing the different simulations.
2. Present the results of the comparisons.
3. Discuss the results of the comparisons.

## 8.2 Method

### 8.2.1 Locations for Comparisons

Interface height and average upper layer temperature were compared throughout each enclosure. The location of these comparison points are summarised in table 8.1.

**Table 8.1. Comparison points for each enclosure.**

Enclosure	Location
1	Vent centre-line, and front corner of enclosure
2	Two thermocouple locations, vent centre-line, and front corner of enclosure

The front corner of the enclosure refers to the corner on the same wall as the vent. The temperature profile was recorded in this corner 0.15m from each wall to ensure that the temperature profile in the stagnation point that occurs near a corner was not recorded (see figure 8.1).

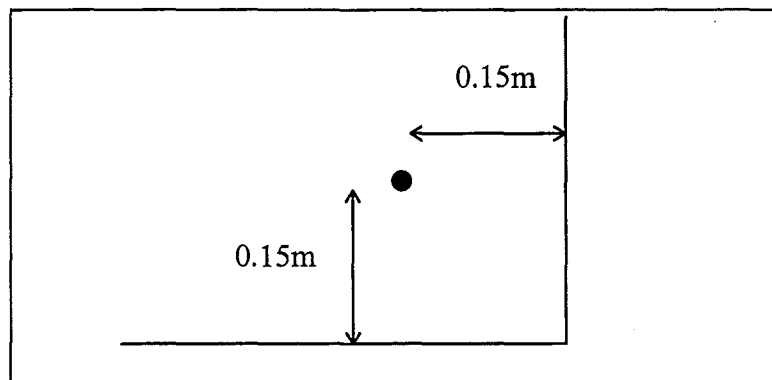


**Figure 8.1. Location of corner temperature measurement (not to scale).**

The locations of the thermocouple trees for enclosure 2 were as per the BRANZ experiments, namely both trees were located along the centre-line of the enclosure and 6m and 15m from the far wall respectively (see figure 8.2).



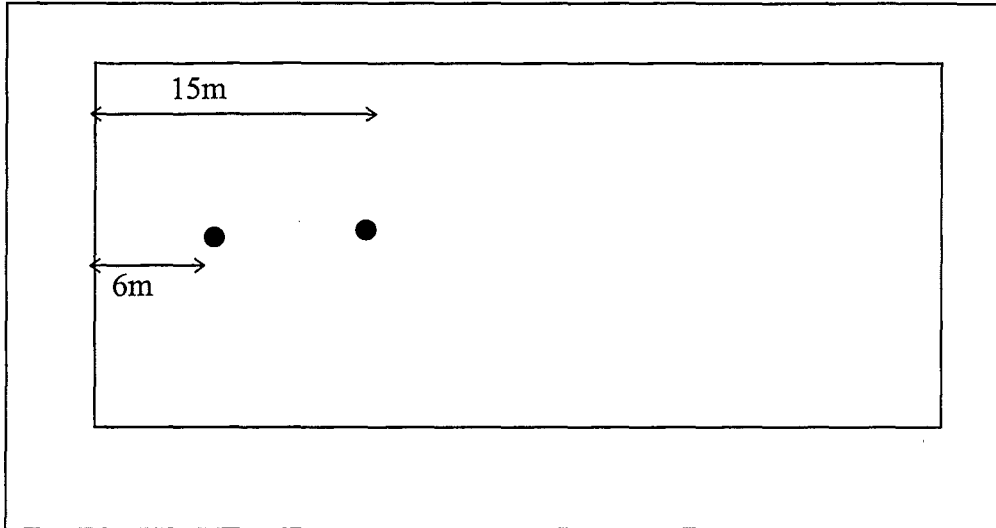


**Figure 8.2. Plan view of the location of the thermocouple trees for enclosure 2 (not to scale).**

## 8.2.2 Interface Height

A CFD model generates a temperature field throughout the computational domain. Unlike a zone model, the CFD model does not generate a “interface height”. Therefore, for comparison purposes, a definition of interface height must be decided upon. Two methods have been used to estimate the location of a hot/cold gaseous interface for this project:

1. Cooper et al.’s N-percent method (Cooper et al., 1982), and
2. a height derivative of temperature method.

### 8.2.2.1 Cooper et al. (1982)

Cooper et al.’s N-percent method was derived for locating the position of the hot/cold layer interface where experimental thermocouple tree data is available.

The method computes a reference upper layer temperature difference  $\Delta T_{ref}$  as per equation 8.1, where  $T(z_{top}, t)$  is the temperature at the top of the thermocouple tree at time  $t$ , and  $T_{amb}(z_{top})$  is the ambient temperature at the top of the thermocouple tree.

$$\Delta T_{ref}(t) = \max[T(z_{top}, t)] - T_{amb}(z_{top}) \quad (8.1)$$

Then, by the N-percent rule, the interface is defined as passing the elevation  $z_i$  when  $z_i$  satisfies equation 8.2:

$$T(z_i, t) - T_{amb}(z_i) = \frac{N\Delta T_{ref}(t)}{100} \quad (8.2)$$

The N-percent method (Cooper et al., 1982) is presented graphically in figure 8.3.

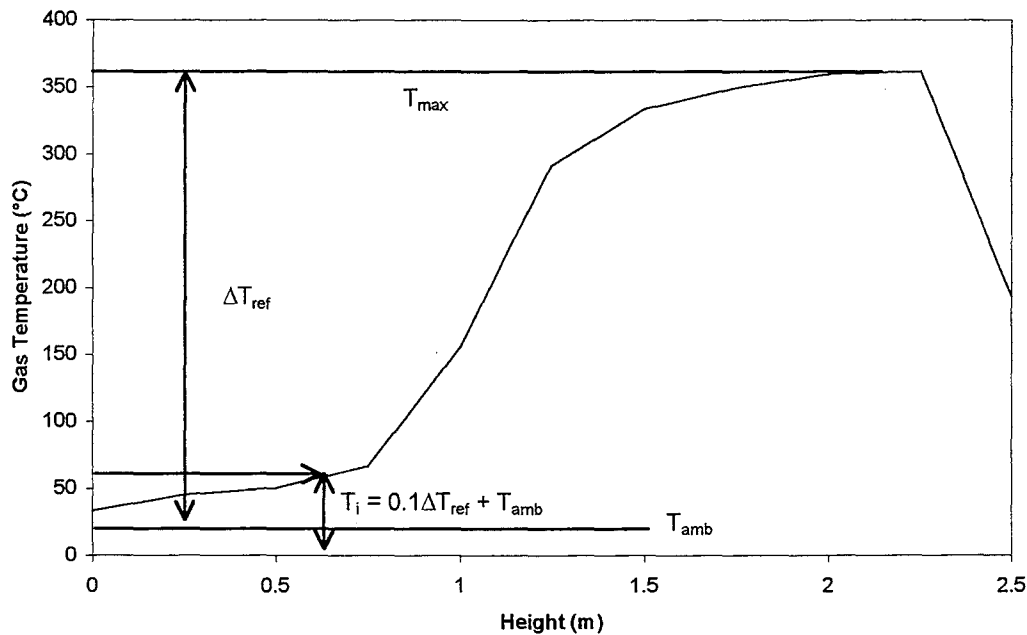


**Figure 8.3. Graphical representation of Cooper et al.'s (1982) N-percent rule at time  $t$ .**

Cooper et al. (1982) state that the rule should only be used where the right-handside of equation 8.2 exceeds some minimum value  $\Delta T_{min}$  where they take  $\Delta T_{min}$  to be  $0.5^\circ\text{C}$ .

Cooper et al. (1982) take  $N$  in equation 8.2 to be 10, and this practise will be followed here.

The interface height derived by the N-percent method (Cooper et al., 1982) is calculated based on the temperature profile in figure 8.3. This profile is constructed from temperature data at vertical intervals of 0.25m, therefore, the uncertainty associated with the value of interface height is  $\pm 0.125\text{m}$ , as no interpolation between points was carried out.

### 8.2.2.2 Height derivative of temperature

This method is used to define where the vertical temperature profile is changing the most rapidly (increasing), thus defining a layer interface. This is achieved by plotting the height derivative of gas temperature ( $dT/dy$ ) versus height, and observing the location of any maxima along this curve.

This method has no theoretical basis other than the anecdotal evidence that there will be a vertical region of high temperature gradient in the location of an interface between relatively hot and cold layers. This method has been previously used by Luo et al. (1997) as a definition of interface height for interpreting the results of CFD simulations.

Figure 8.4 is a gas temperature versus height plot. This plot shows that the maximum slope of the gas temperature plot occurs between 1 and 1.25m. Figure 8.5 shows a plot of  $dT/dy$  versus height derived from the temperature-height information contained in figure 8.4. This plot also indicates a maximum occurring at approximately 1.25m, which is taken to represent an interface location.

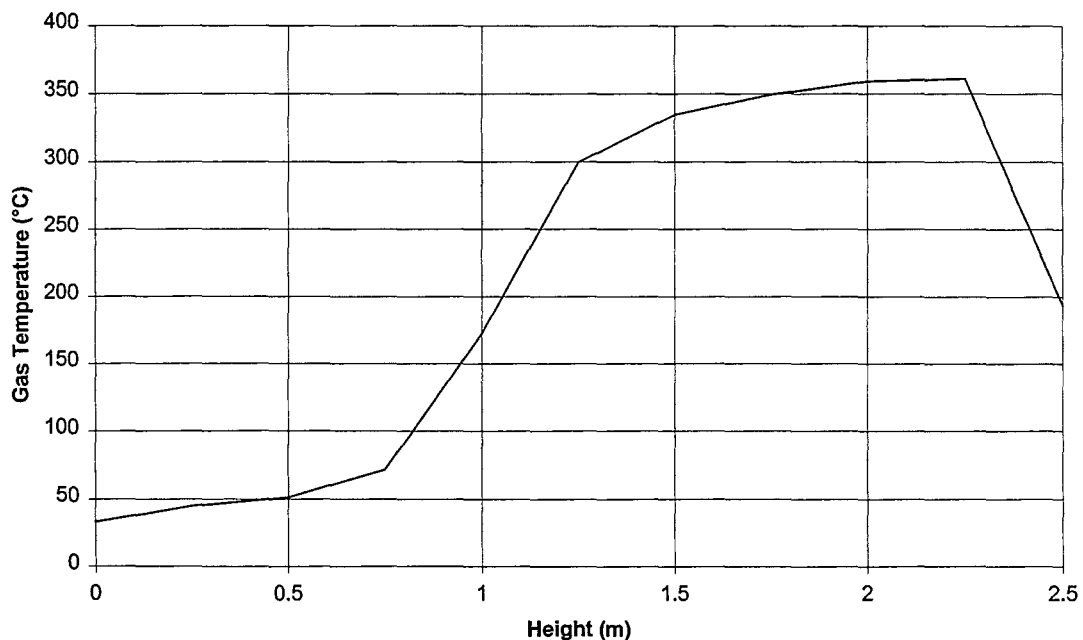


**Figure 8.4. Gas temperature versus height plot used to derive  $dT/dy$  versus height data.**

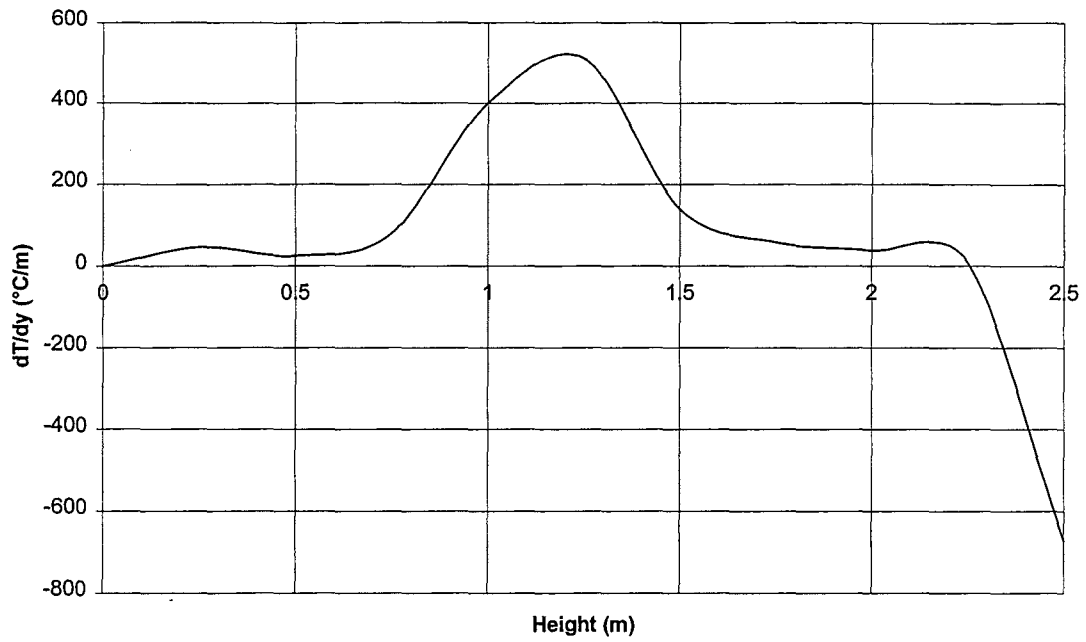


**Figure 8.5.** An example plot of  $dT/dy$  versus height indicating a maximum at approximately 1.25m.

### 8.2.3 Average Upper Layer Temperature

Once the interface location has been defined by one of the two methods above, the temperature profile above the interface height was averaged to yield an average upper layer temperature that was used for comparison purposes.

## 8.3 Results

Results derived from the zone and CFD simulations will be presented for enclosures 1 and 2. These results will compare average upper layer temperature, and interface height at different locations within the enclosures at discrete time intervals. Two different methods of interpreting interface height from CFD results will be used.

Comparisons of doorway centre-line temperature will be made between full-scale data and the CFD simulations for the 330kW fire in enclosure 1.

### 8.3.1 Enclosure 1

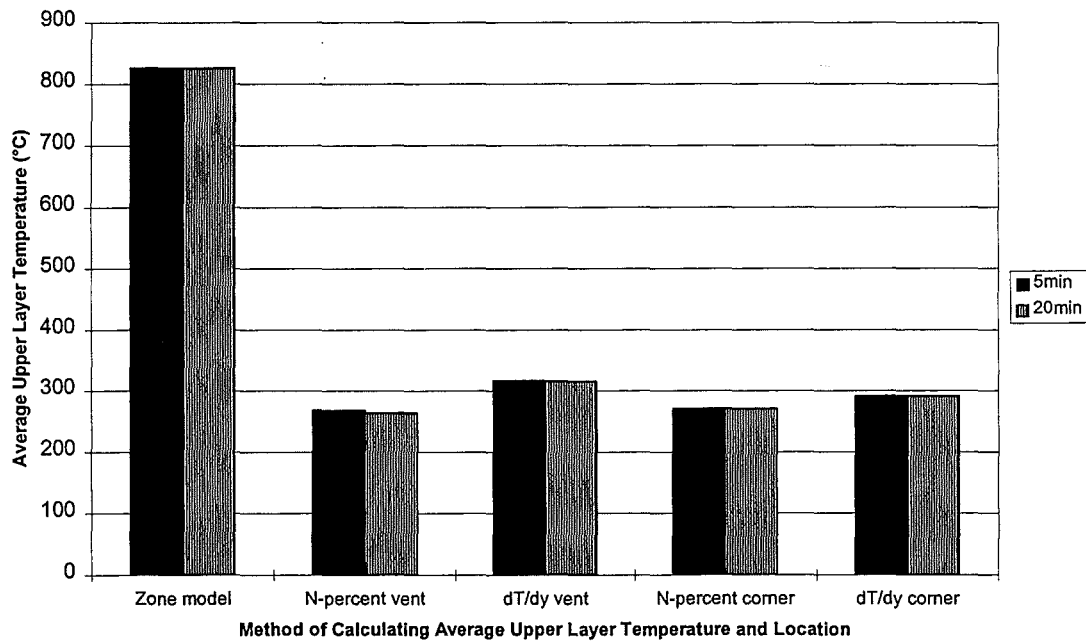


**Figure 8.6. Comparison of average upper layer temperature derived by FAST, N-percent rule, dT/dy for 330kW fire in enclosure 1.**

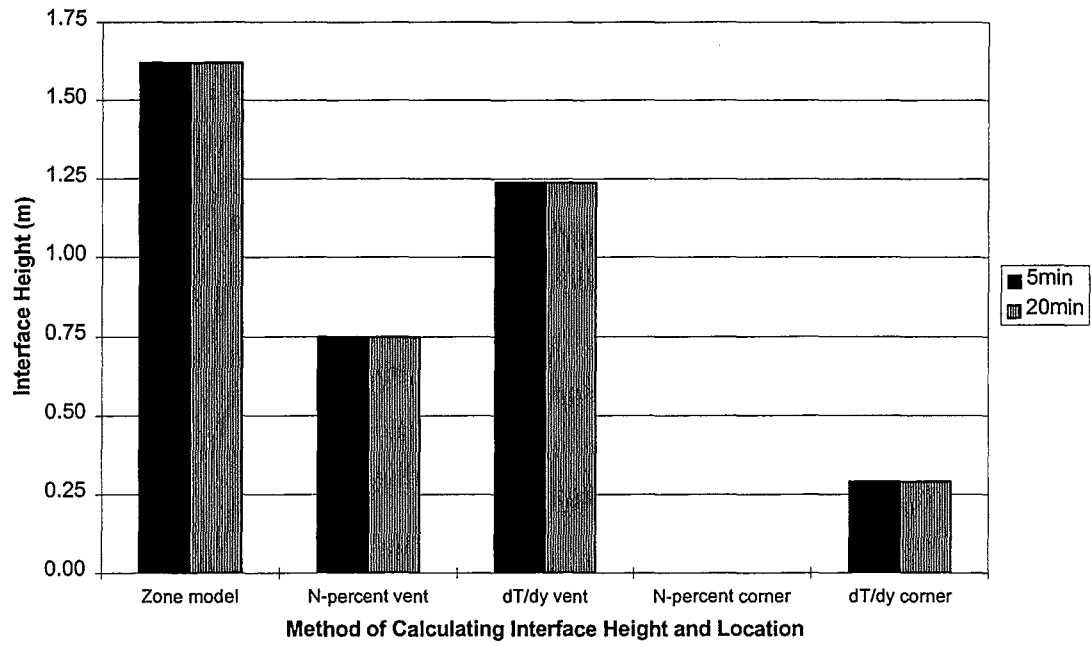


**Figure 8.7. Comparison of interface height derived by FAST, N-percent rule, dT/dy for 330kW fire in enclosure 1.**

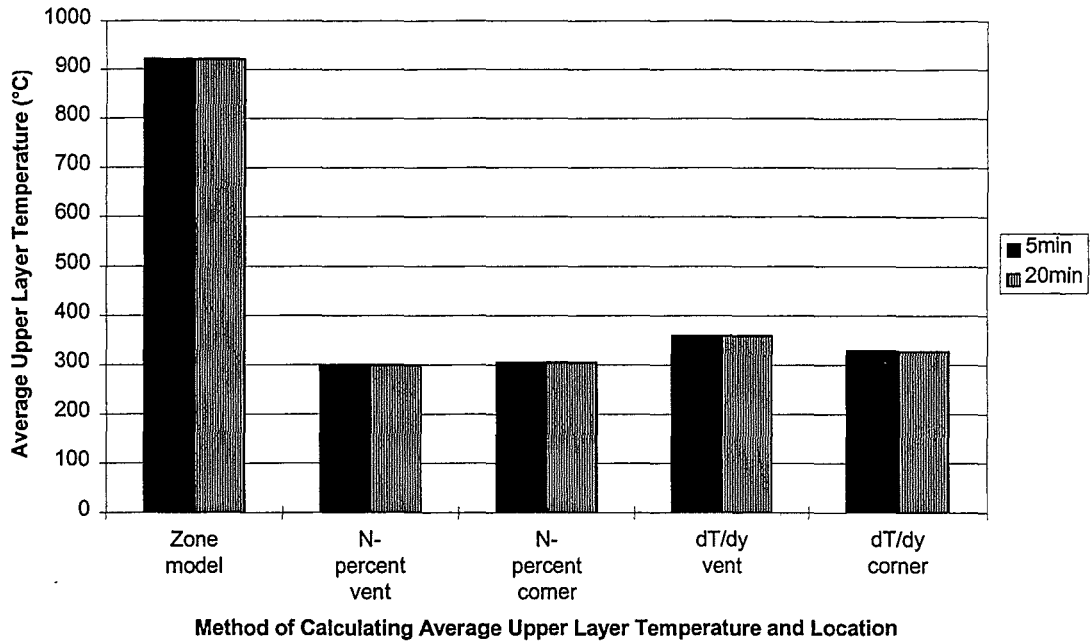


Figure 8.8. Comparison of average upper layer temperature derived by FAST, N-percent rule, dT/dy for 430kW fire in enclosure 1.

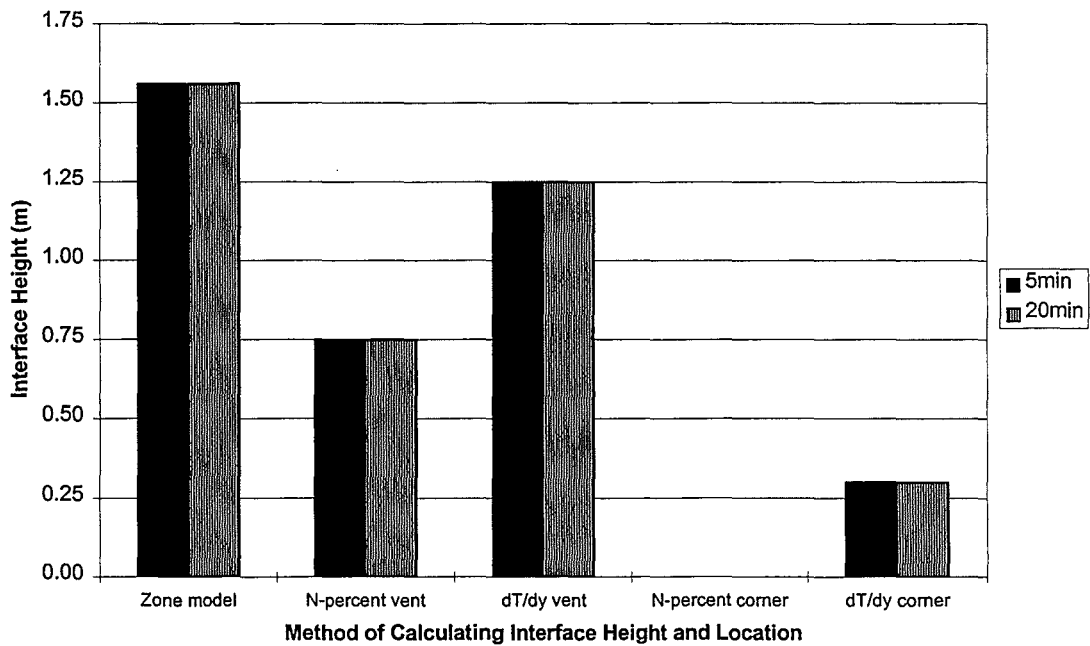


Figure 8.9. Comparison of interface height derived by FAST, N-percent rule, dT/dy for 430kW fire in enclosure 1.

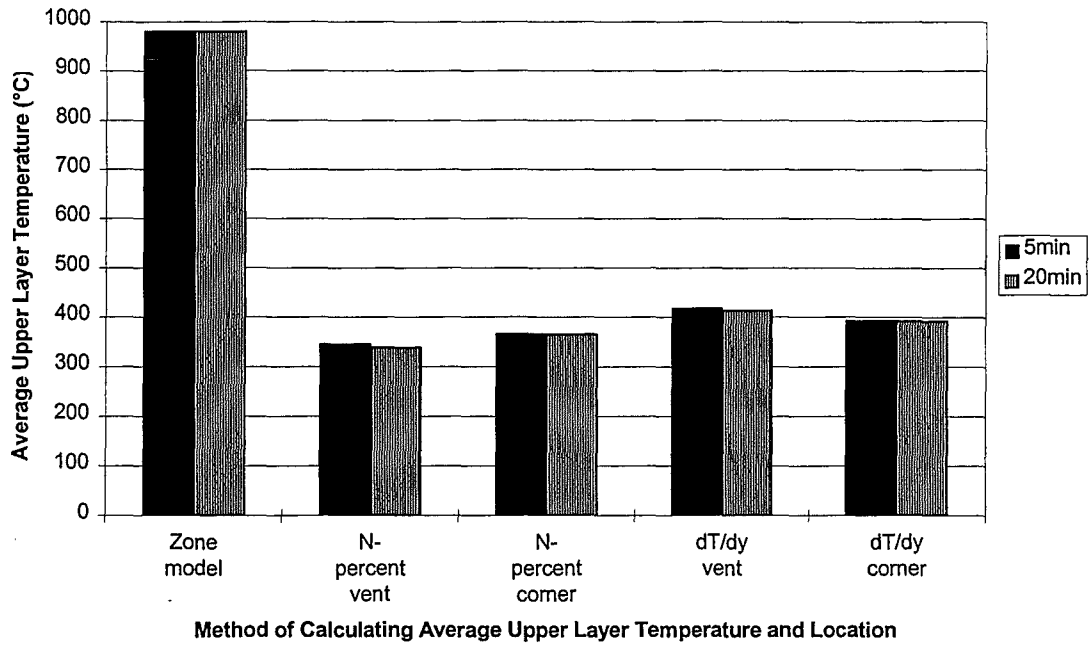


Figure 8.10. Comparison of average upper layer temperature derived by FAST, N-percent rule, dT/dy for 500kW fire in enclosure 1.

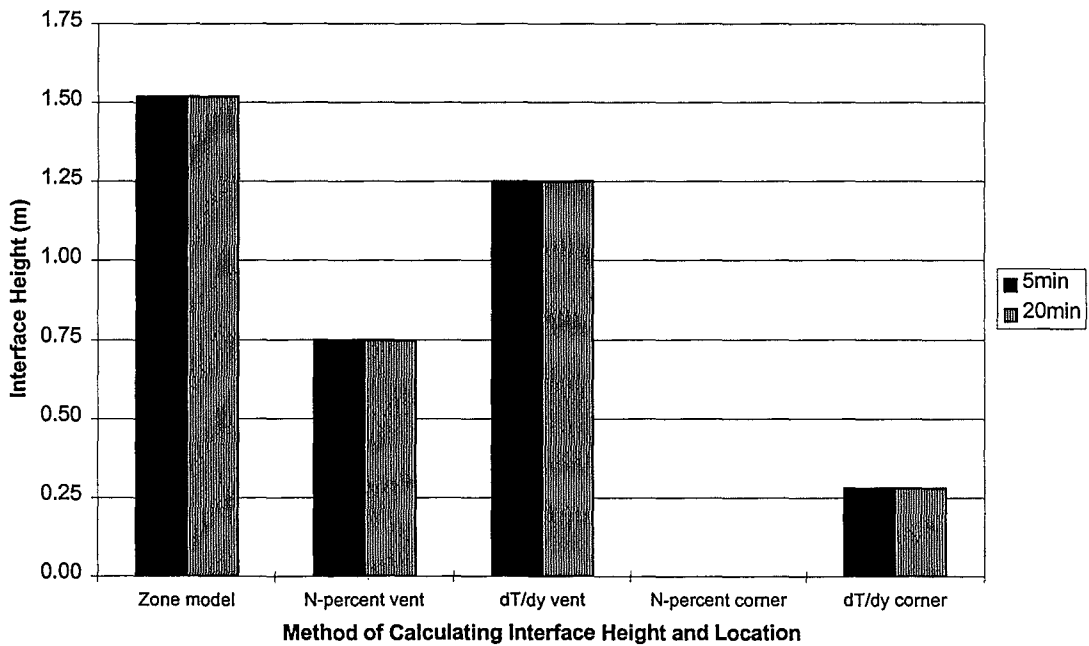


Figure 8.11. Comparison of interface height derived by FAST, N-percent rule, dT/dy for 500kW fire in enclosure 1.



### 8.3.1.1 Summary Results - Enclosure 1

Tables 8.2 and 8.3 list percentage comparisons of average upper layer temperature, and interface height for enclosure 1 for each calculation method in each location. The results are expressed as a percentage of the result from the zone model; a value of less than 100% means the calculation method returned a value less than the zone model.

**Table 8.2. Comparisons of average upper layer gas temperature, based on two different definitions of interface height expressed as percentage of zone model results.**

	Time	N-percent vent	dT/dy vent	N-percent corner	dT/dy corner
1a	5min	32	38	33	35
	10min	32	38	33	35
1b	5min	33	33	39	36
	10min	33	33	39	36
1c	5min	35	37	43	40
	10min	35	37	42	40

**Table 8.3. Comparisons of temperature interface height for N-percent method and dT/dy method expressed as percentage of zone model results.**

	Time	N-percent vent	dT/dy vent	N-percent corner	dT/dy corner
1a	5min	46	76	0	18
	10min	46	76	0	18
1b	5min	48	80	0	19
	10min	48	80	0	19
1c	5min	49	82	0	18
	10min	49	82	0	18

### 8.3.1.2 Remarks

Figures 8.6, 8.8, and 8.10 show average upper layer temperatures derived by FAST, Cooper et al.'s (1982) N-percent method, and the dT/dy method for enclosure 1. These graphs show that the results after 5 minutes are the same as after 20 minutes, indicating a steady-state.

As the heat release rate is increased, the average upper layer temperatures derived by all methods increase. For the methods excluding FAST, the average upper layer temperatures are approximately constant with location in the enclosure. The calculation methods are approximately 30-40% of the FAST results.

Figures 8.7, 8.9, and 8.11 show the interface height derived by FAST, Cooper et al.'s (1982) N-percent method, and the dT/dy method for enclosure 1. These graphs indicate that for the same location in the enclosure, the calculation methods calculate different interface heights. The N-percent (Cooper et al., 1982), and dT/dy calculation methods derives an interface height at the vent centre-line between 50 and 80% of that derived by FAST. For increasing heat release rate (figures 8.7, 8.9, 8.11), the interface height remains approximately constant.

At the corner, an interface height of 0 was derived using the N-percent method (Cooper et al., 1982). The physical significance of this is that the N-percent method (Cooper et al., 1982) calculated an interface temperature which was greater than the temperature at the floor level.

### 8.3.2 Enclosure 2

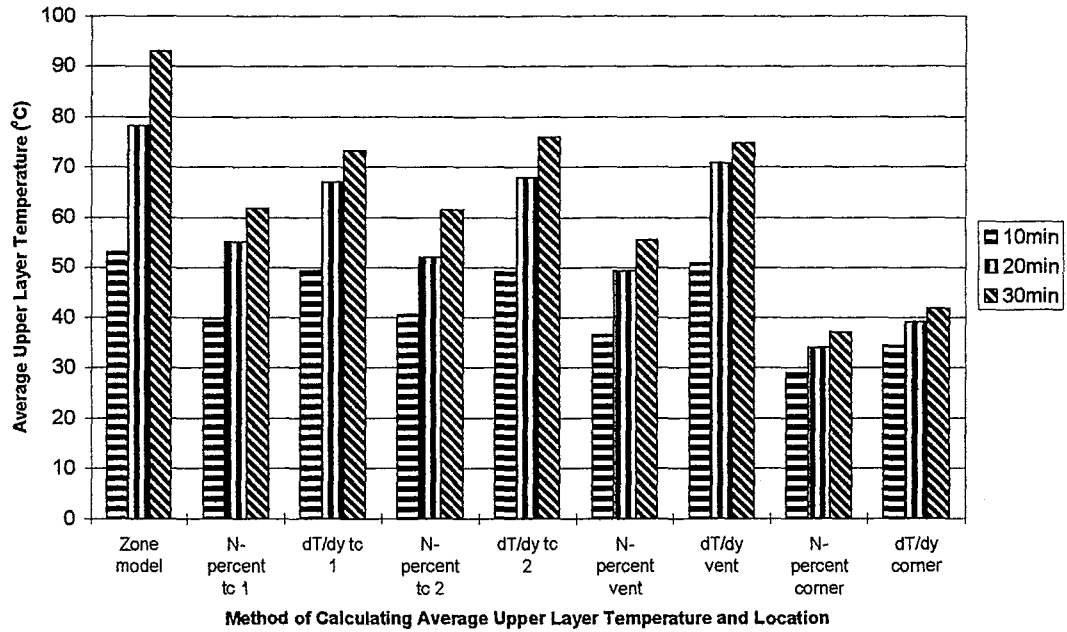


Figure 8.12. Comparison of average upper layer temperature derived by FAST, N-percent rule, dT/dy for 300kW fire in enclosure 2.

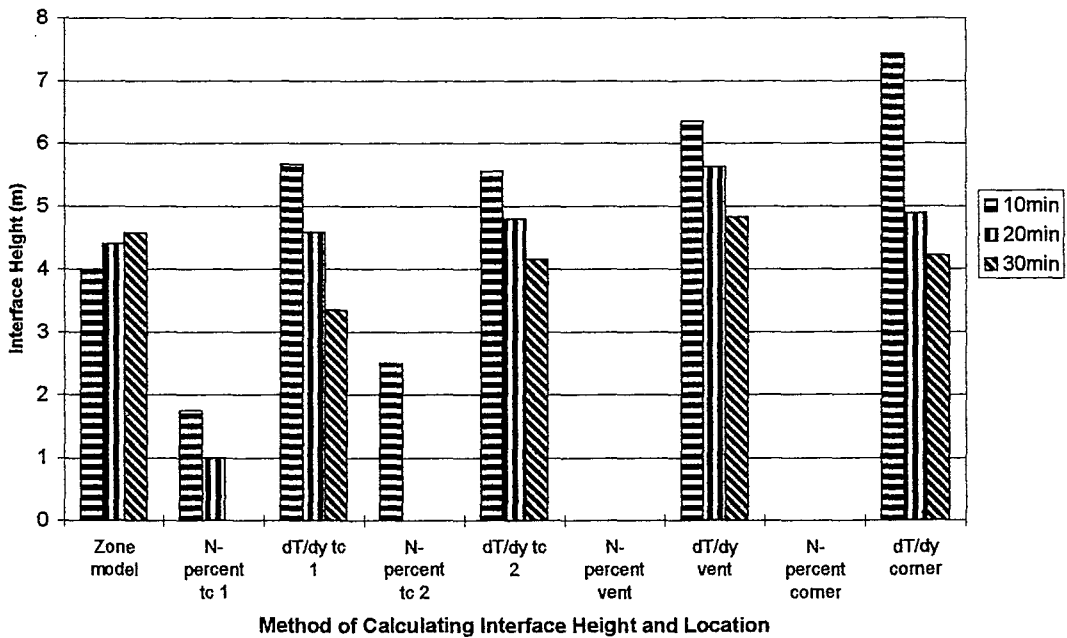


Figure 8.13. Comparison of interface height derived by FAST, N-percent rule, dT/dy for 300kW fire in enclosure 2.

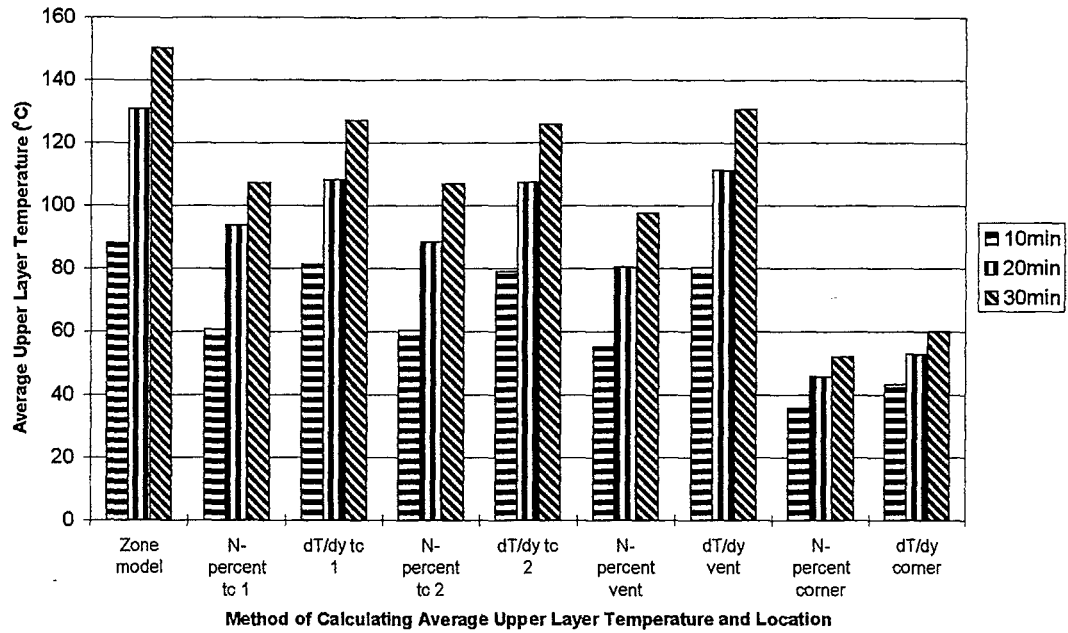


Figure 8.14. Comparison of average upper layer temperature derived by FAST, N-percent rule, dT/dy for 600kW fire in enclosure 2.

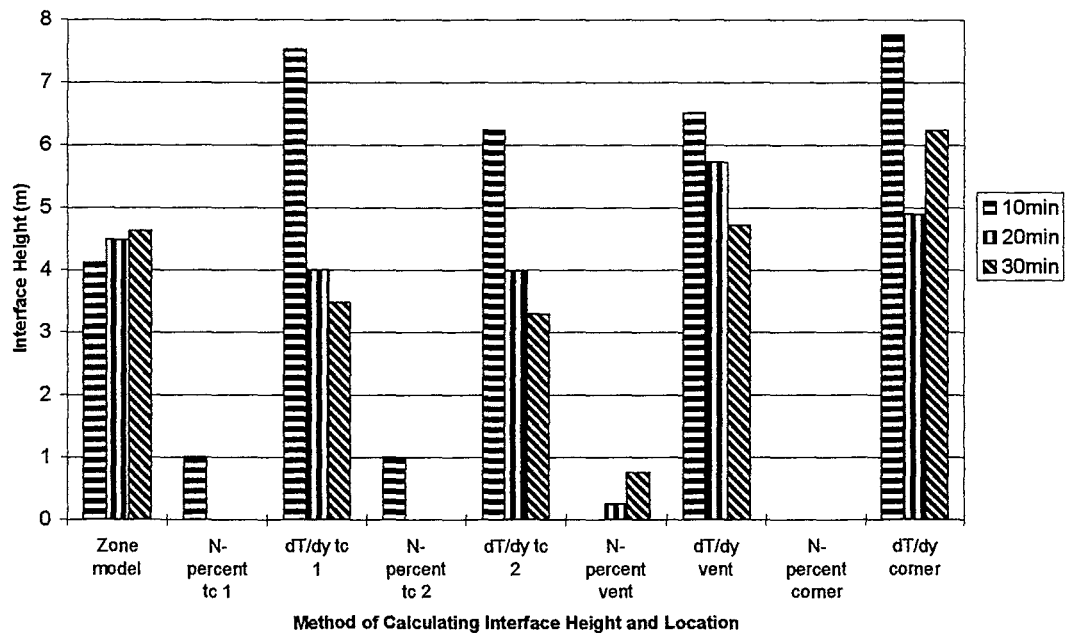


Figure 8.15. Comparison of interface height derived by FAST, N-percent rule, dT/dy for 600kW fire in enclosure 2.

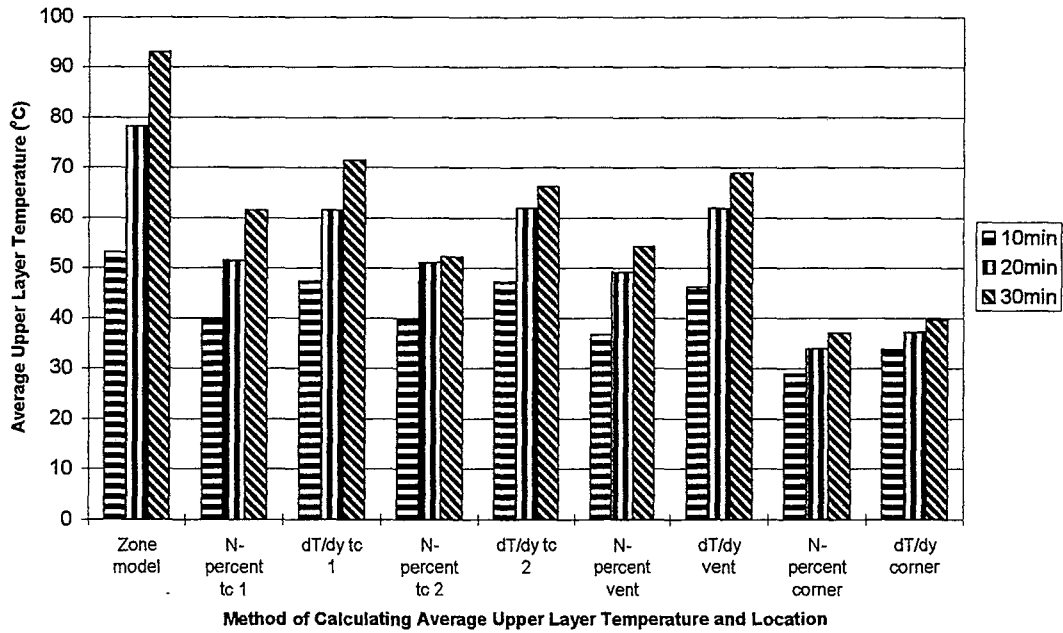


Figure 8.16. Comparison of average upper layer temperature derived by FAST, N-percent rule, dT/dy for a centrally-located 300kW fire in enclosure 2.

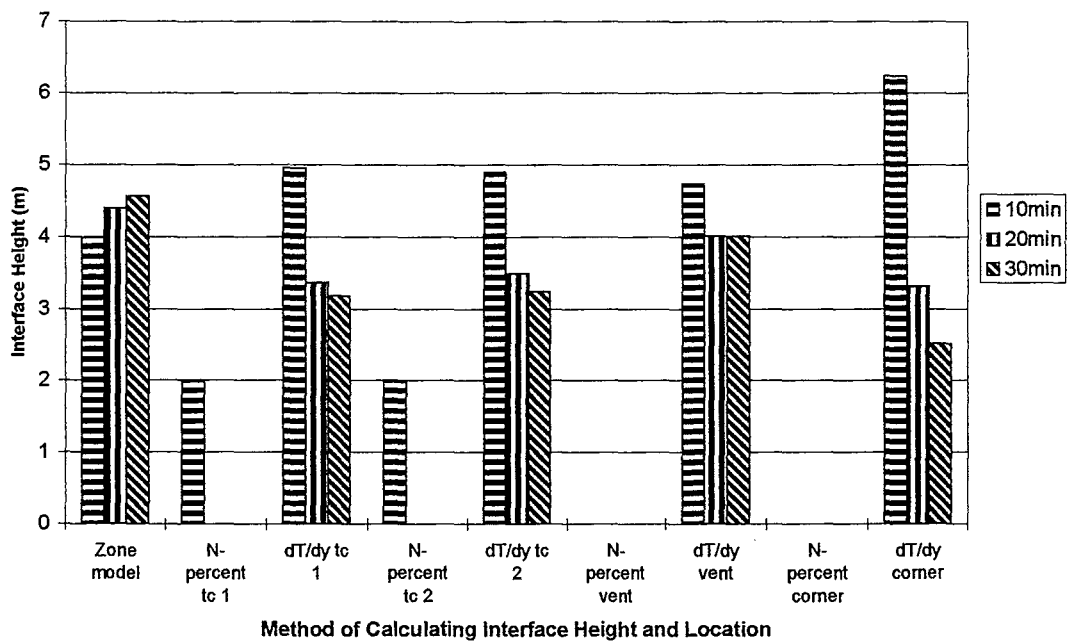


Figure 8.17. Comparison of interface height derived by FAST, N-percent rule, dT/dy for a centrally-located 300kW fire in enclosure 2.

### **8.3.2.1 Summary Results - Enclosure 2**

Table 8.5 and 8.6 list percentage comparisons of interface height and average upper layer temperature for enclosure 2 for each calculation method in each location. The results are expressed as a percentage of the result from the zone model; a value of less than 100% means the calculation method returned a value less than the zone model.

**Table 8.4. Comparisons of average upper layer gas temperature, based on the N-percent method definition of interface height expressed as percentage of zone model results.**

	Time	N-percent tc 1	dT/dy tc 1	N-percent tc 2	dT/dy tc2	N-percent vent	dT/dy vent	N-percent corner	dT/dy corner
2a	10min	75	93	77	93	69	96	54	65
	20min	71	86	67	87	63	91	44	50
	30min	66	79	66	82	60	80	40	45
2b	10min	69	92	69	90	63	91	41	49
	20min	72	83	67	82	61	85	35	40
	30min	71	85	71	84	65	87	35	40
2c	10min	75	89	75	89	69	87	54	64
	20min	66	79	65	79	63	79	43	48
	30min	66	77	56	71	58	74	40	43



**Table 8.5. Comparisons of temperature interface height for N-percent method and dT/dy method expressed as percentage of zone model results.**

Time	N-percent	dT/dy	N-percent	dT/dy	tc	N-percent	dT/dy	N-percent	dT/dy
	tc 1	tc 1	tc 2	2	vent	vent	corner	corner	
2a 10min	44	142	63	140	0	160	0	186	
20min	23	104	0	109	0	128	0	111	
30min	0	73	0	91	0	106	0	92	
2b 10min	24	183	24	152	0	159	0	189	
20min	0	89	0	89	6	128	0	109	
30min	0	75	0	71	16	102	0	135	
2c 10min	50	125	50	123	0	119	0	157	
20min	0	77	0	79	0	91	0	75	
30min	0	70	0	71	0	88	0	55	

### 8.3.2.2 Remarks

Figures 8.12, 8.14, and 8.16 show average upper layer temperatures derived by FAST, the N-percent method (Cooper et al., 1982), and the dT/dy method for enclosure 2. These graphs show that the results after 10, 20 and 30 minutes are all different, which indicates an unsteady-state.

There appears to be reasonable agreement in average upper layer temperature derived by all three calculation methods in all locations except the corner. All three calculation methods predict that the average upper layer temperature will increase in the enclosure with increasing time. Ignoring the comparison at the corner, the calculation methods are between 56 and 96% of the FAST results for all heat release rates.

Figures 8.13, 8.15, and 8.17 show the interface height derived by FAST, the N-percent method (Cooper et al., 1982), and the dT/dy method for enclosure 2. As time increases, FAST predicts that the interface height will increase; the dT/dy method predicts that the interface height will decrease. The N-percent method (Cooper et al., 1982) does not consistently predict an interface height and, therefore, no trend can be assessed.

Figures 8.13, 8.15, and 8.17 also indicate that for the same location in the enclosure, the calculation methods calculate different interface heights. FAST derives an interface height which is generally less than the dT/dy method throughout the enclosure. The dT/dy method predicts an approximately uniform layer height for all heat release rates at all locations except the corner, with the exceptions of the vent centre-line and corner for the 600kW fire and the centrally-located 300kW fire.

## **8.4 Discussion**

### **8.4.1 Enclosure 1**

The performance of the zone model FAST (Peacock et al., 1997) shall be compared to the CFD model based on the average upper layer temperature and interface height.

#### **8.4.1.1 Average Upper Layer Temperature**

The average upper layer temperature derived by the N-percent method (Cooper et al., 1982) and the  $dT/dy$  method are between 30 and 40% of the average upper layer temperature predicted by FAST. This is a significant result and shows that FAST overpredicts the average upper layer temperature for these cases.

The FAST zone model has been shown previously to accurately simulate the upper layer temperatures for the fires considered here when the boundaries were assumed to be non-adiabatic (Dembsey et al., 1995). Therefore, it is postulated that FAST has difficulty in simulating the fires considered here because of the assumption that all boundaries were adiabatic; FAST will produce high average upper layer temperatures for cases where heat losses through the boundaries would be significant. This condition is most likely to be relevant where the volumetric heat release rate in the enclosure is large, i.e., the heat release rate divided by the total volume of the enclosure, as temperature gradients across boundaries are likely to be greater, thus conductive losses through boundaries will be greater. Therefore, the assumption of adiabatic boundaries for this enclosure is not sufficient for accurate comparison between the zone and CFD simulation results.

#### **8.4.1.2 Interface Height**

The interface height derived by the N-percent method (Cooper et al., 1982) and the  $dT/dy$  method was between 50 and 80% of the interface height predicted by FAST. The interface heights derived by the N-percent method (Cooper et al., 1982)

and the  $dT/dy$  method was a function of the location within the enclosure and therefore indicated, unlike FAST, that there was no single interface height throughout the enclosure.

The method by which the interface height was estimated from the CFD results effects the comparison - the interface height predicted by the  $dT/dy$  method was always closer to the FAST prediction than the N-percent method (Cooper et al., 1982).

## **8.4.2 Enclosure 2**

### **8.4.2.1 Average Upper Layer Temperature**

The average upper layer temperature derived by the N-percent method (Cooper et al., 1982) and the  $dT/dy$  method was between 56 and 96% of the average upper layer temperature predicted by FAST. This shows that for these cases in this enclosure the comparison of average upper layer temperature is favourable between the zone and CFD model. The comparisons were more favourable for this sized-enclosure because the volumetric heat release rate was smaller than for enclosure 1, thus conductive losses through the boundaries were less significant.

### **8.4.2.2 Interface Height**

The interface height derived by the N-percent method (Cooper et al., 1982) and the  $dT/dy$  method was between 0 and 183% of the interface height predicted by FAST at all locations throughout the enclosure except at the vent centre-line and the corner. In contrast to enclosure 1, the interface heights derived by the N-percent method (Cooper et al., 1982) and the  $dT/dy$  method were relatively constant with changing location within the enclosure and therefore indicate that there was a more uniform interface layer throughout the enclosure than in enclosure 1.

The interface height at the vent centre-line predicted by the N-percent method (Cooper et al., 1982) and the  $dT/dy$  method was between 0 and 160% of the interface height predicted by FAST. Generally, the interface height predicted by the  $dT/dy$  method was higher than the interface height predicted by FAST.

The method by which the interface height was estimated from the CFD results effects the comparison - the interface height predicted by the  $dT/dy$  method

was always closer to the FAST prediction than the N-percent method (Cooper et al., 1982).

### 8.4.3 Overall

#### 8.4.3.1 Cooper et al.'s (1982) N-Percent Method

The method described by Cooper et al. (1982) to define interface height is not acceptable for use in CFD comparison work. There are two main reasons for this:

1. The lack of any theoretical basis in the approach.
2. The relatively poor performance of this method in the comparisons presented here.

Firstly, due to the nature of the N-percent method (Cooper et al., 1982), the interface temperature defined by the method has no physical significance; it is little more than a guess, and any experimental validation of the accuracy of the approach is fortunate (e.g., Cooper et al., 1982).

Secondly, in the comparisons presented above, the N-percent method (Cooper et al., 1982) performed poorly in two different scenarios:

1. Predicting an interface height in the corner of enclosure 1 and throughout enclosure 2.
2. Predicting the trend in decreasing interface height with increasing time for a given location within an enclosure.

It is apparent that the N-percent method (Cooper et al., 1982) requires a larger temperature difference between the gas temperature at the ceiling and the gas temperature at the floor than Cooper et al. (1982) acknowledge. In the case where the N-percent method (Cooper et al., 1982) predicts an interface height at the floor level, the temperature gradient from the floor to the ceiling is obviously too small (see tables 8.3 and 8.5), because when the N-percent method (Cooper et al., 1982) predicts an interface at the floor level, the temperature which is calculated to correspond to the temperature at the interface is greater than the temperature at the floor level. For these cases where the N-percent method (Cooper et al., 1982) failed to predict an interface (i.e., an interface, defined by Cooper et al. (1982), occurs at the floor), the temperature gradient from floor to ceiling was of the between 300 and 400°C for enclosure 1, and 20 and 30°C for enclosure 2.

Therefore, for the two enclosures considered here, it is evident that the N-percent method (Cooper et al., 1982) of defining interface height should not be used in locations where the temperature gradient from the floor to the ceiling is not greater than 300-400°C for an enclosure measuring 3.7x2.5x2.5m, and 20-30°C for an enclosure measuring 41x11x11m.

The second area where the N-percent method (Cooper et al., 1982) performed poorly was in the prediction of the general trend of decreasing interface height with increasing time at a given location within the enclosure. Because enclosure 1 was at a steady-state at the times considered, this discussion only refers to the performance for the unsteady-state in enclosure 2.

The post-processor visualisations of the temperature profiles throughout enclosure 2 with increasing time clearly show that as time goes by the temperatures increase throughout the enclosure, this would indicate that an interface height would decrease with time; i.e., the layer depth increases with time. This trend was not clearly evident in the predictions of layer height using the N-percent method (Cooper et al., 1982) (see figures 8.12, 8.14, and 8.16). At some locations the interface height decreased with time while in others it did not. In general, the ability to observe and assess trends is affected by the N-percent method (Cooper et al., 1982) not being able to consistently predict an interface height.

In light of the performance of the N-percent method (Cooper et al., 1982) for predicting interface height, the  $dT/dy$  method seems to be a preferable definition for the following reasons:

1. The  $dT/dy$  concept has some physical meaning and interpretation.
2. The  $dT/dy$  method predicted a decrease in interface height with time, as demonstrated by the CFD temperature images.
3. The  $dT/dy$  method is easy to compute for any given temperature profile.



# 9 Conclusions

Zone and CFD fire modelling techniques have been used to simulate three different sized fires in two different sized enclosures:

1. A domestic-sized enclosure measuring 3.7m long x 2.5m wide x 2.5m high.
2. An industrial-sized enclosure measuring 41m long x 11m wide x 11m high.

The fire sizes simulated were 330, 430, and 500kW for the domestic-sized enclosure and 300, and 600kW for the industrial-sized enclosure.

The results of these simulations have been compared based on interface height and average upper layer temperature.

## 9.1 Conclusions from the Zone Modelling Simulations

1. When the enclosure boundaries are assumed to be adiabatic, compared to full-scale results and CFD simulations, zone models over-predict the average upper layer temperature for cases where the volumetric heat release rate is large.
2. Computer run times for simulating fires in enclosures using zone modelling are of the order of minutes.

## 9.2 Conclusions from the CFD Simulations

1. CFD simulations take between 300 and 3000 times as long to reach a solution as an equivalent zone model simulation.
2. Limitations of the CFD solution, including the sensitivity of the solution to the fineness of the grid and the physical sub-models of combustion and thermal radiation, need to be addressed in the future.

## 9.3 Conclusions from the Comparisons

1. The results of the comparisons between zone and CFD simulation results is highly dependant on the definition chosen to represent the interface height.
2. For the domestic-sized enclosure:
  - The CFD results derived average upper layer temperatures between 30 and 40% of the average upper layer temperature derived by the zone model.
  - The CFD results indicated that the interface height was between 50 and 80% of the interface height derived by the zone model.
3. For the industrial-sized enclosure:
  - The CFD results derived average upper layer temperatures between 56 and 96% of the average upper layer temperature derived by the zone model.
  - The CFD results indicated that the interface height was between 0 and 183% of the interface height derived by the zone model.
  - Generally, the interface height predicted by the CFD model was higher than the interface height predicted by the zone model.
4. The N-percent method (Cooper et al., 1982) of defining interface height is not recommended for defining interface height in CFD simulations because:
  - The method did not consistently predict an interface height in locations of small temperature gradient from floor to ceiling.
  - The method failed to predict a decreasing interface height with time.
5. The  $dT/dy$ , height derivative of temperature method is recommended for defining interface height in CFD simulations because:
  - The method has physical meaning.
  - The method successfully predicts a decrease in interface height with time.
  - The method is easy to compute for any given temperature profile.

## **9.4 Further Research**

### **Comparison-related Issues**

1. Further comparisons of both zone and CFD models against full-scale fire test results must be made.
2. A suitable basis for defining layer height in CFD work should be agreed upon and tested against full-scale test results.
3. Simulations that investigate the issue of geometry such as enclosures having high aspect ratios and irregular shaped-geometries should be used for comparison with zone models.

### **CFD-related Issues**

1. The sensitivity of the solution's dependence on grid size needs to be investigated.
2. The flow field at a finer post-processing time resolution (smaller time-step) should be investigated.
3. A thermal radiation sub-model, and non-adiabatic boundaries needs to be included in the simulation and the subsequent effect on the quality of the solution determined.



# 10 Nomenclature

$A$	area
$c$	specific heat
$D$	diffusion coefficient
$E$	activation energy
$f$	mixture fraction
$Fr$	Froude number
$g$	acceleration due to gravity
$G$	turbulence constant
$h$	enthalpy
$H$	heat
$J$	diffusion flux
$k$	thermal conductivity, turbulent kinetic energy
$l$	length scale
$M$	molecular mass
$N$	number of cells/grid points, N-percent factor
$p, P$	pressure
$Pe$	Peclet number
$q, Q$	heat
$R$	Universal gas constant
$s$	stoichiometric oxidiser/fuel ratio
$S$	source term
$t$	time
$T$	temperature
$u$	velocity
$x$	space dimension
$Y$	mass fraction

$z$  interface height

### **Greek Symbols**

$\beta$  Schwab Zeldovich variable  
 $\delta$  Kronecker delta  
 $\Delta$  "change in"  
 $\Gamma$  exchange coefficient  
 $\varepsilon$  rate of dissipation of turbulent kinetic energy  
 $\sigma$  Prandtl/Schmidt numbers  
 $\tau$  time scale, Reynolds stress tensor  
 $\mu$  dynamic viscosity  
 $\nu$  kinematic viscosity  
 $\rho$  mass density  
 $\phi$  general variable

### **Superscripts**

$\cdot$  time derivative  
 $\text{—}$  time average  
 $'$  unsteady variable  
 $"$  density-weighted unsteady variable

### **Subscripts**

$i, j, k$  Cartesian coordinate directions  
amb ambient  
B buoyancy  
c convective, combustion  
f fuel  
i interface  
max maximum  
min minimum  
o oxidant  
p products

# 11 References

ALPERT, R. L. (1972) Calculation of Response Time of Ceiling-Mounted Fire Detectors, *Fire, Tech.*, **8**, 181

ALPERT, R. L., and WARD, E. J. (1983) *Evaluating Unsprinklered Fire Hazards*, SFPE Technology Report 83-2, Society of Fire Protection Engineers, Boston, USA.

BIA (1992) *New Zealand Building Code and Approved Documents*, Building Industry Authority, Wellington, New Zealand.

BILGER, R. W. (1994) Computational Field Models in Fire Research and Engineering, *Proc. Fourth International Symp. Fire Safety Science*, 95-110.

BUCHANAN, A. H. (1994) Fire Engineering for a Performance Based Code, *Fire Safety J.*, **23**, 1-16.

CHOU, P. Y. (1945) On Velocity Correlations and the Solution of the Equations of Turbulent Fluctuations, *Q. Appl. Math.*, **3**, 38-54; **3**, 198.

COLLIER, P. C. (1997) Modelling Fires in Large Spaces, *BUILD magazine*, **42**, 38-39.

COOPER, L. Y., HARKLEROAD, M., QUINTIERE, J., and RINKINEN, W. (1982) An Experimental Study of Upper Hot Layer Stratification in Full-Scale Multitroom Fire Scenarios, *J. Heat Transfer*, **104**, 741-749.

COX, G. (1995a) *Basic Considerations*, in *Combustion Fundamentals of Fire*, Academic Press, London, United Kingdom.

COX, G. (1995b) *Compartment Fire Modelling*, in *Combustion Fundamentals of Fire*, Academic Press, London, United Kingdom.

COX, G. and CHITTY, R. (1982) Some Stochastic Properties of Fire Plumes, *Fire and Materials*, **6**, 127.

COX, G., KUMAR, S., and MARKATOS, N. C. (1985) Some Field Model Validation Studies, *Proc. First International Symp. Fire Safety Science*, 159-171.

DAVIS, W. D., NOTARIANNI, K. A., and McGRATTAN, K. B. (1996) *Comparison of Fire Model Predictions with Experiments Conducted in a Hangar with a 15 metre Ceiling*, NISTIR 5927, National Institute of Standards and Technology, Gaithersburg, Maryland, USA.

DAVIS, W. D., FORNEY, G. P., and BUKOWSKI, R. W. (1997) Developing Detector Siting Rules from Computational Experiments in Spaces with Complex Geometries, *Fire Safety J.*, **29**, 129-139.

DINENNO, P. J. (1995) Appendices to the SFPE Handbook of Fire Protection Engineering, Society of Fire Protection Engineering and the National Fire Protection Association, Quincy, Massachusetts, USA.

DEMBSEY, N.A., PAGNI, P.J., and WILLIAMSON, R.B. (1995) Compartment Fire Experiments: Comparison with Models, *Fire Safety J.*, **25**, 187-227.

EMMONS, H. W. (1995) Vent Flows, chapter 2/5 in *The SFPE Handbook of Fire Protection Engineering*, second edition, Society of Fire Protection Engineering and National Fire Protection Association, Quincy, Massachusetts, USA.

GOTT, J. E., LOWE, D. L., NOTARIANNI, K. A. and DAVIS, W. D. (1997) *Analysis of High Bay Hangar Facilities for Detector Sensitivity and Placement*, NIST TN 1423, National Institute of Standards and Technology, Gaithersburg, Maryland, USA.

HESKESTAD, G. (1995) Fire Plumes, chapter 2/2 in *The SFPE Handbook of Fire Protection Engineering*, second edition, Society of Fire Protection Engineering and National Fire Protection Association, Quincy, Massachusetts, USA.

HINZE, J. O. (1959) *Turbulence - An Introduction to Its Mechanism and Theory*, McGraw-Hill, New York, New York, USA.

HUNT, B. (1995) *Fluid Mechanics for Civil Engineers*, University of Canterbury, Christchurch, New Zealand.



JONES, W. P., and LAUNDER, B. E. (1972) The Prediction of Laminarisation with a 2-equation Model of Turbulence, *Int. J. Heat Mass Transfer*, **15**, 301-314.

KANURY, A. M. (1987) On the Craft of Modelling in Engineering and Science, *Fire Safety J.*, **12**, 65-74.

KARDOS, T. (1996) *Modelling of Smoke Flow Using Computational Fluid Dynamics*, Fire Engineering Research Report 96/4, Department of Civil Engineering, University of Canterbury, New Zealand.

KARLSSON, B. (1997) *Recent work on CFD models at the Department of Fire Safety Engineering, Lund University*, Department of Fire Safety Engineering, Lund University, Lund, Sweden.

KERRISON, L., MAWHINNEY, N., GALEA, E. R., HOFFMANN, N., and PATEL, M. K. (1994a) A Comparison of Two Field Models with Experimental Room Fire Data, *Proc. Fourth International Symp. Fire Safety Science*, 161-172.

KERRISON, L., GALEA, E. R. HOFFMANN, N., and PATEL, M. K. (1994b) A Comparison of a FLOW3D Based Fire Field Model with Experimental Compartment Fire Data, *Fire Safety J.*, **23**, 387-411.

KLOTE, J. H., and MILKE, J. A. (1992) *Design of Smoke Management Systems*, American Society of Heating, Refrigerating and Air-Conditioning Engineers, Inc, and the Society of Fire Protection Engineering, Atlanta, Georgia, USA.

KUMAR, S. (1983) Mathematical Modelling of Natural Convection in Fire, *Fire Mater.*, **7**, 1-24.

KUMAR, S., and COX, G. (1983) The Application of a Numerical Field Model of Smoke Movement to the Physical Scaling of Compartment Fires, in: *Numerical Methods in Thermal Problems*, eds: Lewis, R. A., Johnson, J. A., and Smith, W. R., Pineridge Press, United Kingdom.

KUMAR, S., HOFFMANN, N., and COX, G. (1985) Some Validation of Jasmine for Fires in Hospital Wards, *Numerical Solution of Fluid Flow and Heat/Mass Transfer Processes*.

KUMAR, S., GUPTA, A. K., and COX, G. (1991) Effects of Thermal Radiation on the Fluid Dynamics of Compartment Fires, *Proc. Third International Symp. Fire Safety Science*, 159-171.

LAUNDER, B. E., and SPALDING, D. B. (1972) *Lectures in Mathematical Models of Turbulence*, Academic Press, London, United Kingdom.

LAUNDER, B. E., and SPALDING, D. B. (1974) The Numerical Computation of Turbulent Flows, *Comp. Methods Appl. Mech. Eng.*, **3**, 269-289.

LEWIS, M. J., MOSS, M. B., and RUBINI, P. A. (1997) CFD Modelling of Combustion and Heat Transfer in Compartment Fires, *Proc. Fifth International Symp. Fire Safety Science*, 463-474.

LOCKWOOD F. C., and SHAH N. G. (1981) A New Radiation Solution Method for Incorporation in General Combustion Prediction Procedures, *Proc. 18<sup>th</sup> International Symposium on Combustion*, The Combustion Institute, 1405.

LUO, M., HE, Y., and BECK, V. (1997) A Comparison of Existing Fire Model Predictions with Experimental Results from Real Fires, *J. Applied Fire Science*, **6**, 357-382.

MAGNUSSEN B., and HJERTAGER G. H. (1976) On Mathematical Modelling of Turbulent Combustion with Special Emphasis on Soot Formation and Combustion, *Proc. 16<sup>th</sup> International Symposium on Combustion*, The Combustion Institute, 719-729.

MARKATOS, N. C., MALIN, M. R., and COX, G. (1982) Mathematical Modelling of Buoyancy-Induced Smoke Flows in Enclosures, *Int. J. Heat Mass Transfer*, **25**, 63-75.

MARKATOS, N. C., and COX, G. (1984) Hydrodynamics and Heat Transfer in Enclosures Containing a Fire Source, *PhysicoChem. Hydrodynam.*, **5**, 53-66.

MARKATOS, N. C., PERICLEOUS, K. A., and COX, G. (1986) A Novel Approach to the Field Modelling of Fire, *PhysicoChem. Hydrodynam.*, **7**, 125-143.

MAWHINNEY, R. N., GALEA, E. R. HOFFMANN, N., and PATEL, M. K. (1994) A Critical Comparison of a Phonetics Based Fire Field Model with Experimental Compartment Fire Data, *J. of Fire Prot. Engr.*, **6**, 137-152.

MILES, S. D., and COX, G. (1996) Prediction of Fire Hazards Associated with Chemical Warehouses, *Fire Safety J.*, **27**, 265-287.

MOODIE, K. and JAGGER, S. F. (1992) The Kings Cross Fire: Results and Analysis from the scale model tests, *Fire Safety J.*, **18**, 83-103.

MOSS, J. B., and RUBINI, P. A. (1997a) Coupled Soot and Radiation Calculations in a Compartment Fire, to be published in the proceedings of the *Second International Conference on Fire Research and Engineering*, Gaithersburg, USA.

MOSS, M. B., and RUBINI, P. A. (1997b) SOFIE - Simulation of Fires in Enclosures, *Proc. Fifth International Symp. Fire Safety Science*, 1326

NAM, S. and BILL, R. G. (1993) Numerical Simulation of Thermal Plumes, *Fire Safety J.*, **21**, 231-256.

NOTARIANNI, K. A. and DAVIS, W. D. (1993) *The use of Computer Models to Predict Temperature and Smoke Movement in High Bay Spaces*, NISTIR 5304, National Institute of Standards and Technology, Gaithersburg, Maryland, USA.

PATANKAR, S. V. (1980) *Numerical Heat and Mass Transfer*, Hemisphere Publishing, New York, New York, USA.

PATANKAR, S. V., and SPALDING, D. B. (1972) A Calculation Procedure for Heat, Mass and Momentum Transfer in Three-Dimensional Parabolic Flows, *Int. J. Heat Mass Transfer*, **15**, 1787-1806.

PEACOCK, R. D., FOURNEY, G. P., RENEKE, P. A., PORTIER, R., and JONES, W. A. (1993) *CFAST, the Consolidated Model of Fire Growth and Smoke Transport*, National Institute of Standards and Technology Technical Note 1299, United States Department of Commerce, Gaithersburg, Maryland, USA.

PEACOCK, R. D., RENEKE, P. A., JONES, W. A., and BUKOWSKI, R. W. (1997) *A User's Guide for FAST 3.0: Engineering Tools for Estimating Fire Growth*

*and Smoke Transport*, National Institute of Standards and Technology Special Publication, United States Department of Commerce, Gaithersburg, Maryland, USA.

QUINTIERE, J. G. (1989) Fundamentals of Enclosure Fire “Zone” Models, *J. of Fire Prot. Engr.*, **1**, 99-119.

QUINTIERE, J. G. (1995) Compartment Fire Modelling, chapter 3/5 in *The SFPE Handbook of Fire Protection Engineering*, second edition, Society of Fire Protection Engineering and National Fire Protection Association, Quincy, Massachusetts, USA.

QUINTIERE, J. G., RINKINEN, W. J., and JONES, W. W. (1981) The Effect of Room Openings on Fire Plume Entrainment, *Comb. Sci. Tech.*, **26**, 193-201.

RAPPITSCH, G., PERKTOLD, K., and PERNKOPF, E. (1997) Numerical Modelling of Shear-Dependant Mass Transfer in Large Arteries, *Int. J. Numer. Meth. Fluids*, **25**, 847-857.

RODI, W. (1980) *Turbulence Models and their Application in Hydraulics - A state of the art review*, International Association for Hydrodynamic Research, Delft, The Netherlands.

SIMCOX, S., WILKES, N. S., and JONES, I. P. (1992) Computer Simulation of the Flows of Hot Gases from the Fire at King’s Cross Underground Station, *Fire Safety J.*, **18**, 49-73.

SINAI, Y. L. and OWENS, M. P. (1995) Validation of CFD Modelling of Unconfined Pool Fires with Cross-Wind: Flame Geometry, *Fire Safety J.*, **24**, 1-34.

STECKLER, K. D., QUINTIERE, J. G., and RINKINEN, W. J. (1982) Flow Induced by a Fire in a Compartment, NBSIR 82-2520, National Bureau of Standards, Washington, United States of America.

STROUP, D. W. (1995) Using Field Modelling to Simulate Enclosure Fires, chapter 3/8 in *The SFPE Handbook of Fire Protection Engineering*, second edition, Society of Fire Protection Engineering and National Fire Protection Association, Quincy, Massachusetts, USA.

STULL, D. R., and PROPHET, H. (1971) *JANAF Thermochemical Tables*, National Bureau of Standards, Washington D.C, USA.

VAN DOORMAAL, J. P., and RAITHBY, G. D. (1984) Enhancement of the SIMPLE Method for Predicting Incompressible Fluid Flows, *Num. Heat Transfer*, 7, 147-163.

WALTON, W. D. (1995) Zone Computer Fire Models for Enclosures, chapter 3/7 in *The SFPE Handbook of Fire Protection Engineering*, second edition, Society of Fire Protection Engineering and National Fire Protection Association, Quincy, Massachusetts, USA.

WALTON, W. D., and THOMAS, P. H. (1995) Estimating Temperatures in Compartment Fires, chapter 3/6 in *The SFPE Handbook of Fire Protection Engineering*, second edition, Society of Fire Protection Engineering and National Fire Protection Association, Quincy, Massachusetts, USA.

WATERS, R. A. (1985) Air and Smoke Movement Within a Large Enclosure, in: *Numerical Simulation of Fluid Flow and Heat/Mass Transfer Processes*, Springer-Verlag, Berlin, Germany.

WATERS, R. A. (1989) Stansted Terminal Building and Early Atrium Studies, *J. of Fire Prot. Engr.*, 1, 63-76.

WELCH, S., and RUBINI, P. A. (1996) *SOFIE 2.1 User's Manual*, Cranfield University, Cranfield, United Kingdom.

WOODBURN, P. J. (1995) *Computational Fluid Dynamics Simulation of Fire-Generated Flows in Tunnels and Corridors*, Ph.D thesis, University of Cambridge, United Kingdom.

WOODBURN, P. J., and BRITTER, R. E. (1996) CFD Simulations of a Tunnel Fire - Parts I and II, *Fire Safety J.*, 26, 35-62, 63-90.



# Appendix A Script Files

The purpose of this appendix is to list one example script file for each enclosure. Lines preceded by a '%' signify a comment line.

## A1 Enclosure 1

```
%+++++
% Enclosure 1, 1a.key
% Compartment size 2.5 x 3.7 x 2.5 (i x j x k)
% HRR 330 kW at compartment centre
%
%   Track flow field
%
%   Transient time 1800 seconds
%   Buoyancy corrections to k-e model
%   Eddy breakup combustion model
%   Propane fuel
%   Adiabatic thermal boundaries
%   No radiation
%   One vent (door) to outside centred on i-j plane
%   Plane of symmetry used - parallel to j-k plane
%
%+++++
setup
solution type
heat transfer
turbulence
high-Re k-e
options
buoyancy corrections
end
end
end
combustion
eddy breakup
options
buoyancy corrections
end
end
fuel type
C3H8
end
```

```
transient
buoyancy
end
generate grid
cartesian
x
0
2
10
0.87
% dx
0
1.5
5
0.38
0
0
y
0
2
15
2
0
1.5
4
0.5
0
1.5
z
0
5
10
1.24
1
1.5
5
1.22
0
1.5
10
1.24
0
1.5
2
0.054
0
1.5
10
2
1
1.5
generate
end end
assign blockages
```



```

inactive
% Wall 3
i 2 1-1
j 2 1-1
k 27 28
ok
% Create vent
delete
i 12 16
j 2 16
k 27 28
ok
end
boundary types
% East mirror line of symmetry
fluid
mirror
east
i 1-1 1-1
j f 1
k f 1
ok
fluid
% Vent
staticcp
east
i f 1
j f 1
k 1-1 1-1
ok
fluid
inflow
south
i 13 16
j 2 2
k 12 16
ok
end
boundary values
tke_f
top
i f 1
j f 1
k 1-1 1-1
ok
1
ted_f
top
i f 1
j f 1
k 1-1 1-1
ok
0.1
% fuel inlet

```

```
v_f
south
i 13 16
j 2 2
k 12 16
ok
3.376E-03
mfuel_f
south
i 13 16
j 2 2
k 12 16
ok
1
mfrac_f
south
i 13 16
j 2 2
k 12 16
ok
1
t_f
south
i 13 16
j 2 2
k 12 16
ok
290
end
interior values
solution
tke
fluid
interior
ok
1
solution
ted
fluid
interior
ok
0.1
derived
t
fluid
interior
ok
290
end end
control
solved variables
relax
u 0.1
v 0.1
```

```

w 0.1
end
end
solver control
minimum residual 5.0E-03
maximum timestep iterations 200
pressure correction cycles 20
autosave frequency 100
maximum transient time 1800
end
physical models
ambient temperature 290
end
end
file
problem directory
% problem directory name
la
true
solution directory
% solution directory name
la_sol
true
end
run 60
file
write
solution
export
fieldview
la_1min_fv
end end end
%
run 60
file
write
solution
export
fieldview
la_2min_fv
end end end
%
run 60
file
write
solution
export
fieldview
la_3min_fv
end end end
%
run 60
file
write

```

```
solution
export
fieldview
la_4min_fv
end end end
%
run 60
file
write
solution
export
fieldview
la_5min_fv
end end end
%
run 300
file
write
solution
export
fieldview
la_10min_fv
end end end
%
run 600
file
write
solution
export
fieldview
la_20min_fv
end end end
%
run 600
file
write
solution
export
fieldview
la_30min_fv
end end end
```

## A2 Enclosure 2

```
%+++++
% Enclosure 4, 4Ha.key
% Compartment size 11 x 11 x 41 (i x j x k)
% HRR 300 kW 4m from one end
%
%   Track flow field
%
%   Transient time 1800 seconds
%   Buoyancy corrections to k-e model
%   Eddy breakup combustion model
%   n-Heptane fuel
%   Adiabatic thermal boundaries
%   No radiation
%   One vent (door) to outside centred on i-j plane
%   Plane of symmetry used - parallel to j-k plane
%
%+++++
setup
solution type
heat transfer
turbulence
high-Re k-e
options
buoyancy corrections
end
end
end
%
combustion
eddy breakup
options
buoyancy corrections
end
end
fuel type
n-Heptane
end
transient
buoyancy
end
generate grid
cartesian
x
0
2
10
5.30
0
1.5
```

```

4
0.20
0
0
Y
0
1
15
11
1
1.5
z
0
5
5
3.775
0
1.5
1
0.45
0
0
30
36.775
0.5
1.5
2
0.25
0
1.5
10
2
1
1.5
generate
end end
assign blockages
inactive
% Wall 3
i 2 1-1
j 2 1-1
k 38 39
ok
delete
i 13 15
j 2 1-1
k 38 39
ok
end
boundary types
% East mirror line of symmetry
fluid
mirror
east

```

```
i 1-1 1-1
j f 1
k f 1
ok
fluid
staticp
east
i f 1
j f 1
k 1-1 1-1
ok
fluid
inflow
south
i 12 15
j 2 2
k 7 7
ok
end
boundary values
tke_f
top
i f 1
j f 1
k 1-1 1-1
ok
1
ted_f
top
i f 1
j f 1
k 1-1 1-1
ok
0.1
v_f
south
i 12 15
j 2 2
k 7 7
ok
5.770E-03
mfuel_f
south
i 12 15
j 2 2
k 7 7
ok
1
mfrac_f
south
i 12 15
j 2 2
k 7 7
ok
```

```

1
t_f
south
i 12 15
j 2 2
k 7 7
ok
290
end
solution
tke
fluid
interior
ok
1
solution
ted
fluid
interior
ok
0.1
derived
t
fluid
interior
ok
290
end end
control
solved variables
relax
u 0.1
v 0.1
w 0.1
end
end
solver control
minimum residual 5.0E-03
maximum timestep iterations 200
pressure correction cycles 20
autosave frequency 100
maximum transient time 1800
end
physical models
ambient temperature 290
end
end
file
problem directory
% problem directory name
4Ha
true
solution directory
% solution directory name

```



```
4Ha_sol
true
end
run 60
file
write
solution
export
fieldview
4Ha_1min_fv
end end end
run 60
file
write
solution
export
fieldview
4Ha_2min_fv
end end end
%
run 60
file
write
solution
export
fieldview
4Ha_3min_fv
end end end
%
run 60
file
write
solution
export
fieldview
4Ha_4min_fv
end end end
%
run 60
file
write
solution
export
fieldview
4Ha_5min_fv
end end end
%
run 300
file
write
solution
export
fieldview
4Ha_10min_fv
```

```
end end end
%
run 600
file
write
solution
export
fieldview
4Ha_20min_fv
end end end
%
run 600
file
write
solution
export
fieldview
4Ha_30min_fv
end end end
```

# **Appendix B SOFIE - Lessons Learned**

This chapter illustrates some of the problems encountered during this project, the aim being to present some solutions to simple problems for people who might want to use SOFIE in the future. The first person narrative is used.

## **B1 Communication**

If you are working by yourself, i.e., in an environment where no one else is working with SOFIE, it is very important that you get in contact with other SOFIE users, or CFD code users in general. Possible means of communication is with the SOFIE developers at Cranfield (through the SOFIE bulletin board, or direct person-person email), or the various CFD user internet bulletin boards and chat groups.

The advantage of being in contact with other SOFIE users is that if problems do arise in your work, the chances are that other users have encountered similar problems themselves and know the solutions. This communication can save a lot of time and frustration.

## **B2 Planning**

Run times using CFD codes can be extremely long. Therefore, it is in your best interests to have clearly defined your problem from the outset. This particularly refers to the nature of the grid and fuel source definition: e.g., is the fuel injected at the floor level, or above the floor? Any time that you spend refining the nature of your problem before any simulations are started will pay off because you won't need to run several simulations before getting the problem right.

## **B3 User Manuals**

The current user's manual is the one for SOFIE version 2.04, which is still useful for a description of the basic use of SOFIE. Version 2.06 has introduced a number of changes mostly related to the advanced combustion models and the radiation model. Further developments with SOFIE will entail modifications to the user interface and an updated version of the user's manual will not be available until these modifications have been finished.

Simple heat release/combustion problems are able to be set up using the current manual as a basis and the example script files; in general any differences between the manual and the actual code are easy to identify as you work through setting up a script (most notably you do not need to specifically read polynomial data). If the radiation and/or soot models are required, then further information should be sought from the Cranfield team as information regarding these sub-models is not in the form of a user's manual at this time.

## **B4 Heap Space Memory**

When running SOFIE on a PC there are a number of environment variables that must be set before SOFIE will run. Details of this may be found in the Readme.txt file that comes with installation files. To set the environment variables, you may either write a DOS batch file or within Windows NT, use the Control Panel-System-Environment path.

SOFIE reserves memory for the solution, this is called 'heap space'. If the heap space is insufficient then SOFIE will not run. SOFIE is coded in Fortran77 and thus cannot have adjustable arrays for different sized solutions. However, some C-code is used to dynamically allocate the amount of memory required to run the simulation.

In allocating the heap space, the amount specified must be large enough for your problem to just run. This requires a bit of guess work in changing the environment variable SOFIE\_REAL.

## B5 Databases

SOFIE uses a default fuel of Methane. Changing the fuel type is achieved during setup, look in the menu option for the combustion model and you will see there is a menu called 'fuel type'. You will be prompted for a fuel type and should enter one of those in the SpecificHeat.coe file. You should do this AFTER selecting the eddy breakup combustion model.

Whatever fuel you choose must be defined in the SpecificHeat.coe file. This requires not only H/C ratios but also the specific heat polynomial data. You may add whatever fuels you wish by simply copying the data format.

When appending new data to the SpecificHeat.coe file, consistent SI units (J, kg, K) should be used. Then the scale factor will be unity and the units should be 'MASS'.

SOFIE allows for multiple polynomials spanning the defined temperature range for specific heat. It is possible to use a single constant value.

### **Example: appending new data to the SpecificHeat.coe file:**

The polynomials should be of the form:

2 polynomials

poly 1 from say 273k to 1000k, a 3 term poly of form  $(a + bT + cT^2)$

poly 2 from 1000k to 3000k, a 2 term poly of form  $(a + bT)$

then the datafile would contain:

species name	example	
molecular mass	1234.5	% kg/kmol
heat of formation	-8.31456e+6	% J/Kg
H/C ratio	4	
O/C ratio	2	
units	MASS	
scale factor	1.0	
number polys	2	

upper value            1000  
number coefs           3  
28.11e+3 0.1967e+1 0.4802e-2    % Units of  $C_p$  are J/kg/K  
upper value            3000  
number coefs           2  
132.0 5.432

Note that the majority of data in the SpecificHeat.coe file is taken from the JANAF tables (Stull and Prophet, 1971), where the data is in molar form (units of specific heat are J/kmol/K) which has been normalised by the universal gas constant (hence a scale factor of 8314.510).

## **B6 Grids**

Setting up the grid is the most important part of running SOFIE. I would make the following recommendations regarding grid generation for a project using SOFIE:

1. Investigate the grid dependence of your solutions, i.e., carry out sensitivity studies, and
2. if the fuel source is injected above the floor level, the cells above the floor at the fire source should be blocked.

## **B7 Active Boundaries**

To include a the solid boundary in the calculation and treat the boundary as non-adiabatic, i.e., do a conjugate heat transfer solution in both the fluid and the solid, the boundary must be specified as a number of active blockages (at least two blockages thick). The solid type must also be specified as a material listed in the .coe files. In this case the internal boundary (fluid/solid) need not be specified as the heat transfer coefficient and wall temperature will be calculated. However, an external boundary condition must be specified for the active/inactive blockages (the outside of the wall). It is common to use a specified heat transfer coefficient (based on natural

convection on a vertical wall) and the specified ambient temperature, but this could also be specified as isothermal boundary, which would require the specification of an external temperature.

## **B8 Tracking CO Concentration**

The only way to track CO concentration with the current version of SOFIE is to use a combustion model. The code requires modifications to allow you to specify volumetric source terms for any of the passive scalars.

Unless the flamelet combustion model is used (which Cranfield do not recommend yet), SOFIE does not have a model to describe the production of CO. However, using a passive scalar, (which you could name CO), if you assume that the CO is produced at the fuel source, then it is possible to track where the CO is transported to.

When using the eddy breakup combustion model, you are required to set a mixture fraction at the fuel source equal to unity (and equal to zero elsewhere). This calculation does not contain any CO chemistry, it is simply tracking a scalar. However, by using an empirical relationship for the mass fraction of CO produced at the fuel source, the non-dimensional mixture fraction may then be related to the mass fraction of CO.

## **B9 Convergence Problems**

If there is not a very good energy balance in the solution, then the enthalpy equation may need to be solved more accurately. It is possible to converge the mass and momentum equations, while still not having an energy balance. SOFIE prints out two residual errors:  $q_{flow}$  and  $q_{bnd}$  during the simulation which indicate the energy balance for the fluid and active blockages respectively.

To solve the energy equation more accurately, first, check the under relaxation factor for enthalpy; if the value is 0.5 you may find that increasing to 0.7 will improve things. Secondly, you could change the solver for just the enthalpy to

(for example) sip3d, and you must also increase the number of cycles for enthalpy to say 10.

When there are active cells in the flow domain, it is necessary to have the enthalpy under relaxation values as high as possible. This is because when carrying out solutions with active blockages, because of the large difference in density between solid and fluid there is a big difference in pseudo iteration-time-step (controlled by the under relaxation factor), thus the solution will change more rapidly in one region than in another; this can give large energy imbalances.

A under relaxation factor of 1.0 implies no under-relaxation and hence no pseudo-time-step, thus removing the above problem.

Finally, if you are using the radiation model you should ensure that the minimum number of iterations per time-step is set equal to the frequency at which the radiation solver is called (by default 10). If you are not using the radiation model then this is not an issue, however you may find that to ensure there is an energy balance, setting the minimum number of iterations per time-step to a value like 5 (or greater if you can afford the time) might be a good idea.



## B10 Post-Processing

Transient solutions are not able to be viewed using Fieldview for Windows version 2. Therefore, result files must be written and exported at the time intervals you wish to look at. The reason for this is that the producers of Fieldview are a commercial company who will not support the file formats used in the SOFIE code.

To write out files for post processing the following lines of script file may be used:

```
run 60
file
write
solution
export
fieldview
1a_60seconds_fv
end end end
run 60
```

The above is an example of running the simulation for 60 seconds then writing and exporting a file named 1a\_60seconds\_fv in a format that can be viewed in Fieldview for Windows. Once the file has been written and exported the simulation will now run for another 60 seconds.

It should be noted that the files viewed by Fieldview for Windows are large (5MB+), thus this will probably restrict the number of files (or time-steps) to be able to be exported for a simulation.

In terms of processing the data, it is easy to get attractive pictures of temperature profiles, etc. throughout the domain. However, it is difficult and time consuming to generate data for a simulation using the current form of the Fieldview for Windows software.

## **FIRE ENGINEERING RESEARCH REPORTS**

<b>95/1</b>	<b>Full Residential Scale Backdraft</b>	<b>I B Bolliger</b>
<b>95/2</b>	<b>A Study of Full Scale Room Fire Experiments</b>	<b>P A Enright</b>
<b>95/3</b>	<b>Design of Load-bearing Light Steel Frame Walls for Fire Resistance</b>	<b>J T Gerlich</b>
<b>95/4</b>	<b>Full Scale Limited Ventilation Fire Experiments</b>	<b>D J Millar</b>
<b>95/5</b>	<b>An Analysis of Domestic Sprinkler Systems for Use in New Zealand</b>	<b>F Rahmanian</b>
<b>96/1</b>	<b>The Influence of Non-Uniform Electric Fields on Combustion Processes</b>	<b>M A Belsham</b>
<b>96/2</b>	<b>Mixing in Fire Induced Doorway Flows</b>	<b>J M Clements</b>
<b>96/3</b>	<b>Fire Design of Single Storey Industrial Buildings</b>	<b>B W Cosgrove</b>
<b>96/4</b>	<b>Modelling Smoke Flow Using Computational Fluid Dynamics</b>	<b>T N Kardos</b>
<b>96/5</b>	<b>Under-Ventilated Compartment Fires - A Precursor to Smoke Explosions</b>	<b>A R Parkes</b>
<b>96/6</b>	<b>An Investigation of the Effects of Sprinklers on Compartment Fires</b>	<b>M W Radford</b>
<b>97/1</b>	<b>Sprinkler Trade Off Clauses in the Approved Documents</b>	<b>G J Barnes</b>
<b>97/2</b>	<b>Risk Ranking of Buildings for Life Safety</b>	<b>J W Boyes</b>
<b>97/3</b>	<b>Improving the Waking Effectiveness of Fire Alarms in Residential Areas</b>	<b>T Grace</b>
<b>97/4</b>	<b>Study of Evacuation Movement through Different Building Components</b>	<b>P Holmberg</b>
<b>97/5</b>	<b>Domestic Fire Hazard in New Zealand</b>	<b>KDJ Irwin</b>
<b>97/6</b>	<b>An Appraisal of Existing Room-Corner Fire Models</b>	<b>D C Robertson</b>
<b>97/7</b>	<b>Fire Resistance of Light Timber Framed Walls and Floors</b>	<b>G C Thomas</b>
<b>97/8</b>	<b>Uncertainty Analysis of Zone Fire Models</b>	<b>A M Walker</b>
<b>97/9</b>	<b>New Zealand Building Regulations Five Years Later</b>	<b>T M Pastore</b>
<b>98/1</b>	<b>The Impact of Post-Earthquake Fire on the Built Urban Environment</b>	<b>R Botting</b>
<b>98/2</b>	<b>Full Scale Testing of Fire Suppression Agents on Unshielded Fires</b>	<b>M J Dunn</b>
<b>98/3</b>	<b>Full Scale Testing of Fire Suppression Agents on Shielded Fires</b>	<b>N Gravestock</b>
<b>98/4</b>	<b>Predicting Ignition Time Under Transient Heat Flux Using Results from Constant Flux Experiments</b>	<b>A Henderson</b>
<b>98/5</b>	<b>Comparison Studies of Zone and CFD Fire Simulations</b>	<b>A Lovatt</b>
<b>98/6</b>	<b>Bench Scale Test of Light Timber Frame Walls</b>	<b>P Olsson</b>
<b>98/7</b>	<b>Exploratory Salt Water Experiments of Balcony Spill Plume Using Laser Induced Fluorescence Technique</b>	<b>E Y Yii</b>

School of Engineering  
University of Canterbury  
Private Bag 4800, Christchurch, New Zealand

Phone 643 364-2250  
Fax 643 364-2758